TECHNICAL DOCUMENTS LIAISON OFFICE
UNEDITED ROUGH DRAFT TRANSLATION

OPERATING CYCLES IN HEAT ENGINES (COLLECTION OF ARTICLES)

BY: Various Authors

ENGLISH PAGES: 328

THIS TRANSLATION HAS BEEN PREPARED IN THIS MANNER TO PROVIDE THE REQUESTER/USER WITH INFORMATION IN THE SHORTEST POSSIBLE TIME. FURTHER EDITING WILL NOT BE ACCOMPLISHED BY THE PREPARING AGENCY UNLESS FULLY JUSTIFIED IN WRITING TO THE CHIEF, TECHNICAL DOCUMENTS LIAISON OFFICE, MCLTD, WP-AFB, OHIO	PREPARED BY: TECHNICAL DOCUMENTS LIAISON OFFICE MCLTD WP-AFB, OHIO

R

RABOCHIYE PROTSESSY V TEPLOVYKH DVIGATEL'NYKH USTANOVKAKH

Vyp. 119

Gosudarstvennoye Nauchno-Tekhnicheskoye
Izdatel'stvo Oborongiz, Moskva 1960

Pages: 174

TABLE OF CONTENTS

The present collection of articles deals with transition cycles in engine chambers and the effect of regeneration on the engine's characteristics; the results of theoretical and experimental investigation of spraying fuel by spray nozzels with colliding jets are examined, and the possibility of utilizing higher temperatures in a turbine and testing it with model gas is studied; an electric canal arc is examined which makes it possible to investigate the plasma as a new working substance of heat engines.

The book is meant for specialists studying the theory and design of heat engines.

FORWORD

The present collection of articles contains papers written by the collaborators of the chair for aviation engines, which deal with individual problems of the theory of heat engines.

D. I. Abugov's paper gives a profound analysis of the combustion process and establishes a number of hitherto unknown regularities in the development of this process. The author widens the field of application of the heat theory of fuel combustion, taking account in his computations not only the heat transfer from the reacting mixture to the surrounding medium but also the exchange of mechanical work. The author draws interesting conclusions about the inverse effect of the development of the reaction on its initial stimulation. The author juxtaposes the regularities thus obtained and the combustion cycles in engines; in so doing, he sets forth test data and evaluates additional phenomena preceding the fundamental ignition cycle of the gaseous phase.

An important device for the study of problems of heat transfer and gas exchange in flows, one of which has a high temperature, is represented by the electric canal arc or plasmotron. A high-temperature jet with a high content of plasma is formed under very complex

conditions and the problems regarding the characteristics of plasmotron products are far from being solved. V. B. Tikhonov and Ye. A. Yakovlev describe the design of the most commonly used type of plastmotron, enumerate the problems arising when studying plasmas and utilizing plasmotrons, and set forth a tentative solution of two problems which determine the properties of the jet obtained. The authors who have worked with a plasmotron bring the results of spectrograms processing taken of the plasma jet, and the approximate distribution of temperatures along the transverse section of the jet. Moreover, the theoretical computations of the authors show that the parts played by electrical forces in the acceleration of the jet is quite irrevelant. Upon reading the paper it becomes clear that engineers without special training, when working with plasmotrons, must first acquire some knowledge in new fields of physics unknown to them.

The problem dealt with in the paper of I.G. Panevin " On Spraying Liquids by Spray Nozzles with Colliding Jets" is referred to the initial moment of fuel mixture formation. The theoretical part of the paper analyses the stability of film motion, shows which perturbations destroy films and how the formation of such

perturbations is affected by more substantial parameters of (injection elements.

In the end, the author calculates the mean size of a drop for a two-jet spray nozzle and successfully corroborates his computations by tests.

In his second paper, Panevin studies the distribution of the liquid in the jet formed by two colliding jets. The author offers an alternative theoretical solution of the problem and sets forth the result of his own tests. He examines in detail the effect of the parameters of two-jet spray nozzles on the distribution of fuel consumption and the component ratio in fuel jets.

In his paper "Investigations of the Spreading of an Axially Symmetrical Jet along the Wall", V.A. Kurochkin determines the velocities and the thickness of the liquid film at various distances from the point where the jet meets the wall. Experimental investigations have confirmed the theoretical scheme proposed by the author. To measure the film thickness, the author utilized the radiation of the isotope Sr^{90}.

Obtaining a steady operation of engines with basic and transient cycles is one of the principal problems for the further development of engines. As is shown in the paper by L. A. Latyshev, N. B.

Rutovskiy and V. B. Tikhonov, forced mechanical oscillations of turbine fuel pipes can cause perturbations which may bring about unsteadiness. The experiments described in the paper show that oscillations in the fuel conduit bring about oscillations in the spray nozzle feed and fluctuations in the cycle of fuel mixture formation. All this, complicated as it is by the invert effect of the chamber on the feed system, represents an undesirable complex of phenomena which interfere with the steady operation of the engine. The literature does not deal with the problems tackled by the authors, hence the paper may be of interest for the specialists. Worth noting is the original design of the assembly causing the oscillation of the pipe conduit.

In his paper "Heat Regeneration in ZhRD", A. V. Kvasnikov discusses the possibility of improving the efficiency of ZhRD by utilizing regeneration. On the basis of the data cited in the paper it becomes clear why external regeneration is not used in practice. At the same time it is shown that in separate specific cases the utilization of regenerating devices may turn out to be expedient.

The two papers at the end of this collection examine a turbine which represents one of the elements of the feeding system of

an engine. In his paper "Cooling of short turbine blades", A. F. Shtyrlin determines the temperatures of simple and covered turbine blades with a cooled butt. Among the many cooling systems the author selected the simplest one. The desire to improve the quality of gas generator products, the discovery of new working substances, the increasing capacity of turbines, all this calls for the application of high-temperature turbines. By utilizing a number of assumptions and examining the linear problem of the distribution of heat in a covered blade, A. F. Shtyrlin sets forth a computation method for the determination of temperatures by the height of the blade and the temperature gradients in the covering material. By the results of his computations and experimental checks of individual cases, the author shows that the utilization of coverings protecting the surfaces of the blade or removing heat to the butt makes it possible to lower the temperature of the blade. This temperature reduction is small and can be of practical significance only for blades of small height. A. F. Shtyrlin's paper can be utilized for comparing various methods of turbine blade cooling and when developing mehtods for the computation of blade temperatures.

V. M. Tyugin's paper "On the possibility of utilizing binary

alloys for tests with model turbines" belongs to a cycle of works by the chair on the problem of utilizing model working substances for the investigation of processes in turbines or other blade engines. Such substances include mixtures consisting of gases which differ widely in their molecular weight. Can the gases belonging to such a mixture be demixed when the flow is reversed; will there be an equilibrium flow of such a mixture in the nozzle channel, and will it be necessary to take into account the secondary processes mentioned above when computing the fundamental process? V. M. Tyugin's paper answers these questions.

The members of the chair believe that this collection of articles as a whole may be of interest for specialists working in the field of jet engines.

TRANSIENT COMBUSTION PROCESSES IN ENGINES

by

Candidate of Technical Sciences D. I. Abugov

The investigation of transient combustion processes (ignition, extinction, change of combustion into detonation) is of the greatest interest. In fact, the difficulties encountered when seeking a practical solutions of problems relating to combustion cycles processes in engines, are, in many cases, associated with transient cycles processes.

The experimental work required for overcoming the difficulties encountered, frequently is empirical in character and, while requiring considerable expenditures in terms of means and time, it does not provide sufficient understanding of the nature and regularities of the phenomena under investigation.

The theoretical analysis of transient combustion processes is considerably complicated by their unsteady nature and the necessity of taking into account the final rate of chemical reactions. For this reason, when studying these processes, it becomes necessary to introduce substantial simplifications.

In the present paper, on the basis of the heat theory of combustion, we examine the ignition cycle of a homogeneous (preli-

minarily mixed) gaseous mixture of fuel and an oxidizing agent, thus making it possible to eliminate the study of mixture formation processes and evaporation, thereby considerably simplifying our task; in addition, other substantial simplicfications have also been introduced. The application of the results obtained to actual combustion chambers where combustion takes place under considerably more complicated conditions, is discussed on the basis of individual examples.

The heat theory (1, 2, 3) regards ignition as a result of preflame chemical reactions which take place in the fuel mixture. [redacted] At the final rate of the chemical reactions, the igniting capacity of the fuel mixture depends on the energy exchanged between the reactant and the surrounding medium. If the heat released by the chemical reaction accumulates in the reacting system, then the inverse effect [redacted] of the development process of the chemical reaction (temeperature increase) on the original process of its stimulation (initial heating of the fuel mixture) leads to a sizable increase (almost staggered in nature) in accordance with the exponential expression $e^{-\frac{E}{RT}}$

of the reaction rate which, during the transient ignition period, is relatively small. As a result of this, there arises an unsteady, progressively accelerated cycle of the chemical reaction, i.e., there occurs ignition. However, if the heat from the chemical reaction is divereted into the surrounding medium and the heatup of the reactent is irrelevant, there takes place a stationary cycle of slow reaction, i.e., ignition does not occur.

The extinction procedure, or the cessation of the propagation of the flame, is similar to the ignition procedure. Here, too, the energy exchanged between the reactent and the surrounding medium is of decisive importance. In this case, the transition of the stationary rapid reaction to the non-stationary, progressively decreasing reaction depends on this exchange.

The heat theory of combustion usually regards the energy interaction between the reactent and the surrounding medium as a form of heat transfer. The interaction of a thermodynamic system with the surrounding medium, however, takes place in two different ways; as heat transfer and performance of mechnical work, while in the case of an open system there also takes place an exchange of substance (mass) with the surrounding medium. Depending upon the conditions under which

combustion takes place, it will be necessary to take account of this or the other form of exchange between the reacting system and the surrounding medium. In particular, in the case of variations in the state of the gas with high velocities and great specific performance, exchange of mechanical work will be of prevailing importance as compared to heat transfer.

The investigation of ignition and extinction processes requires the joint solution of a system of equations which includes the chemical kinetics equation and the equations of gas dynamics.

In order to simplfy the writing of the formulas, we adopted the system of physical units (excepting individual numerical examples).

§ Chemical Kinetics Equation

In accordance with the concepts of heat theory we assume that the rate of the complex process of chemical transformation during combustion can be expressed approximately by an equation where the rate of reaction is a function of the concentration of the initial substances and the temperature $W=-\frac{d\rho_i}{dt}=f(\rho, T)$, and can be written as

$$W=K\rho_i^n e^{-\frac{E}{RT}}. \qquad (1)$$

where ρ_i is the concentration of the original substance (in

mass units per volume unit);

T is the temperature;

K is the constant coefficient;

E is the activation energy;

n is the exponent which depends upon the order of the reaction.

Equation (1) should be regarded as an approximate dependence where the values E, K and n are constants determined experimentally. In the case of complex reactions, variations in the mechanism are possible and , hence, variations in the values for the kinetic parameters at various temperature ranges may also occur. In these cases, the above values should be regarded as the mean values for the variables in the interval under investigation.

According to test data for the combustion reaction of commercial fuels, the above order of reactions corresponds in most cases to n=2.

The sharply nonlinear character of the exponential dependence of the reaction rate on the temperature ($W \sim e^{-\frac{E}{RT}}$) (Arrhenius' Law) brings about substantial peculiarities in the transient combustion processes.

The rate of heat emission owing to chemical reaction, referred

to volume unit and time unit, equals HW, where H is the thermal effect of combustion reaction.

Equations of Gas Dynamics

When gaseous mixtures are burnt, the gas mass remains constant, hence the mass conservation equation has the usual form. The equations of gas motion (conservation of the quantity of motion) also remain unchanged.

When writing the energy equation, we can substitute the processes of chemical transformation by such a fictitious external heat supply which, according to its energy results, would be equivalent to the chemical reactions, i.e., we regard combustion as an external heat source.

In the general case of space motions of the gas, without taking account of viscosity, the laws of mass conservation, quantity of motion and energy are expressed by the following equations (according to Euler):

$$\left.\begin{aligned} \frac{d \ln v}{dt} &= -\operatorname{div} u \\ \frac{du}{dt} &= -v \operatorname{grad} p \end{aligned}\right\} \qquad (2)$$

$$c_p\rho\frac{dT}{dt}=HW+\operatorname{div}(\lambda\,\operatorname{grad}T)-p\frac{d\ln v}{dt}. \tag{3}$$

Equation (3) can also be written as:

$$c_p\rho\frac{dT}{dt}=HW+\operatorname{div}(\lambda\,\operatorname{grad}T)+\frac{dp}{dt}. \tag{3'}$$

Thexex
We examine an ideal gas and do not take account of the variation in the number of molecules during combustion, and write the equation of state as

$$pv=RT. \tag{4}$$

Here, p, T, v are the pressure, temperature and specific pressure of the gas;

$\rho=1/v$ is the gas density;

u is the gas velocity;

c_v и c_p are the thermal capacity of the gas with constant volume and pressure, respectively;

R is the gas constants;

λ is the heat condustion coefficient;

t is the time.

Thus, the complete system of equations of gas dynamics and chemical kinetics is composed of seven equations (the law of the conservation of quantity of motion yields three equations of motion) which determine seven parameters: u_x, u_y, u_z, p, z, T and W. In the general case, all of these values are functions of the coordinates x, y and z, and of the time t.

The equations mentioned above have a general character and, for the time being, are in no way connected with the course of the combustion processes under investigation.

By assigning initial and boundary conditions, such a connection can be established in principle. The solution of a system of differential equations under the assigned conditions would make it possible to find the distribution of gas temperature as a function of time and coordinates, i.e., find a solution for the problems under investigation.

In the case of ignition, there takes place an abrupt transition from small temperature variations to large ones, and rapid temperature increases (from the slow stationary reaction to the progressive accelerated reaction). By determining the temperature variation in time, it is possible to determine the effect borne by the variation of the outer parameters on ignition, etc., as well as to

establish the course of the ignition process in time.

Under different initial conditions, it is possible to determine in a similar way the typical conditions of extinction, i.e., the abrupt transitions to rapid and great temeprature drops.

Unfortunately, the solution of the problem in the most general form for a gas in motion, taking into account the spatial distribution of all the parameters inside the combustion chamber and on its boundaries, is impracticable owing to unsurmounting mathematical difficulties of integrating the systems of nonlinear differential equations with partial derivatives. The assignment of boundary conditions indispensable for such a solution is also connected with great difficulty.

We may gain some ideas about the transient combustion processes in a gas in motion by analyzing the systems of equations (2), (3) in a general way.

Since these equations comprise total derivatives, it is possible to follow the variations in the state of a gas particle in motion.

As is seen from equation (3), in the case of incompressible motions (ρ=const) at $HW + \operatorname{div}(\lambda \operatorname{grad} T) > 0$ the temperature of a given

gas particle and, hence, the pressure will grow, whereas they will decrease if these terms are negative. Yet, in the case of a nonuniformly heated gas, its density changes also under the effect of temperature variation, hence, even with a sufficiently small velocity, it is impossible to consider its density constant.

For compressible motions the relationships are even more complex.

If at $HW+\operatorname{div}(\lambda \operatorname{grad} T)>0$ the density of a given particle decreases, then its temperature increase will be less than in the case of incompressible flows, and it may even drop. If, on the other hand, the density of the given particle increases, then its temperature and pressure increase to a greater degree than in the case of incompressible flows.

It is known that in the case of one-dimensional flows with flow velocities within the range of M numbers $1/\sqrt{k}$ and 1, the supply of heat, for example, owing to combustion, leads to a drop in temperature. This is explained by the fact that the sum of kinetic energy growth and the work performed exceeds the quantity of heat supplied (in the same way as when to a mass of gas contained

in a cylinder with a piston, heat is supplied and at the same time the piston is moved in such a way that the dilation performed exceeds the quantity of heat supplied).

The mathematical difficulties were found to be extremely great also in the case of unidimensional problems where all the parameters, excepting time, depend only on one coordinate. The investigation of nonstabilized nonisentropic gas flows is a field of gas dynamics which has not been sufficiently explored as yet.

Owing to this situation it becomes necessary to resort to considerable simplifications when setting up and solving the problems.

In the present paper, the main attention is devoted to the thermal aspect of combustion (the effect of temperature conditions on the rate of heat emission from the chemical reaction)[6], which is of particular significance for the transition processes; the chemical and gasodynamic aspect of combustion are almost entirely ignored.

1. THEORY OF IGNITION

In the simplest case of ignition of a fuel gas mixture contained in a container with constant volume (1),

tained in a container with constant volume (1), the energy equation (3), considering the gas motionless and assuming

$$\operatorname{div}(\lambda \operatorname{grad} T) = -\xi(T, x_i), \tag{A}$$

can be written as

$$c_v \rho \frac{\partial T}{\partial t} = HW - \xi(T, x_i). \tag{5}$$

Integration of equation (5) with partial derivatives and taking into consideration the dependence of temperature on time and on the coordinates is connected with great mathematical difficulites, so that we are forced to resort to further simplifications.

In the theory of heat ignition, developed by N.N. Semenov (4) and which has become the basis for any further studies in this field, the author regards the dependence of temperature on time without considering the distribution of temperature in space. With $\rho V = M$ и $V\xi(T, x_i) = \alpha F(T - T_{ст})$ equation (5) assumes the form

$$c_v M \frac{dT}{dt} = HVW - \alpha F(T - T_{ст}), \tag{5'}$$

(1) Where dv=0, i.e., account is taken only of the heat exchange between the reacting gas and the surrounding medium.

where V и F are the volume and surface of the container;

α is the coefficient of heat transfer from the gas to the container walls;

T_{cr} is the temperature of the walls.

(j)

Such a research method (nonstationary method) makes it possible to establish the critical conditions of ignition as well as the course of the ignition process in time. All this is of particular interest for technical applications.

The nonstationary theory of ignition, considering only the thermal interaction of the reacting gas with the surrounding medium, has been developed in detail by O.M. Todes (2).

Yet, ignition can be investigated also following another procedure. If we analyze the temperature distribution in space and do not take account of this distribution with regard to time, then, in the case of heat transfer by pure conduction inside the container, equation (5) can be written as

$$HW + \operatorname{div}(\lambda \operatorname{grad} T) = 0. \qquad (B)$$

The solution of this equation under given boundary conditions (constant temperature on the inner surface of the container walls)

yields a stationary distribution of temperature in the reacting fuel mixture. The critical ignition conditions are looked for as conditions under which a stationary temperature distribution becomes impossible (3).

The stationary method for the study of ignition does not afford the possibility of establishing the course of the process in time, and, hence, its application to the solution of technical problems is forcibly limited.

In actual engines, ignition occurs under conditions where there takes place a thermal and mechanical interaction of the reacting fuel mixture with the surrounding medium (5).

The study of ignition, taking into consideration mechanical interaction, makes it possible to determine new properties in the course of ignition, in particular, a singular form of transition (kinetic) curves which are not found in the case of ignition in a container with a constant volume.

Basic Assumptions

In order to simplify our task and obtain general conclusions, we are going to investigate ignition under the following conditions:

1. Investigation of a closed system, i.e., a system capable

of exchanging heat and mechanical work with the surrounding medium, but incapable of exchanging substance (mass).

In an open system, the gas mass can change on account of the exchange taking place with the surrounding medium, which renders considerably more difficult the determination of the gas state parameters.

The results obtained for a closed system can also be applied to the study of ignition in an open system.

2) It is assumed that pressure and temperature are identical at any point of the reacting system and that the temperature gradient is localized at the walls of the combustion chamber. Assumptions regarding pressure do not give rise to objections if the condition mentioned at the end of the following paragraph is regarded as satisfied.

Assumptions regarding temperature are usually accepted when ignition is studied by the nonstationary method. This means that each individual element of the overall fuel mixture volume reacts on its own, without transferring heat and substance to other elements; only the transfer of heat from the whole reacting system to the surrounding medium is taken into consideration.

The assumption of an identical temperature by the volume of the reacting fuel mixture in the case of heat transfer to the surrounding medium can be accurate only for elementary volumes. If the volume attains final temperatures, it is necessary to introduce a mean temperature for the volume. The rate of the chemical reaction, however, cannot be regarded as a function of the mean temperature; owing to the extremely close dependence of the rate of reaction on temperature, the substitution of the true temperature distribution by an average can change the reaction rate. In the case of intensive turbulent mixing of the reacting gas, the assumption in question is a close approximation, but even in this case, owing to temperature fluctuations, the difference between the mean value of the action rate and the reaction rate at a mean temperature value may turn out to be sufficiently substantial.

Experimental data show (6) that in most cases ignition has a local character: individual foci are formed from where the flames spread, thus creating simultaneously new foci. This type of ignition is apparently connected with the non-uniform distribution of temperature over the volume of the reacting fuel mixture.

Another method of investigation can also be applied: it

consists of dividing the volume of the fuel mixture where ignition takes place into a large number of elements and proceed to investigate the ignition process in these small fuel volumes. This leads to the study of the open system, inasmuch as the volumes singled out are going to exchange with one another not only heat but also substance. For this reason, when undertaking general investigations, utilization of this method will be difficult, whereas when studying concrete problems it may be readily applied.

The assumption of an identical (or mean) temperature for the volume of the reacting fuel mixture is a rough approximation which, in certain cases, may lead to substantial errors. Yet, if we give up this assumption it may be difficult, if at all possible, to obtain ~~xnee~~ generalized results.

3. It is assumed that the change in the volume of the fuel gas mixture with the time which determines the exchange of energy of the latter with the surrounding medium in the form of mechanical work, results from external agents and is determined directly by the specifications of the problem, i.e., V(t) is assigned.

Generally, the exchange of mechanical work may not only be the result of the effect of external factors not depending on the

process, but may also be closely associated with the course of the ignition process proper. Calculation of such interconnections may be difficult in a general form.

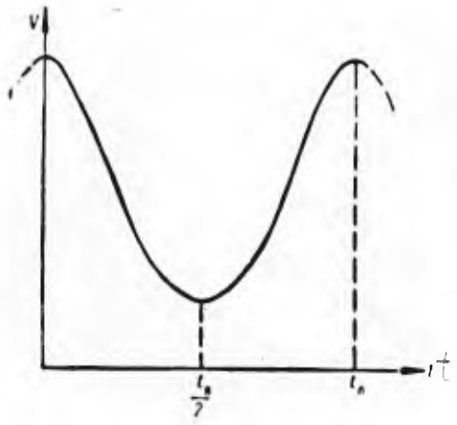

Fig. 1. Curve of function V(t).

On the other hand, obtaining results under the above assumption facilitates the study of individual problems where mechanical interaction is associated with the development of the ignition process.

The function V(t) may have various aspects. Of more general interest is the case of a periodically varying function V(t) and a mechanical interaction varying not only in magnitude but also

in its sign, viz., ignition under conditions of compression and dilation. Without interfering with the general assumptions, let us assume that V(t) is a continuous periodical function whose period t_p can be divided into two intervals in each of which V(t) is monotonic; let us also assume that function V(t) is even, i.e., it is a symmetry of the first order (Fig. 1).

The assumption of an identical pressure and temperature in the volume of the reacting fuel mixture imposes certain specific limitations on the magnitude of the period of the function.

If the gas volume changes, the pressure and, hence, the temperature will change uniformly at any point, i.e., there will be no local variations in the pressure and temperature provided the condition

$$t_n \gg \frac{l}{c}, \qquad (C)$$

is satisfied. Here, l is the characteristic linear dimension of the system under investigation; and

c is the velocity of sound in the gas.

This condition means that the time for the change of the gas volume is long in comparison with the time l/c during which a sound

signal covers the distance l. When satisfying this condition, the diffusion of mechanical interactions in the gas may be regarded as instantaneous.

4. The effect on the rate of reaction by the change in the concentration of the initial gas owing to burning out is not taken into consideration.

Ignition, i.e., the transition from a slow reaction to a progressively accelerated one, usually takes place with a small burnup. Moreover, temperature variation has a prevailing effect on the reaction rate. We may therefore disregard the change in the concentration when studying ignition, without running into any sizeable error.Yet, the assumption in question leads to a limitation of computations of temperature variations in time with the aid of the equation of only the initial ignition stage given below.

In order to simplyfy mathematical calculations and obtain results more simple in form, let us additionally introduce the following assumptions (when solving concrete problems, most of these simplifications can readily be dispensed with):

a) We shall examine the reactions of the first order (n=1). Let us note that this assumption does not contradict the fact that

changes in the concentration of the initial gas owing to burnup are disregarded. In this case, the order of the reaction determines the effect on the reaction rate of the initial concentration of the fuel mixture and the effect of the change in this concentration due to the change in volume of the reacting gas.

If we disregard the change in the concentration with the change in volume, then, in the final formulas, we may take account of the case of a reaction of the second order.

b) We assume the heat capacity of the gas to be constant.

c) We disregard the variation in the number of moles during combustion.

d) In computing the heat transferred from the gas into the surrounding medium we assume F=const, where α is the heat transfer coefficient which depends on the gas temperature and pressure as well as on the turbulence characteristics; F is the cooling surface of the gas which changes when the volume changes. In the case of a predominant value for the energy exchanged in the form of mechanical work, this assumption will not introduce substantial errors.

Initial Equations

With the assumptions mentioned above, the energy equation (3)

may be written as

$$\frac{dT}{dt} = \frac{H}{c_v}\frac{W}{\rho} - \frac{p}{c_v \rho}\frac{d\ln V}{dt} - \frac{\alpha F}{c_v M}(T - T_{cr}). \qquad (6)\,(x)$$

the equation of the reaction rate will then take the form of

$$W = K\rho c^{-\frac{E}{RT}}. \qquad (7)$$

By combining equation (6) with (7), and after minor transformations, we obtain

$$\frac{dT}{dt} = \frac{H}{c_v} K c^{-\frac{E}{RT}} - (k-1)\frac{d\ln V}{dt} T - \frac{\alpha F}{c_v M}(T - T_{cr}), \qquad (8)$$

where $k = c_p / c_v$.

The terms on the right of this equation determine the effect of heat emission due to chemical reaction on the rate of temperature variation of the fuel gas (first term) and the energy exchanged with the surrounding medium in the form of mechanical work (second term) and in the form of heat transfer (third term).

The possibility of a rapid variation of the mechanical work

(x) This equation can readily be derived directly from the first law of thermodynamics.

performed by the gas not only in magnitude but also in the sign, whereas heat transfer takes place only in the direction of decreasing temperature, i.e., from the gas into the surrounding medium (considering that T is always greater than T_{const}), leads us to discover new peculiarities in the development of the ignition process which are not encountered in the case of thermal interaction alone.

Ignition processes with a predominant effect of mechanical interaction take place in engines of the pulsating type (piston and air jet engines as well as steady-flow jet engines during starting and oscillating combustion cycles). The investigation of such processes is of interest for the application to the ignition of shock and detonation waves as well as for the explanation of the mechanism of transition from combustion to detonation.

In a number of cases, instead of equation (8) , it is more convenient to use the following analogic equation:

$$\frac{dT}{dt} = \frac{H}{c_p} K e^{-\frac{E}{RT}} + \frac{k-1}{k} \frac{d \ln p}{dt} T - \frac{\alpha F}{c_p M}(T - T_{cr}). \qquad (8')$$

To write equation (8) in a dimensionless form we introduce the dimensionless variables

$\tau = t/t_f$ — dimensionless time

$\theta = T/T_0$ — relative temperature.

As a unit of dimensionless time we took the characteristic time $t_f = 1/2\pi f$, where f is the frequency of the function V(t).

In units of dimensionless time, the variation period of the functions V(t) and dV/dt will be equal to $(= 2\pi)$. The quantity t_f is the natural time scale for the ignition process under the condition of a predominant value of the mechanical interaction.

As a unit for relative temperature we took the gas temperature T_0 at the initial time instant $(\tau = 0)$. Let us note that the temperature T_0 cannot serve as a rate for the temperature variation during ignition; the latter is given below.

We obtain the dimensionless rate (φ) of the change in volume of the fuel mixture by introducing dimensionless time:

$$(k-1)\, t_f \frac{1}{V}\frac{dV}{dt} = (k-1)\frac{d\ln V}{d\tau} = \varphi. \qquad \text{(A 17)}$$

For the convenience of further calculations let us introduce the dimensionless volume $\varepsilon = V_{max}/V$.

Let us also introduce the dimensionless parameters:

$b = \frac{E}{RT_0}$ — Relative activation energy;

$q = \frac{H}{c_v T_0}$ — Relative heat of reaction (let us note that with $V = \text{const}$ $q = \frac{T_{max} - T_0}{T_0}$);

$d = K t_f = \frac{K}{2\pi f}$;

$g = \frac{aF}{c_v M} t_f = \frac{aF}{c_v M 2\pi f}$

(c 17) Dimensionless coefficient in the reaction rate equation; Relative rate of heat transfer from the gas to the surrounding medium.

By introducing into equation (8) the dimensionless variables and parameters, and assuming that $T_{const} = T_o$ and denoting qd by C (x), we obtain

$$\frac{d\sigma}{d\tau} = Ce^{-\frac{h}{\sigma}} - \psi\sigma - g(\sigma - 1) \qquad (9)$$

(The initial conditions being $(\sigma=1)$ with $\tau=0$).

We assume here that at the initial moment there is a fuel mixture $(C>0)$, but we can also assume that the fuel mixture has been found at a given moment $(\tau_{cm}>0.)$. In this case, in addition to equation (9), we have the following conditions:

$C=0$ $\tau < \tau_{CM}$

(1 17) with (j 17) non-reacting gas;

$C>0$ $\tau \geq \tau_{CM}$

(k 17) with (1 17) fuel mixture.

Let us note that for the conditions in engines (T = 250 to 750°)

(x) The parameter C represents the rate of increase of dimensionless temperature owing to the chemcial reaction taking place at an infinitely high temperature.

considering $E \approx 20 \cdot 10^3 \div 40 \cdot 10^3$, we obtain $\bar{b} \approx 20 \div 80$, $q \approx 10 \div 5$ and less (for mixtures differing considerably from stoichiometric compounds).

The solution of equation (9) makes it possible to determine the dependence of the ignition limit on various factors as well as the effect of the latter on the course of the ignition process in time.

The character of the curves $\lambda \sigma(\bar{b}, \cdot)$ is determined by the values for the parameters C, b and g as well as by the aspect of function [illegible] .

Under unfavorable conditions (small value for C, large values for b and g) the temperature variation [illegible] in time will differ slightly from the temperature variation in the case of C=o (non-reacting gas). Under different conditions, beginning from a certain moment [illegible] , there takes place a very sharp increase of [illegible] as compared with the case of C=o, which corresponds to ignition.

The non-linearity of equation (9) engenders serious difficulties for the mathematical anlysis of ignition conditions. A numerical integration of this equation may yield results relating to particular

cases. In order to obtain general results, let us utilize quantitative investigation methods.

Investigation of Ignition Conditions

Without integrating equation (9) we analyze it using the method of graphical plotting of integral curves which gives a good general idea ~~of~~ about the nature of solutions. For this purpose we found the coordinate of the extremum points $(d\sigma/d\tau = 0)$ (~~n 18~~) and inflection points $(d^2\sigma/d\tau^2 = 0)$ (~~o 18~~) of integral curves according to equations:

$$Ce^{-\frac{h}{\sigma}} - \psi\sigma - g(\sigma - 1) = 0, \tag{10}$$

$$\left(C\frac{h}{\sigma^2}e^{-\frac{h}{\sigma}} - \psi - g\right)\frac{d\sigma}{d\tau} - \sigma\frac{d\psi}{d\tau} = 0. \tag{11}$$

Let us assume that the zero time reference $(\tau = 0)$ (~~e 18~~) is the moment for which $\varepsilon = 1$ $(T \text{ e. } V = V_{MAX})$ (~~f 18~~) ; then we have $\varepsilon - \varepsilon_{MAX}$ (~~g 18~~) with $\tau = \pi$ (~~h 18~~) and $\varepsilon = 1$ (~~i 18~~) with $\tau = 2\pi$ (~~j 18~~) .

If $C=\theta$ and $g=\theta$, equation (9) corresponds to the isentropic variation of the state of the gas. Integration of this equation ~~xxi~~ yields $\sigma_s = \varepsilon^{K-1}$ (~~k 18~~) . The corresponding integral curves $\sigma_s(\tau)$ (~~l 18~~) (isentropic curves) reach their extremum points $(\gamma = 0)$ (~~m 18~~) when $\tau = 0, \tau = \pi$ and $\tau = 2\pi$ (~~n 18~~) (with $\tau = 0$ (~~o 18~~) and $\tau = 2\pi$ (~~p 18~~) -minimum, with $\tau = \pi$ (~~q 18~~)

-maximum) and the inflection points with and .

With C=0 equation (9) corresponds to the variation of the state of non-reacting gas. In this case, integration of equation (9) yields approximately corresponding integral curves (curves of non-reacting gas) have their extremum points with , and their inflection points with . Compared with the preceding case (isentropic variation), all these points are shifted towards since condition yields , and condition yields . The shift is the greater, the greater the value for g in comparison with .

If (fuel gas) we find the coordinates of the extremum and inflection points of the unknown integral curves by solving equations (10) and (11) (assuming that the parameters C,b,g as well as are assigned.

Figure 2 shows the graphical method for the solution of equation written in the form of

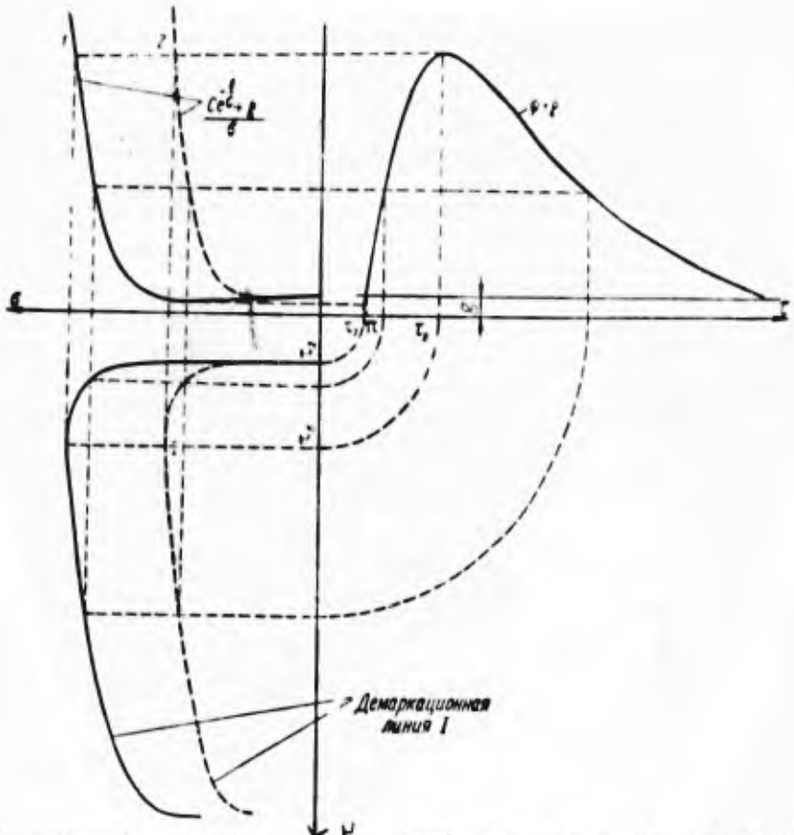

Fig .2. Graphical solution of equation (10). Curve 1 is plotted for b_1, curve 2 for b_2, $b_1 > b_2$. a-demarcation line I.

The graph shows the effect of the variation in the magnitude of the parameters on the value of the ordinate of the curve of extremum points (this curve will be called demarcation line I). With C increasing or b, ψ and g decreasing, σ_1 decreases and vice versa. These parameters exert a similar effect on the ordinates of the curve of inflection points (this curve will be called demarcation line II).

Let us note that with moderate values for the relative tempera-

ture σ (~~d 19~~) (i.e., the beginning of demarcations lines I and II) the abscissas of the points of demarcation lines I and II coincide with the abscissas of the extremum and inflection points of the non-reacting gas. This is explained by the exponential character of the dependence of the rate of the chemical reaction on ~~temperatur~~ temperature: at moderate and fairly low temperatures, the reaction rate is found to be actually equal to zero (although mathematically $W \neq 0$ (~~a 20~~)).

Demarcation line I divides the plane (b'20) into two parts: the integral curves within the area traced by demarcation line I have $d\sigma/d\tau < 0$ (~~b 20~~), and $d\sigma/d\tau > 0$ (~~c 20~~) outside of it.

Demarcation line II separates the area where $d^2\sigma/d\tau^2 < 0$ (~~d 20~~), i.e., the integral curves are convex upward; outside this area $d^2\sigma/d\tau^2 > 0$ (~~e 20~~) and, hence, the integral curves are concave with the trend upward.

If $\tau = \tau_B$ (~~f 20~~) then $d\psi/d\tau = 0$ (~~g 20~~), hence $\sigma_I = \sigma_{II}$ (~~h 20~~) here, i.e., demarcation lines I and II intersect $(d\sigma/d\tau = d^2\sigma/d\tau^2 = 0)$ (~~22 20~~). To the left of point B, demarcation line I is a curve of maximum point of the integral curve # $\sigma(\tau)$ (~~j 20~~) since $d^2\sigma/d\tau^2 < 0$ (~~k 20~~); to the right

of point B it becomes a curve of minimum points since here

$d^2\sigma/d\tau^2>0$

By solving equation $d^3\sigma/d\tau^3=0$ and plotting the corresponding curve against the plane $\sigma-\tau$, we find point A for which $d^2\sigma/d\tau^2=d^3\sigma/d\tau^3=0$. To the left of point A, demarcation line II is a curve of maximum points for the function $\sigma'(\tau)$ (since here $d^3\sigma/d\tau^3<0$); to the right of point A it becomes a curve of minimum points for the function $\sigma'(\tau)$ (since here $d^3\sigma/d\tau^3>0$).

Figures 3 to 5 show the draft $\sigma(\tau)$ against which are plotted the demarcation lines I and II as well as the curves $\sigma_H(\tau)$ for the non-reacting gas (dotted line). The relative position of these curves enables us to determine the conditions for ignition.

First of all we should point out the difference of conditions for the development of ignition with $\tau<\tau_2$ and with $\tau>\tau_2$.

If $\tau<\tau_2$, $d\sigma_H/d\tau>0$ or $[\gamma\sigma+q(\sigma-1)]<0$

i.e., the resulting exchange of energy between the non-reacting gas and the surrounding medium leads to an increase in temperature in the latter. Hence, with $\tau<\tau_2$ we shall always have $d\sigma_H/d\tau>Ce^{-\frac{b}{\sigma}}$

If $\tau > \tau_i$ (~~$\tau \geq 0$~~), $d\sigma_H/d\tau \leq 0$ (~~≤ 0~~), i.e., $[\psi_\sigma + g(\sigma-1)] > 0$ (~~≥ 0~~)

this means that the resulting exchange of the non-reacting gas with the surrounding medium leads to a decrease in the gas temperature (either because the relative heat transfer to the surrounding medium exceeds the mechanical work imparted to the gas by the surrounding medium, or because of the overall influence of the heat and mechanical work transferred from the gas to the surrounding medium). Hence it follows that with $\tau > \tau_i$ (~~$\tau \geq 0$~~) we have always $d\sigma/d\tau \leq (\tau \geq 0) C e^{-\frac{b}{\sigma}}$.

We show below that the ordinates of the special points A and B make it possible to fix the limits of the ignition sectors ~~with~~ in accordance with the transition cycle.

By dividing the time interval 2π (~~≥ 0~~) which corresponds to the period of variation of function ψ (~~≥ 0~~), taking account of the peculiarities mentioned above, we obtained four sectors with different ignition conditions.

Let us examine several characteristic cases of ignition cycle. Let us assume that the fuel mixture is formed at the instant $\tau = 0$ (~~≥ 0~~)

If C is small (Fig.3) demarcation lines I and II run above the

curve of the non-reacting gas, hence the integral curve $\sigma(\tau)$ which in sectors 1 and 2 practically coincides with the curve of the non-reacting gas, intersects demarcation line II (i.e., from concave it becomes convex) and further on, by meeting demarcation line I it bends downward. At the same time there occurs a slight increase in temperature $(\sigma - \sigma_H)$ owing to chemical reaction (heating) and ignition does not take place. The quantity of heat developed by the chemical reaction can be evaluated approximately by applying to the curve of the non-reacting gas at the borders of sectors 2 and 3 a tangent with a slope $tg\beta = \left(\frac{d\sigma}{d\tau}\right)_{\sigma_H} = Ce^{-\frac{b}{\sigma_H}} - q(\sigma_H - 1)$

With great values for C (Fig. 4) the relative position of the demarcation lines and the curve of the non-reacting gas change substantially; The integral curve runs above the demarcation line II, and at the end of sector 1, or in sector 2, there takes place a noticeable temperature increase from chemical reaction, and as a result of the progressive temperature increase and the reaction rate ignition takes place.

In the intermediate case (Fig. 5), the integral curves can fall into sector 3 in the area between demarcation lines I and II and, running between them with a relatively small temperature increase,

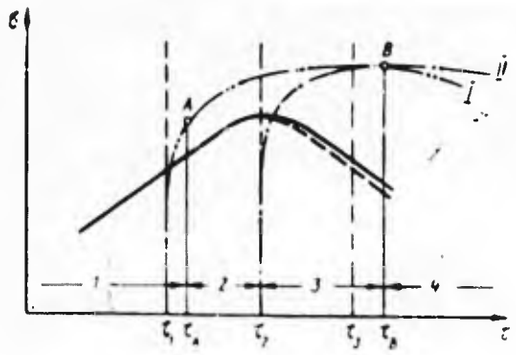

Fig. 3. Variation of relative temperature depending on dimensionless time (no ignition occurs). I and II demarcation lines.

intersects demarcation line II as a result of which an accelerated temperature increase will occur, i.e., ignition will take place, or intersect demarcation line I and turn downward (no ignition occurs).

Thus, $d^2\sigma/d\tau^2 = 0$ (~~d 21~~) is the condition for ignition in sector 3, while $d\sigma/d\tau = 0$ (~~e 21~~) is the condition for the absence of ignition.

Towards the end of sector 3 the converging points of demarcation line II (inflection points) and I (extremum points) yield a critical condition on the ignition boundary

$$\frac{d\sigma}{d\tau} = \frac{d^2\sigma}{d\tau^2} = 0. \qquad \text{(A 22)}$$

That the ignition boundary is at the end of sector 3 (provided the formation of the fuel mixture took place considerably earlier) results from the fact that in sector 4 demarcation line I becomes a

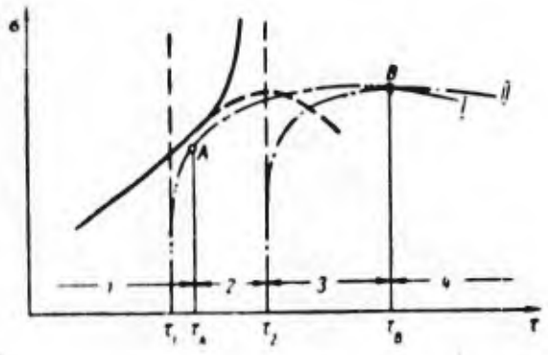

Fig. 4. Variations of relative temperature depending on dimensionless time (ignition takes place in sector 1). I and II demarcation lines.

curve of minimum points owing to which the condition for ignition is $d\sigma/d\tau = 0$ (a 22), hence the maximum temperature increase due to chemical reaction can be obtained no later than at the end of sector 3.

Let us set the threshold value for the temperature increase

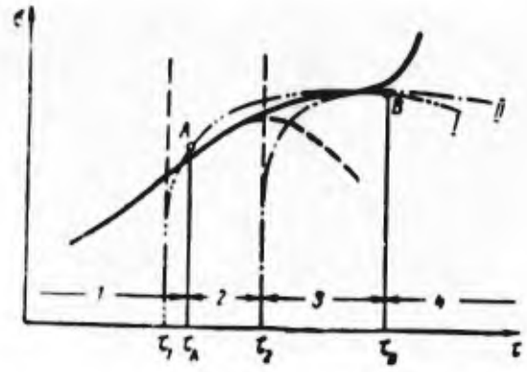

Fig. 5. Variation of relative temperature depending on dimensionless time (ignition takes place in sector 3). I and II-demarcation lines.

from chemical reaction on the ignition boundary. approximately this can be effected in the following way. Keeping in mind that owing to the exponential character of the temperature dependence of the reaction rate, a reaction at temperatures close to maximum under given conditions are of basic importance, let us take as a determinant the temperature θ_{γ} which corresponds to the moment τ_2.

The value for the temperature increase $(\sigma-\sigma_2)$ (b 23) is found from the conditions of tangency of the straight line drawn from the point (t_{23}, σ_2) (a 23) with a slope corresponding to $tg\beta=(d\sigma/d\tau)_{\sigma_2}$ (e 23), with demarcation line I.

We assume that the determining temperature $\sigma_2=\sigma_{H_2}$ (f 23) (maximum temperature of the non-reacting gas). In computing the threshold value for the temperature increase from reaction $(\sigma-\sigma_2)$ (g 23) we assume that g=0. This assumption does not exclude the possibility for further correlations for the ignition boundary, to take into consideration the heat transferred into the surrounding medium, i.e. consider $q>0$ (h 23).

Let us write the equation for the straight line under consideration as

$$\sigma=\sigma_{H2}+Ce^{-\frac{b}{\sigma_{H2}}(\tau-\tau_2)} \qquad \text{(A 23)}$$

or

$$\frac{\sigma-\sigma_{H2}}{Ce^{-\frac{b}{\sigma_{H2}}}}=\tau-\tau_2. \qquad \text{(B 23)}$$

The equation of demarcation line I, allowing for the linearization of function ψ (i 23), i.e., assuming $\psi=a(\tau-\tau_2)$ (j 23), where a is constant, can be written as

$$\frac{Ce^{-\frac{b}{\sigma}}}{a\sigma} = \tau - \tau_2. \qquad (C\ 23)$$

On the basis of the tangency condition of the lines under investigation, we obtain

$$\frac{\sigma - \sigma_{H2}}{Ce^{-\frac{b}{\sigma_{H2}}}} = \frac{Ce^{-\frac{b}{\sigma}}}{a\sigma} \qquad (12)$$

and

$$\frac{d}{d\sigma}\left(\frac{\sigma - \sigma_{H2}}{Ce^{-\frac{b}{\sigma_{H2}}}}\right) = \frac{d}{d\sigma}\left(\frac{Ce^{-\frac{b}{\sigma}}}{a\sigma}\right) \qquad (13)$$

or

$$\frac{1}{Ce^{-\frac{b}{\sigma_{H2}}}} = \frac{Ce^{-\frac{b}{\sigma}}}{a\sigma^2}\left(\frac{b}{\sigma} - 1\right). \qquad (13')$$

dividing (12) by (13') we find

$$\sigma - \sigma_{H2} = \frac{\sigma^2}{b - \sigma} \qquad (D\ 23)$$

or, considering that ~~$(\sigma - \sigma_{H2})$~~ $\sigma \ll b$, we obtain approximately

$$\sigma - \sigma_{H2} = \frac{\sigma_{H2}^2}{b}. \qquad (A\ 24)$$

thus, on the ignition boundary, the temperature increase from chemical reaction is approximately equal to σ_{H2}^2/b ~~$(b - \sigma_{H2})$~~. It can be shown by using the approximate expression for the exponent (3) that

$$e^{-\frac{b}{\sigma_{H2} + \frac{\sigma_{H2}^2}{b}}} = e^{-\frac{b}{\sigma_{H2}}} e, \qquad (B\ 24)$$

i.e., the temperature increase thus obtained causes the rate of the chemical reaction to increase by e times (the value σ^2/b ~~(σ_{H2})~~ will

be called the characteristic temperature interval).

Now the critical ignition condition $d\sigma/d\tau = 0$ (~~d 24~~), considering approximately that the ignition boundary corresponds to the end of sector 3 where $\psi = \psi_{MAX}$ (~~e 24~~) (since $\frac{d\psi}{d\tau} = 0$ (~~f 24~~)), can be written as

$$\frac{Ce^{-\frac{b}{\sigma_{M2}}}}{\psi_{max}\left(\sigma_{M2}+\frac{\sigma_{M2}^2}{b}\right)+g\left(\sigma_{M2}+\frac{\sigma_{M2}}{b}-1\right)} = \frac{1}{e}, \tag{14}$$

or, disregarding the temperature increase $\sigma^2_{H_2}/b$ (~~g 24~~) in the denominator, which introduces a negligible error,

$$\frac{\tau_p}{\tau_n} = e, \tag{15}$$

where $\tau_p = \frac{\frac{\sigma_{M2}^2}{b}}{Ce^{-\frac{b}{\sigma_{M2}}}}$ is the characteristic time of reaction, i.e., the time required for the temperature [redacted] of the gas (with no energy exchange with the surrounding medium) to increase by one characteristic interval from the chemical reaction occurring at an invariable rate which corresponds to the maximum temperature of the non-reacting gas;

$$\tau_n = \frac{\frac{\theta_{H2}^2}{b}}{\psi_{max}\theta_{H2} + g(\theta_{H2} - 1)}$$

the characteristic time of losses, i.e; the time required for lowering the gas temperature (with no chemical reaction) by one characteristic interval owing to an exchange of energy with the surrounding medium which takes place at an invariable rate corresponding to the maximum temperature of the non-reacting gas and the maximum value of ψ (~~3-24~~) .

From expression (15) it ensues that on the ignition boundary the characteristic reaction time is at a constant ratio to the characteristic time of losses; ignition occurs only if the characteristic reaction time does not exceed by more than e-times the characteristic ~~xxx~~ time of losses.

Equation (14) connects all the parameters and variables on the boundary of ignition. In particular, with the assigned values $\psi_{MAX.}$ (~~a-25~~) , g, C and b it is possible to determine the critical value of temperature ~~θ_H~~ θ_{H2} (~~b-25~~) , below which ignition turns out to be impossible:

$$\sigma_{H2} = \frac{b}{1 + \ln C - \ln|\psi_{max}\sigma_{H2} + g(\sigma_{H2} - 1)|} . \qquad (A\ 25)$$

Let us point out the "logarithmic" connection between temperature σ_{H2} and the relative activation energy b on the one hand, and the remaining parameters on the other. For this reason, a "logarithmic" accuracy in the estimation of the value for the latter will be sufficient: in particular, without noticeable errors, it is possible to disregard the temperature increase σ_H^2/b in the denominator of the expression (14), as this is the case with formula (15).

Taking the value σ^2_H/b as assigned, it is possible to find the critical value for b (with assigned C, ψ_{MAX} and g,) or C (with assigned b ψ_{MAX} and g), etc., from equation (14); it is also possible to establish the connection between the various parameters on the boundary of ignition, etc.

In the case of ignition taking place in the container V=const, i.e., with no energy exchange in the form of mechanical works, assuming $\psi = 0$ and $\sigma_{H_2} = 1$ (*), we obtain from equation (14)

$$qde^{-b}e = g\frac{1}{b} \qquad (B\ 25)$$

(*) in the case under investigation of the absence of energy exchange in the form of mechanical work, the moment τ_2 corresponds to the initial moment, hence $\sigma_{H2} = 1$.

or, introducing the time for complete combustion at a constant reaction rate, corresponding to the initial temperature, $\tau_r = 1/de^{-b}$

and the time of thermal relaxation (decrease in the difference of gas and container wall temperatures by e times during cooling) $\tau_c = 1/g$, we find

$$\frac{\tau_c}{\tau_r} = \frac{de^{-b}}{g} \approx \frac{1}{bqe}. \qquad (C\ 25)$$

The critical ignition condition was found in this form by O. M. Todes (2) by analyzing the equation for the heat balance for the reacting gas enclosed in a container at V=const.

Ignition Conditions at Sectors 1 and 2.

Let us investigate the ignition conditions at sectors 1 and 2 keeping in mind as before that the fuel mixture is formed at the instant $\tau = 0$.

In these sectors $d\sigma_u/d\tau > 0$, i.e., there takes place a supply of energy (in the form of mechanical work) to the gas from the surrounding medium owing to which the demarcation line I is absent (equation $d\sigma/d\tau = 0$ has no roots). In most of sector 1, the condition $d^2\sigma/d\tau^2 > 0$ is also satisfied; only at the end of this sector does the demarcation line II make its appearance. Here

it represents a curve of maximum points of the function $\sigma'(\tau)$.

If in sector 1 the integral curve intersects demarcation line II, it changes its direction of convexity and the increase in temperature is slowed down. For this reason, ignition in sector 1 is possible only if $d^2\sigma/d\tau^2 > 0$, i.e., the integral curves run above demarcation line II.

In sector 2, demarcation line II represents a curve of minimum points of the function $\sigma'(\tau)$. If the integral curve which in sector 1 was found to be below demarcation line II, intersects the latter in sector 2, the process of temperature increase is accelerated owing to the heat evolved by the chemical reaction, and ignition does take place. Hence, ignition condition for sector 2 is $d^2\sigma/d\tau^2 = 0$.

Let us note that in sectors 1 and 2 where we have always $d\sigma/d\tau > 0$, a sizeable temperature increase owing to the chemical reaction will only take place immediately before ignition (see below). For this reason the possibilities of ignition in sectors 1 and 2 can be determined by examining the relative position of the curve for the non-reacting gas (with which the integral curve coincides almost until the very moment of actual ignition) and demarcation line II.

The ignition process in sectors 1 and 2 can be observed in more detail by utilizing the method of successive approximations:

1) First we find $\sigma(\tau)$, taking into consideration only the reaction rate owing to the change in temperature of the non-reacting gas, and disregarding the variation in the reaction rate connected with the temperature increase due to the heat developed by the chemical reaction;

2) Then we investigate the accelerating effect of $\sigma(\tau)$ on the development of the chemical reaction and, hence, ignition.

Assuming that $\sigma = \sigma_H + \Delta\sigma$, we can write equation (9) in the following way:

$$\frac{d\sigma}{d\tau} = Ce^{-\frac{b}{\sigma_H+\Delta\sigma}} - \psi(\sigma_H+\Delta\sigma) - g[(\sigma_H+\Delta\sigma)-1]. \tag{16}$$

here, $\Delta\sigma$ is the temperature increase ensuing from the heat developed by the chemical reaction and the increase in relative mechanical work and relative heat removal connected with it:

$$\frac{d\sigma}{d\tau} = \frac{d\sigma_H}{d\tau} + \frac{d(\Delta\sigma)}{d\tau}. \tag{A 26}$$

If $\Delta\sigma$ is small in comparison with σ_H, as this is the case during the initial stage of ignition, we can disregard the temperature variation ensuing from the increase in relative mechanical work

and relative heat removal, i.e., we can assume that $\psi \Delta\sigma = 0$ (a 27) and $\Delta\sigma = 0^{*}$ (b 27) (x). Then we obtain from equation (16)

$$\frac{d\sigma}{d\tau} = Ce^{-\frac{b}{\sigma_H + \Delta\sigma}} + \frac{d\sigma_H}{d\tau} \qquad \text{A 27}$$

or

$$\frac{d(\Delta\sigma)}{d\tau} = Ce^{-\frac{b}{\sigma_H + \Delta\sigma}}. \qquad \text{B 27}$$

using approximate expansion of the exponent we find

$$\frac{d(\Delta\sigma)}{d\tau} = Ce^{-\frac{b}{\sigma_H}} e^{\frac{\Delta\sigma b}{\sigma_H^2}}. \qquad (16')$$

By integrating equation (16') with the boundary conditions

$\Delta\sigma = 0$ (c 27) with $\tau = 0,\ \Delta\sigma \to \infty$ (d 27) with $\tau = \tau_{i_{0N}}$ (e 27) (ignition (1)),

we obtain approximately

$$\int_0^{\infty} e^{-\frac{\Delta\sigma b}{\sigma_H^2}} d(\Delta\sigma) \approx \frac{\sigma_H^2}{b} \approx C \int_0^{i_{0N}} e^{-\frac{b}{\sigma_H}} d\tau. \qquad (17)$$

Thus, the temperature increase of the gas due to chemical reaction cannot exceed the quantity σ_H^2/b (f 27) without ignition not taking place.

(x) Let us note that in sectors 1 and 2, ψ (h 27) and g have different signs; this reduces the error associated with the assumption under investigation.

(1) The ignition condition, provided one does not take into account the variation of concentration, can be represented as (i 27) $\Delta\sigma \to \infty$.

The time of development of the ignition process as a whole is basically determined by the time required for the temperature to increase by one characteristic interval as a consequence of chemical reaction. The inverse effect of the development process of the reaction on the original process of its excitation (in the given case, temperature increase of the gas following its compression) leads to a substantial increase in the reaction rate which, during the transition cycle of ignition, is generally small.

For sector 1, the condition under which the interval curve $\sigma(\tau)$ begins to deviate from the curve of the non-reacting gas can be written as

$$\frac{d}{d\sigma}\left(Ce^{-\frac{b}{\sigma}}\right) \geqslant \frac{d}{d\sigma}\left[-\psi\sigma - g(\sigma-1)\right] \tag{C 27}$$

or

$$\frac{b}{\sigma^2} Ce^{-\frac{b}{\sigma}} \geqslant -(\psi+g). \tag{D 27}$$

By introducing the characteristic time of reaction τ_p, we obtain

$$\tau_p \leqslant \frac{1}{-(\psi+g)}. \tag{18}$$

Expression (18) can be regarded as the condition for the ignition on sector 1; it is similar to expression (17).

On the Delay Period of Ignition

From the investigation conducted it ensues that, depending on the magnitude of the parameters C, b and g as well as the function ψ, ignition takes place at a given instant of dimensionless time, i.e., at a specific phase of function ψ.

The shift of the instant of fuel mixture formation, i.e., $\tau_{cM} > 0$, does not effect the ignition instant as long as τ_{cM} falls into an area where $Ce^{-\frac{b}{\sigma}}$ is very small. We can assume that this will be the case as long as $Ce^{-\frac{b}{\sigma}} \leq \sigma^2/b$, where σ^2/b is the characteristic value for the temperature variation during ignition; the latter inequation is equivalent to the condition for $\tau_p \gg 1$ - the time for a temperature increase due to chemical reaction by one characteristic interval is greater compared to a unit of dimensionless time.

For this reason, the "previous history" of the fuel mixture becomes important only from a certain instant on.

In sectors 1 and 2 where $d\sigma/d\tau > 0$ the chemical reaction becomes "perceptible" and its consideration becomes necessary only immediately before the beginning of ignition. This is explained by the exponential character of the dependence of the

reaction rate on temperature as well as by the peculiar characteristics in these sectors of the conditions of the inverse effect of the reaction development on the original process of its exitation.

If ignition occurs in sector 3, the importance of the previous history of the fuel mixture was found to be more considerable. In order to realize critical conditions corresponding to the ignition boundary (as the end of sector 3) , it is necessary that the fuel mixture be formed in sector 2 ($T_{CM} < T_i$) and the ignition process begin with an increasing temperature of the non-reacting gas (and, accordingly , with increasing pressure). At the same time here, too, the displacement of the moment of fuel mixture formation within wide limits covering sector 1 and a considerable part of sector 2, will have no effect on the ignition conditions. Yet, if the fuel mixture formation takes place in sector 3 ($T_{CM} > T_i$) , following which the ignition process will start with a decreasing temperature of the non-reacting gas (and, hence, with decreasing pressure), then ignition conditions deteriorate abruptly. In this case, in order to ensuure ignition, a considerable increase in C or a decrease of b, etc., as compared with the preceding case, will be required.

In connection therewith, the concept of a delay period of ignition (induction period) as a period during which development of the ignition process takes place, becomes quite conditional. An even greater discrepancy between the concept of a delay period of ignition and the actual physical value of the corresponding time interval was found in those cases (frequently encountered when investigating piston engines with injection of liquid fuel) where the fuel mixture is formed later than the possible instant of ignition. Under these conditions, the quantity (delayed ignition) determined experimentally characterizes mainly the time required for the formation of fuel mixture rather than the time of development of the ignition cycle.

Keeping in mind the considerable significance of the magnitude of the delay of ignition when applying it to combustion in engines, it is necessary in each actual case to determine the physical value attributed to this concept.

The Shape of [redacted] (Kinetic) Ignition Curves

In the table below are summarized the conditions under which ignition occurs and those under which ignition does not occur in the sectors 1 to 4.

TABLE (page 29)

1.	2.		5.
	3.	4.	
1	$\frac{d^2\sigma}{d\tau^2} > 0$	$\frac{d^2\sigma}{d\tau^2} = 0$	
2	$\frac{d^2\sigma}{d\tau^2} = 0$	$\frac{d^2\sigma}{d\tau^2} < 0$	
3	$\frac{d^2\sigma}{d\tau^2} = 0$	$\frac{d\sigma}{d\tau} = 0$	Критические условия воспламенения в конце участка 3 (граница воспламенения): $\frac{d^2\sigma}{d\tau^2} = \frac{d\sigma}{d\tau} = 0$
4	$\frac{d\sigma}{d\tau} = 0$	$\frac{d\sigma}{d\tau} < 0$	Необходимое условие воспламенения на участке 4: $\tau_{см} > \tau_B$

1) Sector 2) Ignition 3) Occurs 4) Does not occur 5) Remarks

6) Critical ignition conditions at the end of sector 3 (ignition boundary); 7) Essential condition for ignition in sector 4:

When intersecting certain particular points on the demarcation lines (points A and B) the conditions under which ignition does not take place change into such under which ignition does occur.

When crossing the boundary between sectors 2 and 3 the condition under which ignition does take place remains unchanged, but the change of the sign of the overall energy exchange leads to a

substantial change in the conditions of the inverse effect of the reaction development process on the ignition cycle.

If the fuel mixture contained in the container of permanent exchange is ignited, we have a relationship $\frac{d\sigma}{d\tau} < Ce^{-\frac{b}{\sigma}}$, and only for the ideal boundary case (g=0) (x) we obtain $\frac{d\sigma}{d\tau} = Ce^{-\frac{b}{\sigma}}$.

When computing the interaction of the reactant with the surrounding medium in the form of heat transfer and performance of mechanical work, which is the more general case, it was found that there exist two different cycles of ignition:

$$1.\ \frac{d\sigma}{d\tau} > Ce^{-\frac{b}{\sigma}}, \qquad 2.\ \frac{d\sigma}{d\tau} < Ce^{-\frac{b}{\sigma}}. \tag{A 30}$$

Thus, computation of mechanical interaction leads to the establishment of new regularities in the development of the ignition process, and in particular, of various shapes of tangents (kinetic) ignition curves.

If ignition takes place in sector 1, the cycle proceeds more

(x) It is assumed that the container wall temperature does not exceed the initial temperature of the fuel mixture.

rapidly since $\frac{d\sigma}{d\tau} > Ce^{-\frac{b}{\sigma}}$ ($\sigma \to 0$) and $\frac{d^2\sigma}{d\tau^2} > \frac{d}{d\tau} Ce^{-\frac{b}{\sigma}}$ ($\frac{d\sigma}{d\tau} \to 0$).

At the same time, on the curves $\sigma(\tau)$ ($\sigma \to 0$) and $\sigma'(\tau)$ ($\sigma' \to 0$) there appears no initial phase inhibiting the cycle (Fig. 6).

In sector 2, the ignition cycle is characterized by the relationships $\frac{d\sigma}{d\tau} > Ce^{-\frac{b}{\sigma}}$ ($\sigma \to 0$) and $\frac{d^2\sigma}{d\tau^2} < \frac{d}{d\tau} Ce^{-\frac{b}{\sigma}}$ ($\frac{d\sigma}{d\tau} \to 0$); on curve $\sigma(\tau)$ ($\sigma \to 0$) and especially on curve $\sigma'(\tau)$ ($\sigma' \to 0$) there appears the initial inhibiting phase (Fig. 7).

In sector 3, the ignition process is retarded since $\frac{d\sigma}{d\tau} < Ce^{-\frac{b}{\sigma}}$ ($\sigma \to 0$); at the same time, on the curves $\sigma(\tau)$ ($\sigma \to 0$) and $\sigma'(\tau)$ ($\sigma' \to 0$) there clearly appears the initial inhibiting phase (Fig.8).

Under conditions below the ignition boundary (but close to it) curves $\sigma(\tau)$ ($\sigma \to 0$) and $\sigma'(\tau)$ ($\sigma \to 0$), if $\tau \geq \tau_i$ ($\sigma \to 0$), somewhat depart from the corresponding curves of the non-reacting gas owing to heatup from the chemical reaction.

The above characteristics of the transient (kinetic) ignition curves in various sectors become apparent with particular sharpness with the coordinates (p, τ) ($\sigma \to 0$) and $(d\rho/d\tau, \tau)$ ($\sigma \to 0$).

The results obtained are evidence of the significant effect borne by the sign of the overall energy exchange on the conditions

of the inverse effect of the reaction development process on the initial process of its excitation.

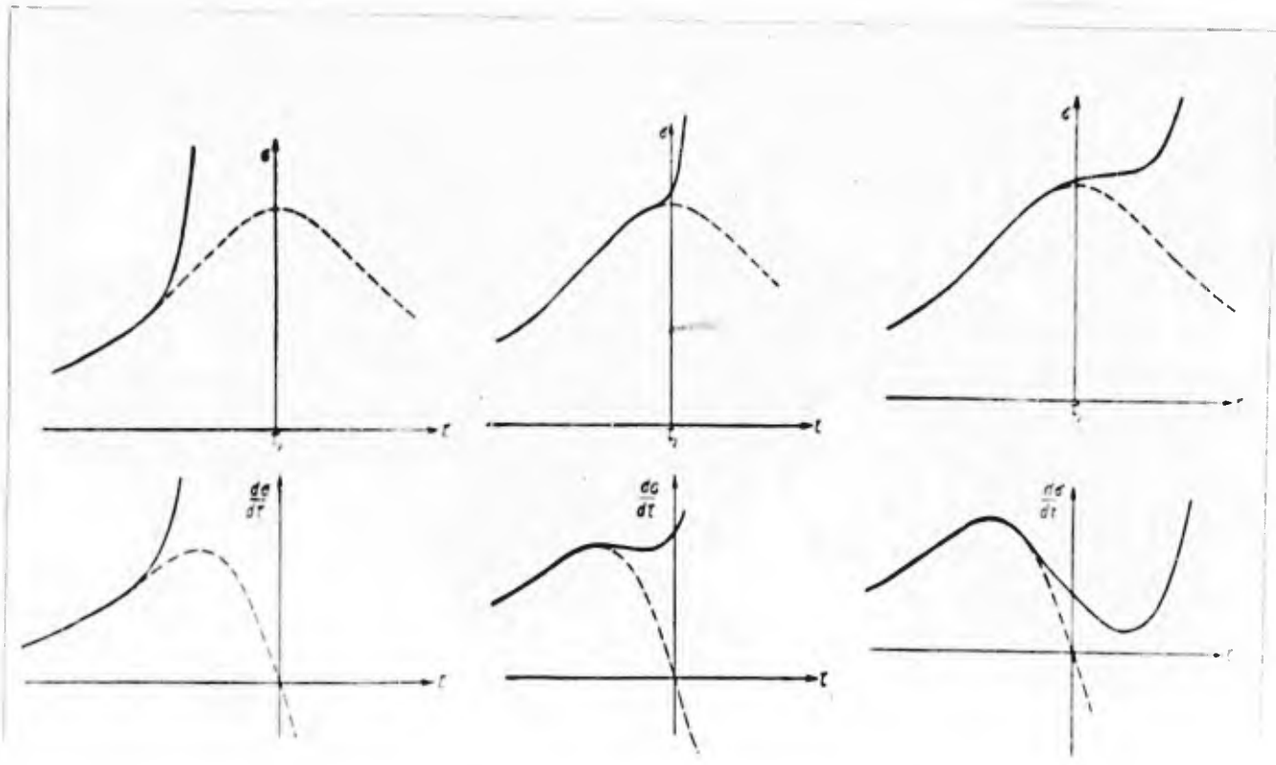

Fig.6. Transient (Kinetic) curves if ignition takes place in sector 1.

Fig.7.Transient (kinetic) curves if ignition takes place in sector 2.

Fig.8.Transient (kinetic) curves if ignition takes place in sector 3.

During ignition, the develoment of the process is inhibited by the initial phase. If ignition begins with an increasing temperature (pressure) of the non-reacting gas, in that temperature range

where the reaction rate is relatively low and the temperature increase due to the latter is slow, an accelerated temperature increase is insured by means of performing work with the surrounding medium on the reactant. In so doing, the conditions of the inverse effect of the reaction develoment process on the ignition cycle are most favorable.

If, on the contrary, ignition is started at dropping temperatures (pressure), then in the temperature range where the reaction rate is relatively low and the temperature increase due to the latter is slow, there occurs an additional delay in the temperature increase owing to the exchange of energy between the reactant and the surrounding medium, and the conditions of the inverse effect of the reaction development process on the ignition process are found to be extremely unfavorable. This leads to an elongation of the transient (kinetic) ignition curves or to the cessation of ignition at the stage of preflame reactions. These characteristics of the transient ignition curves were occasionally attributed (without sufficient foundation) to the multistage ignition cycle with various procedures of chemical reaction, whereas actually they result from the change in the ignition development cycle

under the effect of energy exchange between the reactant and the surrounding medium with an invariable mechanism of chemical reaction. Depending on the sign and the intensity of energy exchange between the reactant and the surrounding medium, the initial stage of the ignition process can proceed in an accelerated fashion, be protracted or, if conditions are unfavorable, completely discontinued.

The varying character of transient (kinetic) ignition curves under conditions of increasing and decreasing pressure can have an extreme bearing upon the transition of combustion into detonation.

2. EXPERIMENTAL INVESTIGATION OF IGNITION PROCESSES WITH VARIOUS FORMS OF ENERGY EXCHANGE

The experimental study of ignition processes and the determination of inhibiting quantities with varying temperatures and pressures is carried out by various methods, in particular, in rapid compression installations (6). Here, a fuel gas and air mixture prepared beforehand is rapidly compressed and the value for inhibition is determined as the time interval from the end of compression to the beginning of a rapid increase in pressure (or to the instant when

maximum pressure is obtained). In this case, the "previous history" of the fuel mixture (during compression) is not taken into consideration. The theory mentioned above, taking into consideration that $\psi = 0$ (~~a-33~~) with $\tau \geq \pi$ (~~b-33~~), can be applied to rapid compression installations. The reason for the discrepancies between experimental data obtained at various installations for one and the same fuel under identical initial and final conditions, is to be sought in the development of ignition already during the process of compression. The shorter the measured magnitude of the delay period, the greater the error resulting from neglecting the chemical reaction during compression and the increase in the temperature of the fuel gas mixture resulting from it. The longer the compression time (especially at the end of compression) the shorter the measured time of delay, all other conditions being equal.

At high temperatures and pressures, the time of delay at rapid compression installations equals zero or is negative, i.e., the error resulting from neglecting the "history" of the gas fuel mixture during the compression period leads to a complete distortion of the physical picture of the phenomenon.

The relationships cited above make it possible to evaluate

the possible magnitudes of similar errors and thus to outline the field of experimental investigation where, at the given rapid compression installation, sufficiently correct results are obtainable.

Tests undertaken at installations for rapid compression-expansion are also of great interest for the study of general regularities ruling ignition at thermal and mechanical interaction between the reacting system and the surrounding medium as well as their application to combustion in piston and other types of engines. Such tests were performed by the author at an installation designed on the basis of a four-cycle, single-cylinder, small-displacement (approximately 0.6 l) engine with variable compression and injection of fuel into the combustion chamber through a cycle. Utilization of an electric motor-generator for the starting and braking of the installation insured that the tests were performed with a constant number of rotations. Pressure and the rate of pressure change in the combustion chamber were recorded with the aid of a MAI (indicator) with a piezoquartz data unit and a cathod oscillograph. In a number of tests we used a stroboscopic electrocontact indicator. The analysis of transient (kinetic) ignition curves was facilitated by the presence on the charts of lines corresponding to the cycle without fuel

injection. The tests were carried out with various fuels (kerosene, gasoline, diesel fuel, diethyl ether, etc.).

The results obtained confirmed the conclusions drawn from theoretical investigations. In particular, the tests carried out with various types of fuels showed that the specific features of transient (kinetic) ignition curves are associated with the sign and intensity of the energy exchange between the reacting system and the surrounding medium. The "two-stage" character of transient curves was always observed in charts $p = \varphi$ (c 23) in the case of ignition in sector 3 (see Fig. 5), i.e., when the combustion chamber volume was increased (Fig. 9), and in charts $dp/d\varphi - \varphi$ (c 34) when ignition occurred in sector 2 (Fig. 10). The conditions for a development of ignition deteriorate sharply if the pressure drops. For this reason a displacement of the moment of gas fuel formation towards the end of sector 2 (by decreasing the injection angle of the fuel into the combustion chamber) brings ignition to a stop. If ignition takes place under conditions of a decreasing combustion chamber volume, we observe an abrupt increase in the rate of pressure increase accompanied by splutter.

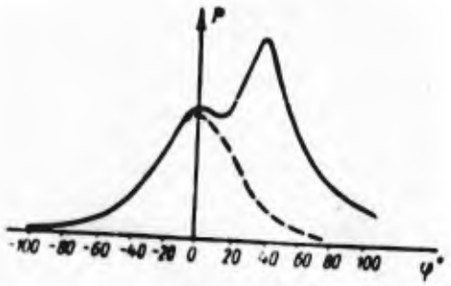

Fig. 9. Pressure oscillogram in combustion chambers. Installation for rapid compression-expansion $\varepsilon = 10$ (b 24), n=900 revolutions per minute).

In certain tests (7), (8), performed at installations for rapid compression-expansion, the presence of a two-stage ignition with varying mechanisms of chemical reaction is determined mainly on the basis of pressure diagrams as well as emanation registrations. This approach, however, has to be regarded as lacking sufficient foundations from the viewpoint of methodical research.

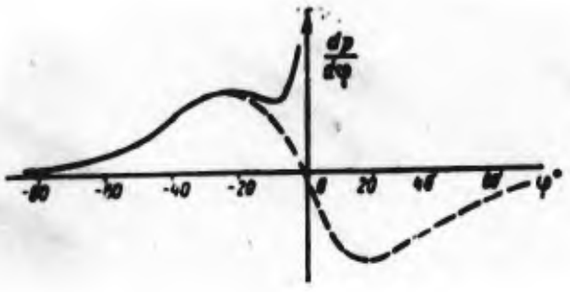

Fig. 10. Oscillogram of the rate of pressure variation in combustion chambers. Installations for rapid compression-expansion ($\varepsilon = 10$ ~~$\varepsilon = 34$~~

n=900 revolutions per minute).

3. MATHEMATICAL SIMULATION OF IGNITION PROCESSES

The application of modern methods of mathematical simulation, based on continuous-performance electronic devices (9), to the solution of equations determining ignition cycles makes it possible, with a minimum loss of time, to obtain results for a wide range of values for the initial parameters.

In an initial investigation, the author together with B.Ya. Kogan solved the problem under investigation with regard to the conditions existing in an installation for rapid compression-expansion.

In solving equation (9) on a simulating installation, the function $\psi = (\kappa-1)\frac{d\ln V}{d\tau}$ (a 35) was computed in correlation for a crank shaft mechanism;

$$\frac{d\ln V}{d\tau} = \frac{-\sin\tau + \frac{\lambda}{2}\sin 2\tau}{\frac{\varepsilon_{max}+1}{\varepsilon_{max}-1} + \cos\tau + \frac{\lambda}{4}(1-\cos 2\tau)}. \qquad \text{A 35}$$

with the aid of the Nusselt fromula for the α coefficient of heat transfer from the gas to the conduction chamber walls $\alpha = \text{const}\,\tau\sqrt[3]{\rho^2\tau}$ (b 35) the last term on the right side of equation (9) was obtained approximately in the form of $C_1\sigma(\sigma-1)$ (c 35).

In solving the problem, the time was chosen in such a way that during simulation the cycles proceeding proceeded with a frequency comprised in the transmission band of the solver units.

In accordance with this, the unit of dimensionless time (representing the characteristic time of the simulated cycle) corresponded to 2.5 sec. By introducing the time $t_m = \frac{1}{m}t$ (d 35) (where m=0.4) and taking into consideration the above expression for the

last term, we obtain an equation, subject to being solved by the simulating installation, in the form of

$$\frac{d\sigma}{dt_m} = mC_1 e^{-\frac{\sigma}{\sigma}} - m\varphi_3 - mC_3\sigma(\sigma - 1) \tag{19}$$

(initial conditions: $\sigma(0) = 1$ (~~$\sigma = 35$~~)).

The greatest difficulties in simulating arouse in connection with the reproduct reproduction of the first term (the exponential term) of the right side of equation (19). We used two functional devices connected in series, of which one was designed according to the scheme of simulation of the neutral zone, and the other had diode elements on the basis of piecewise linear approximations. The great steepness of the characteristic of the dependence under investigation required additional measures by which to reduce it. Yet, the accuracy of reproduction of the exponential term was found to be insufficient. In spite of the shortcomings mentioned above, however, the results obtained have a specific interest. Figures 11 and 12 show the oscillogram of the solutions.

Mathematical simulation may turn out to be extremely useful for the determination of numerical values for the kinetic parameters

(E, K and n) on the basis of test results of experimental installations. Electronic solver devices make it possible to render more complex the initial equations by introducing reactions of the second order, computation of burnout, etc.

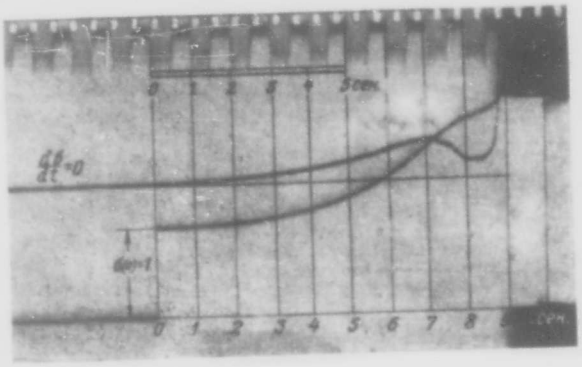

Fig. 11. Simulation of the ignition process in an installation for rapid compression-expansion. Oscillogram of the solution of equation (19) with the following parameter values: b=40, $mC_1 = 3.8 \times 10^7$, $\varepsilon_{max} = 8$ (~~=96~~), $mC_2 = 0.01$.

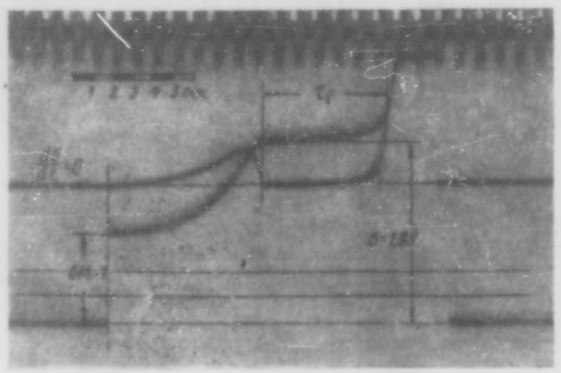

Fig. 12. Simulation of the ignition process in an installation for rapid compression. Oscillogram of the solution of equation (19) when $\psi = 0$ (a-36) with $\tau \geq \pi$ (b-36) ($b=80$, $mC_1 = 1.5 \times 10^{15}$, $\varepsilon_{max} = 8$ (c-36), $mC_2 = 0.005$).

Simulation of ignition processes makes it possible to determine the effect of the instant of fuel mixture formation (forcing τ_{CH} (a-37) to run through the values from $\tau = 0$ (b-37) to $\tau = \tau_2$ (c-37)), the effect of the variation in the magnitude of relative heat removal, the effect of the variation in the frequency of function ψ (d-37), etc., on the ignition cycle.

Simulation methods can readily reproduce the ignition conditions in a rapid compression installation by introducing the condition $\psi = 0$ (~~e 37~~) with $\tau \geq \pi$ (~~f 37~~) (Fig.12) or in the cylinder of a piston engine with shut-off valves in order to explain the behavior of the fuel mixture below the ignition boundary with several successive cycles of compression-expansion; it is possible to simulate the ignition cycle of a fuel mixture by compressing it with a moving flame front, and with a varying combustion chamber volume (with respect to conditions existing in combustion chambers of piston engines with spark ignition), the ignition cycle in an impact fuze, etc. In many cases such investigations ("mathematical experiments") can be helpful in executing physical experiments, reduce their volume, and, after exhaustive study of the phenomena under investigation, replace the physical experiments.

4. ON IGNITION CYCLES IN ENGINES

Piston Engines

The results of the theoretical investigation expounded above can be applied directly to piston engines.

The problem of ignition conditions and the character of transition cycles when the fuel mixture ignites in front of the

flame is of great interest for engines with spark ignition in connection with the problem of knocks (detonation). Experiments have shown that engine knocks are connected with ignition of the fuel mixture in front of the flame. Apparently, knocks depend on the rate of ignition development, which, in turn, depends on the initial temperature and pressure of the fuel mixture in front of the flame as well as the rate of change in its volume owing to the movement of the piston and the expansion of combustion products. The accumulation of all these factors and their complex interrelation render difficult the study of the problem under investigation.

The application of mathematical simulation methods to the solution of the ignition equation for the case under investigation with varying initial values for the temperature and pressure of the fuel mixture, varying conditions corresponding to the change in the advance sparking angle, the rate of flame travel, the flame area, etc., can yield data with which to determine the part played by the various factors in the formation of knocks. For this purpose, it is convenient to use equation (8') as the initial equation, with $p=f(V,x)$ where $V(t)$ is the combustion chamber volume, and $x(t)$ is the

portion of burntout fuel mixture (with respect to its mass). Hence

$$\frac{dp}{dt} = \left(\frac{\partial p}{\partial V}\right)_x \frac{dV}{dt} + \left(\frac{\partial p}{dx}\right)_V \frac{dx}{dt}, \qquad \text{(A 37)}$$

and since

$$\left(\frac{\partial p}{\partial V}\right)_x = -k\frac{p}{V}, \qquad \text{(A 38)}$$

then

$$\frac{1}{p}\frac{dp}{dt} = -k\frac{d\ln V}{dt} + \frac{1}{p}\left(\frac{\partial p}{\partial x}\right)_V \frac{\partial x}{dt}. \qquad \text{(B 38)}$$

In this equation the first term depends on the compression degree (ε) (a 38) and the position of the piston with respect to VMT;; the second term, approximately equalling $\frac{F_{fl} u_{fl} q}{V(1+xq)^{\frac{k-1}{k}}}$ (B 38) depends on the thermal characteristic of the fuel mixture (q), the rate of flame travel (u_{fl}) and its surface (F_{fl}).

Let us point out, as one of the possible systems, the following mechanism for the formation of a detonation wave in the fuel mixture in front of the flame.

The ignition cyclex spreads in the fuel mixture whose density increases owing to the movement of the piston and the expansion of combustion products ~~of~~ in the flame front. We mentioned earlier that the pressure and temperature of the fuel mixture when it changes volume, will change uniformly at any point of the latter provided a

specific condition is met which can be represented as the relationships

$$t' \gg \frac{l}{c} \qquad (6.58)$$

where t' is the magnitude of the time interval during which the pressure of the fuel mixture undergoes a noticeable change;

l is the characteristic linear dimension of the system under investigation;

c is the velocity of sound in the gas located in front of the flame.

The meaning of this relationship is as follows: the time during which a sound signal covers the distance l is short in comparison with the time t' during which there occurs a sizable change in the fuel mixture pressure owing to the reduction of its volume.

If this condition is not satisfied, then, when the volume of the fuel mixture is reduced, there must arise in it a shock wave which travels at a given velocity. A chemical reaction wave will be traveling in the mixture at the same velocity (assuming that the fuel mixture is in a state of chemical activity, i.e., the reaction rate referred

to a unit of dimensionless time is "perceptible"). The heat released by the chemical reaction is supporting and increasing the pressure wave.

The rate of propagation of such quasi-detonation waves may be considerably less than the rate of normal detonation owing to the fact that there takes place in them a partial release of chemical energy.

Estimates show that the above relationship may or may not be fulfilled in the combustion chamber of an engine depending on its operating conditions.

In the case of engines with compression ignition, liquid fuel is injected into the combustion chamber. The cycle of fuel mixture formation (evaporation of fuel drops and intermixing of the vapors with air) takes up a specific time interval. For this reason, the moment of the actual formation of the fuel mixture is displaced with respect to the moment of liquid fuel injection. In such engines there may be a considerable inhomogoneity of the fuel mixture composition with regard to the chamber, and there may take place a variation of this composition in time. In connection therewith,

the assumptions adopted in the present investigation, represent a threshold idealization if applied to engines with injection of liquid fuel. It was found, nevertheless, that the application of the results obtained to the ignition cycle of such engines is quite useful.

By analyzing the critical ignition conditions for (equation(14)) it becomes possible to determine the basic factors which affect ignition and to establish, their mutual relationship. The calculated dependences are in agreement with experimental data.

The problem of "knocks" in engines resulting from compression ignition is closely associated with the peculiarities of transient (kinetic) ignition curves.

A thorough study of the ignition cycle may also be useful for the solution of problems relating to the selection and competitive experiments of fuel for high-power engines.

Jet Engines

These engines are started by means of self-igniting fuels on the basis of nitric acid. When certain compounds (aromatic and aliphatic amines, polyatomic phenols, etc.) are in contact with concentrated nitric acids (or compounds of nitric acid and nictric oxides) at normal

or below normal temperatures, they react rapidly and ignite. As self-igniting fuels for fuels on the basis of nitric acid we used dimethyl hydrazine, a mixture of furfuryl alcohol (70%) and aniline (30%), a mixture of triethylamine (50%) and xylidine (50%), etc.

At the present time there is available a vast amount of experimental data on the ignition of such fuels. These data are reviewed in Ya. M. Paushkin's (10) book.

It is interesting to investigate the complex cycle of ignition of the fluid components from the point of view of the heat theory, without dwelling on the chemical aspect of the problem.

Schematically, we can single out the following two fundamental stages during ignition:

1) The stage of chemical reaction in the liquid phase,

2) the stage of chemical reaction in the gaseous phase.

At normal and below normal temperatures, the chemical reaction in the liquid phase takes place at high rates. High reactance of the liquid phase is the basic property of substances used as

self-igniting components. These components cannot be intermixed, and reaction occurs basically on the boundary between them. The great density of the substance in the liquid state is one of the causes for the high rate of reaction.

Reaction in the liquid phase is accompanied by the liberation of heat, formation of intermediate oxidation products (partly in the solid state) heating and evaporation of a part of the initial components. Under the conditions existing in the combustion chamber of an engine, the size of the interface of components where the chemical reaction in the liquid phase takes place and, hence, the quantity of the vapor-gas mixture formed during a time unit, depends greatly upon the cycles of injection and spraying of the components, in particular, on the type, number and position of the spray nozzles, the diff pressure differential on them, viscosity and xmrfxnexxtxnx surface tension of the liquid, the pressure inside the combustion chamber, etc.. Under constant conditions of injection, the interface will be proportional with fuel consumption.

Which part of the chemical energy of the components are participating in the reaction in the liquid phase changes into heat? The maximum temperature attainable in the liquid is limited by the boiling

point corresponding to external pressure; when the boiling point is reached, there takes place a change in the aggregate state accompanied by an intermittant change in the properties of the substance, in particular, a sharp decrease in its density. As a result of chemical reaction in the liquid phase, only a small part of the chemical energy of the fuel changes into heat since the boiling point is also considerably below the temperature of combustion products. Thus, the part of the first stage of ignition consists of the formation of the vapor-gas mixture; its initial temperature is equal to its boiling point (in the case of components which are complex compounds, we may approximately take the mean boiling point of the components) and depends on the pressure inside the combustion chamber.

The further development of the ignition cycle takes place in the gaseous phase. Experimental investigations of ignition cycles of liquid components (high-speed filming) show that the duration of reaction in the liquid phase is short in comparison with the delay period of ignition in the vapor-gas mixture (smaller by at least one order). This fact is not surprising if we consider that when a liquid changes into gas, density decreases by hundreds of times. This can

cause an abrupt decrease in the rate of reaction.

When investigating the cycle of ignition of liquid components in time, it is possible to disregard approximately the first stage, reaction in the liquid phase (assuming that correct injection and spraying of the components ensures its negligible quantity) and examine only the second stage, reaction in the gaseous phase. With such an approach it becomes possible to apply the results obtained above to the complex process of ignition of liquid components. In so doing, it is necessary, of course, to take into account the peculiarities and additional circumstances associated with the part played by the first stage and the conditions existing in the combustion chamber of engines. Let us point out the most important ones.

In the given case it is necessary to investigate the open system capable of exchanging with the surrounding medium not only heat and mechanical work, but also substance (mass). With a continuous injection of components into the combustion chamber, reaction in the liquid phase becomes the source of substance (gaseous phase) while the nozzle becomes a discharge.

An increase in the pressure inside the combustion chamber owing to its being filled with the vapor-gas mixture forming as a result of the liquid phase reaction, as well as to the heat production from the reaction in the vapor-gas mixture, leads to an additional increase in the rate of reaction in the gaseous phase (both on account of compression of vapor-gas mixture formed earlier, and the increasing temperature in the newly forming mixutr mixture).

The vapor-gas mixture inside the combustion chamber is considerably heterogeneous in concentration and temperature. This is due, in particular, to its varying "age". For this reason, ignition has a focal character. Moreover, the development of ignition is substantially affected by heat transfer and mass exchange of the forming foci with the surrounding medium.

If the temperature of the surrounding medium drops and liquid components are injected into the combustion chamber, and if the rate of chemical reaction in the liquid phase remains sufficiently high (as this is the case with several fuels), the ignition delay can only change as a consequence of increased heat transfer from the reacting vapor-gas mixture. This should not affect considerably the quantity

τ_c

(~~τ_1~~) .

With a decreasing pressure of the surrounding medium the boiling point of the fuel drops and, hence, the temperature of the forming vapor-gas mixture drops as well. In this case, the change in the value for the ignition delay is determined by the well known relationships $\left(\tau_c \sim e^{\frac{E}{RT}}\right)$

If data for the values of kinetic parameters (E,K, and n) are available for the reaction of the vapor-gas mixture, it becomes possible to determine approximately by calculation the effect on the change of pressure in time, when starting the engine with self-igniting components, the variations of temperature and pressure of the surrounding medium, the consumption of components, and other factors.

I take this occasion to express my gratitude to O. M. Todes for his valuable remarks and suggestions relating to the first section of this work.

REFERENCES

) Semenov N; N., Teplovaya Teoriya Goreniya i Vzryvov, "Uspekhi fizicheskikh nauk" (The Heat Theory of Combustion and Explosions; "Progress of the Physical Sciences"), vol. 23, No. 3, 1940.

2) Todes O. M., Teoriya Teplovogo Vzryva, "Zhurnal Fizicheskoy Khimii" (The Theory of Thermal Explosions, "Journal of Physical Chemistry"),vol. 13, No. 7 and 11, 1939.

3) Frank-Kamenetskiy D. A., Diffuziya i Teploperedacha v Khimicheskoy Kinetike, Izdatel'stvo Akademii Nauk SSSR (Diffusion and Heat Transfer in Chemical Kinetics, Press of the Academy of Sciences of the USSR), 1947.

4) Semenov N. N., K Teorii Protsessov Goreniya, "Zhurnal Russkogo Fiziko-khimicheskogo Obshchestva" (On the Theory of Combustion Processes, "Journal of the Russian Physico-Chemical Society" (Physcial Theory Section)), vol. 60, No. 4, 1928.

5) Abugov D. I., O Vosplamenenii Gazov Pri Razlichnykh Formakh Energeticheskogo Obmena s Okruzhayushchey Sredoy, "Doklady AN SSSR" (On the Ignition of Gases With Varying Forms of Energy Exchange with the Surrounding Medium, "Transactions of the Academy of Sciences of the USSR"), vol. 100, No. 2, 1955.

6) Taylor, C. F., Taylor E.S., Livengood J. C., Russel W.A. Leary W. A., Ignition of Fuels by Rapid Compression, SAE Quarterly Transaction, 1950, vol. 4,No. 2.

7) Pastell D. L., Precombustion Reactions in a Motored Engine. SAE Quarterly Transaction, 1950, vol.4, No. 4.

8) Levedahl W. J., Autoignition of Engine Fuels, Fifth Symposium (International) on Combustion, New York, 1955, p.372-385.

9) Trapeznikov V. A. and Kogan B. Ya., Printsipy Postroeniya Modeliruyushchikh Ustanovok Dlya Issledovaniya Sistem Avtomaticheskogo Regulirovaniya, "Avtomatika i Telemekhanika" (Design of Simulating Installations for the Investigation of Systems of Automatic Control "Automation and Telemechanics"), 1952, No.6.

10) Paushkin Ya. M., Khimicheskiy Sostav i Svoystva Reaktivnykh Topliv, Izd. AN SSSR (The Chemical Composition and Properties of Fuels for Jet Engines, Press of the Academy of Sciences of the USSR), 1958.

HIGH-TEMPERATURE, HIGH-POWER STABILIZED ELECTRIC ARCS (ELECTRIC ARC PLASMOTRONS) by Candidate of Technical Sciences V. B. Tikhonov and Eng. Ye. A. Yakovlev

In recent years, high-temperature, high-power stabilized electric arcs (electric arc plasmotrons) have been designed and applied for practical purposes.

Under stationary conditions, electric arc plasmotrons produce plasma jets by means of a relatively simple technical procedure. This is their great advantage over such devices for short-term plasma generation as wire explosion, impact tubes, superpower sparks, etc.

Utilization of electric arc plasmotrons makes it possible to simulate under laboratory conditions the effect of aerodynamic heating of bodies during flights with high Mach numbers, investigate the properties of various materials at high temperatures, etc. Moreover, electric arc plasmotrons open new outlooks for the realization of various physical investigations, viz., determination of the probabilities of a transition of atoms and ions from one energy state to another, study of the radiation capacity of plasma, determination of effective transverse sections of atoms and ions, investigation of problems relating to the heat and electric conductivity of plasma, etc.

Thus, electric arc plasmotrons are a highly effective means for the study of the properties of matter at high temperatures (of the order of several thousands of degrees).

Abroad, experimental work for designing plasmotrons and utilizing them for the solution of the above problems is most widespread in the Federal German Republic and the U.S.A.

Table 1 gives the parameters of some d.c. electric arc plasmotrons. As is seen, the highest temperature attained in a plasmotron channel amounted to 52,000° abs. Accordingly, the numerical values for the jet temperature are ranging from 8,000 to 14,000° abs.

Table 2 brings as an example the approximate values of temperatures obtained by various methods (8, 10, 21).

1. DESIGN AND OPERATION OF ELECTRIC ARC PLASMOTRONS

Electric arc plasmotrons are heavy-current electric arcs for d.c. or a.c. whose channel is stabilized in some way in order to eliminate transverse widening.

The most important parameters determining the temperature of the gas inside the channel of the electric arc are current density and the effective ionization potential of the arc discharge plasma.

TABLE I

Characteristics of Some Experimental Plasmotrons

№ по пор.	Тип плазмотрона	Название научно-исследовательской организации	Геометрические параметры канала *мм*		Электрические параметры			Температура в канале °абс.	Параметры струи		Литература
			диаметр	длина	мощность *квт*	ток *а*	напряжение *в*		температура °абс.	скорость *м/сек*	
1	Дуга Гердиена	Физический институт Высшей технической школы, Ганновер	3,5	10	250	55—500	500	34 000	—	—	[20]
2	Каналовая дуга	Институт экспериментальной физики Кильского университета	1,4	13	80	250	320	35 000	—	—	[22]
3	Каналовая дуга	То же	2,3	—	—	100—1500	—	52 000	—	—	[15]
4	Трубчатая дуга	•	8,0	—	10	50	175—200	12 650	—	—	[25]
5	Плазмотрон с односторонним истечением струи плазмы через цилиндрическое отверстие	•	7,0	—	—	150	—	—	13 200	1200	[26]
6	Плазмотрон с односторонним истечением струи плазмы через сопло Лаваля	Лаборатория Сименс—Шуккерт, Эрланген	—	—	30	200	150	12 500	8 000	6500	[24]
7	То же	Лаборатория Г. Джианнини, Санта-Анна, штат Калифорния	—	—	—	—	—	17 000	10 000	3000	[8]
8	•	Голландская научно-исследовательская лаборатория фирмы „Дженерал электрик", штат Филадельфия (запроектирована установка на 10 000 *квт*)	—	—	70	—	—	—	14 000	1200	
9	•	Проект плазмотрона научно-исследовательской лаборатории Чикагского университета	—	—	8000	—	—	—	—	—	

Legend of Table 1. 1) No. 2) Type pf plasmotron 3) name of scientific research organization 4) geometrical parameters of the channel, in mm 5) electric parameters 6) temperature in channel, ° abs. 7) jet parameters 8) literature 9) diameter 10) length 11) power in kw 12) current in a 13) voltage, in v 14) temperature, ° abs 15) velocity, m/sec 16) Gerdien arc 17) channel arc 18) channel arc 19) tubular arc 20) plasmotron with one-sided outflow of plasma jet through a cylindrical hole 21) plasmotron with one-sided outflow of plasma jet through a Laval nozzle 22) the same 23) Physical Institute of the Polytechnicum, Hannover 24) Institute of Experimental Physics of Kiel University 25) the same 26) Siemens-Schuckert Laboratories, Erlangen 27) G. Giannini Laboratories, Santa Anna, Calif. 28) Nollz Scientific Research Laboratory of "General Electric", Philadelphia (Installation for 10,000 kw) 29) plasmotron projetc of the Scientific Research Laboratory of Chicago University.

Table II

№ по пор.	Способ получения плазмы	Диапазон температур °абс.
1	Ртутные лампы	6000—7000
2	Свободногорящие слаботочные электрические дуги с графитовыми электродами	7000
3	Взрыв тонких металлических проволочек при пропускании электрического тока	8000—20 000
4	Свободногорящие сильноточные электрические дуги с графитовыми электродами	10 000—11 000
5	Ударные трубы	17 000—20 000
6	Искровые разряды	35 000—60 000

Legend of Table II. 1) No. 2) method for obtaining plasma 3) temperature, ° abs 4) mercury tubes 5) free-burning, weak-current electric arcs with graphite electrodes 6) explosion of thin metal wires when current is fed through them 7) free-burning, heavy-current electric acrs with graphite electrodes 8) impact tubes 9) spark discharges.

We shall henceforth assume that the arc discharge plasma is formed by thermic ionization of oxygen, hydrogen and nitrogen atoms for which the ionization potential is sufficiently high and amounts as an average to 13.5 to 14.5 electron volts.

The temperature in the channel of electric arc discharges depends on the magnitude of specific energy, which, in turn, depends linearly on current density.

In the case of usual (so-called free-burning) electric arcs the density of the current changes with its intensity.

It has been established by tests (12, 23) that when the current increases its density in the arc channel tends towards a specific boundary value. For this reason, the temperature of free-burning electric arcs cannot exceed a specific limit. As is shown in Table 2, for free-burning, weak-current electric arcs with graphite electrodes, this limit is close to 7,000° abs, while in the case of free-burning, heavy-current electric arcs with graphite electrodes the temperature increases to 10,000 to 11,000° abs with a current of 1500 a.

The reason for this phenomenon has to be sought in the transverse widening of the channel of free-burning electric arcs when

the current increases.

An increased current density, and hence a high temperature in the arc channel can be obtained by limiting the possibility of transverse widening of the arc channel. This can be achieved by various methods.

One of the first was the method realized in the so-called Beck electric arc (10). In order to limit the widening of the cross section of the lectric arc channel, graphite electrodes with a central channel containing salts of various metals were used. S. Lammer used another system. He increased the density of the current by burning an electric arc in a compressed gas. Nevertheless, the above methods do not afford the possibility of increasing to any considerable extent the temperature inside the electric arc channel.

For small powers, stabilization of the arc discharge channel by means of solid walls was used, for example, by obtaining an arc discharge inside a tube (10, 12).

The applicability of this method is limited by the heat resistance of the material of which the tube is made.

A somewhat increased arc discharge power is obtainable if the tube is cooled from the inside by water which forms a heat-protective film on the walls.

[redacted] The stabilized tubular electric arcs are designed [redacted] accordingly (12, 22, 25).

All the methods listed above make it possible to increase but slightly the current density and temperature in the electric arc channel.

A considerable step forward in the design of high-temperature, stabilized high-power electric arcs was made by the investigations carried out by G. Gerdien and A. Lotz in Germany from 1920 to 1922 (10, 12, 20, 21, 22).

For the stabilization of the electric arc channel, G. Gerdien and A. Lotz used a diaphragm to whose central opening water was fed through a large number of tangential [redacted] channels (Fig. 1). The water film thus formed protects the walls of the diaphragm opening from the high temperatures [redacted] developed in this stabilized portion of the arc discharge channel. Moreover, owing to heating, a part of the cooling water [redacted] turns into steam which later dissociates thermally and ionizes changing into plasma.

The first spectral investigations of the radiation of the arc channel section stabilized by the diaphragm already revealed the presence in the plasma of repeatedly ionized oxygen atoms which

Fig. 1. Design of the Stabilizing Diaphragm Proposed by G. Gerdien. a) water.

indicated the existence of temperatures above 20,000° abs.

The electric arc stabilized by a diaphragm of the above design was called "Gerdien arc".

The first systematic investigation of the radial distribution of temperatures in the Gerdien arc was undertaken by R. Larenz. He found that the maximum temperature along the axis of the Gerdien arc attained 34,000° abs (20).

The next step in the development of high-temperature, sta-

bilized high-power electric arcs was made by H. Maecker who improved the Gerdien arc by creating the so-called channel arc (Fig. 2), whose channel is contained entirely in the air chamber of a centrifugal sprayer (10, 12, 21, 22, 25).

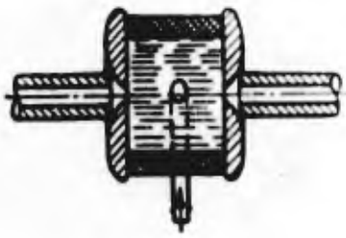

Fig. 2. Design of H. Maecker's channel arc.

The electrodes are placed along the axis of the sprayer. In order to record the radiations of the arc channel, tubular electrodes were used. The water fed by a tangential tube formed inside the sprayer a rotating water whirl with a central air channel where the arc discharge takes place. Owing to the increased length of the stabilized section, the specific power of the channel arc increased by about 50 times as compared with the Gerdien arc, amounting to approximately 11,600 kw/cm^3 (or 10^{13} kcal/m^3 hour) (x) (23).

In stabilized, high-temperature, high-power electric arcs great current densities in the electric discharge channel are obtained by the action of two factors: decrease in the section of the current-carrying channel by cooling the outer layers of the arc channel with a stabilizing agent, and compression of the arc channel by magnetic forces (8, 21). The electric chart of a high-temperature electric channel arc stabilized with water is shown in Fig. 3 (15).

(x) In combustion chambers of rocket engines, thermal stress equals 10^8 to 10^{11} kcal/m^3 hour.

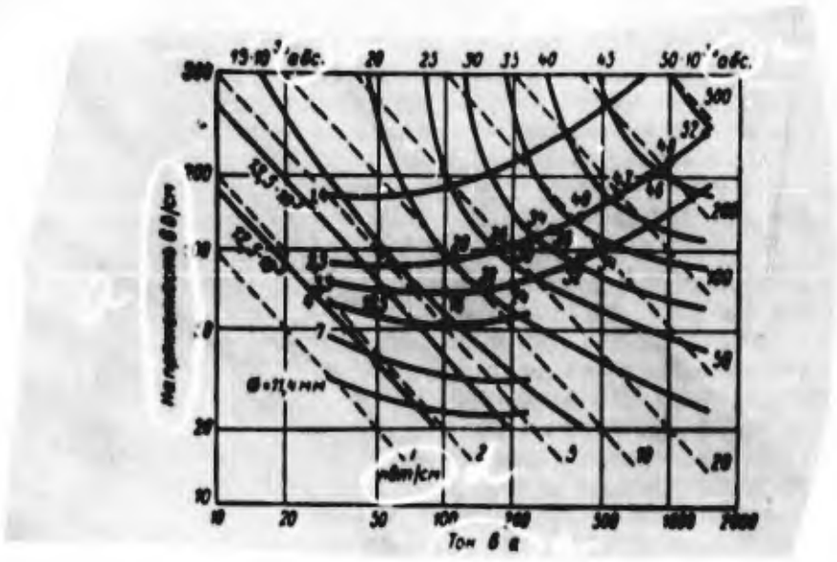

Fig.3. Electric chart of a stabilized channel arc. a) Intensity in v/cm b) abs c) abs d) kw/cm e) current, in [redacted] a.

The above electric chart has two branches: a descending left one and an ascending right one. The isotherms drawn in solid lines show that both branches join at a temperature [redacted] arc channel of about 15,000° abs. In the temperature range below 15,000° abs the electric conductivity of the arc channel increases with [redacted] growing current density. This increased electric

conductivity is connected with an increased concentration of electrons owing to thermal ionization of atoms.

For water vapor plasma, at a pressure of 1 atmospheres and a temperature of about 15,000° abs, the electron concentration in a volume unit is maximum. With a further increase in the temperature, it drops on account of the decreased plasma density ; this results in the appearance on the electric chart of the stabilized arc of an ascending branch. In the diagram the inclined broken lines correspond to the constant values for the energy released by a length unit of the arc's channel.

In order to insure an orderly discharge of the plasma jet formed in the channel of a high-temperature, stabilized electric arc, several plasmotron designs are proposed. Let us investigate some of them (11, 12, 24).

The chamber of an electric arc plasmotron shown in Fig. 4 is partly filled with water which evaporates during arcing. As a consequence, the pressure in the chamber rises to 50 atmospheres. Owing to the fact that the graphite ring electrode has the shape of a Laval nozzle, the rate of discharge of the plasma attains values of up to 6,500 m/sec (24).

Fig. 4. Electric arc plasmotron with one-sided plasma jet discharge through a Laval nozzle. a – water

The most widespread type of electric arc plasmotrons with one-sided plasma jet discharge is shown in Fig. 5. The coolant, which can consist of both fluids and gases, is continuously fed through a tangential channel into the cylindrical plasmotron chamber where the arc discharge takes place. The anode of the electric arc consists

of a cylindrical electrode which travels along the chamber axis, while the cathode consists of the graphite bottom of the chamber with the nozzle.

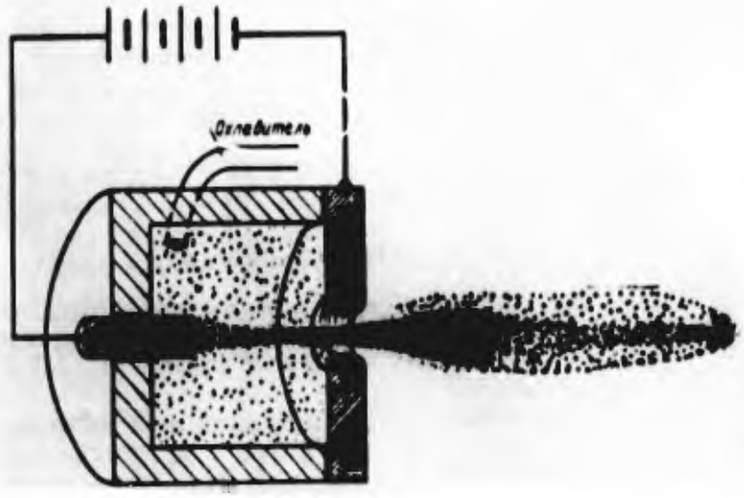

Fig. 5. Electric arc plasmotron with one-sided plasma jet discharge through a Laval nozzle and a tangential feed of the stabilizing fluid into the chamber. a) cooling agent.

At the present time there are electric arc plasmotrons operating

with triphase a-c ~~xxxx~~[1]. The schematic design of such plasmotrons is shown in Fig. 6.

Fig. 6. Electric arc plasmotron for triphase a-c with air stabilization.

(1) See American Aviation, 1957, vol. 21, No. 7, p. 41 to 42; Aviation Week, 1958, Vol. 69, No. 2, p. 71, 73.

In the cylindrical plasmotron chamber, three electrodes are arranged axially. Atmospheric air or an inert gas is fed under pressure through the tangential channel into the upper part of the plasmotron chamber. The electric arc is generated between the electrodes and the earthed graphite cover containing a nozzle for the plasma jet discharge. In the plasmotron chamber, three arcs are formed alternatively, which increases the magnitude of magnetic compression in the arc channel.

The advantages of electric arc plasmotrons for triphase a-c consists in that there is no need in electric d-c generators devised for high powers and currents.

Electric arc plasmotrons operating with triphase a-c are built in the U.S.A. in NACA scientific research laboratories (700 kw) and "General Electric" laboratories (20,000 kw).

To conclude our brief review, let us point out another type of electric arc plasmotron with pulse operation, constructed for the BBC research center in the U.S.A.(1)

(1) See Aviation Week, 1958, vol. 68, No.8, p. 34 to 35.

This plasmotron operates with energy stored in a huge induction coil . The electric arc is formed in the chamber with an initial air pressure of 35 to 140 atmospheres. When the induction coil discharges and a powerful electric arc is generated, a plasma jet [redacted] flows out at a velocity of 14,400 m/sec at a temperature above 20,000° abs and a pressure of about 2,100 atmospheres.

The present paper deals with problems relating to d-c electric arc plasmotrons (8, 10, 12).

ARC DISCHARGE PLASMA

In the course of numerous experimental and theoretical investigations of free-burning electric arcs it has been possible to establish the thermal nature of processes occurring in arc discharges (2, 4, 14, 17, 23).

In the channel of a stabilized electric arc [redacted] are developed such high temperatures that, alongside processes of thermal excitation and dissociation, there also occur processes of thermal ionization of the components constituting the plasma of arc discharges (15, 20).

As a result of thermal ionization, ions of atoms and free electrons are formed.

With the appearance of such particles, the gas changes into a new state which is called plasma.

As a rule, it can be assumed that plasma is formed at temperatures exceeding 10,000° abs since the plasma components have a high ionization energy equalling approximately 13.5 to 14.5 electron volts.

Alongside high electric and thermal conductivity, plasma possesses also a high radiation capacity.

Let us examine some of the specific properties of [redacted] arc discharge plasma.

The plasma of an arc discharge occurring under atmospheric pressure is usually called isothermic plasma; this is emphasized the fact that the plasma is in a state of thermodynamic equilibrium where all of its components have approximately the same quantity of mean kinetic energy of progressive motion, i.e., they have the same temperature (2, 4 ,17, 23).

A closer examination reveals that under service [redacted] conditions the processes of radiation, diffusion of electrons and ions of atoms in the arc discharge lead to certain deviations from the state of thermodynamic equilibrium (20). Moreover, in the electric

discharge pixx channel the plasma is found to be current-conducting.

Nevertheless, the utilization of the theory of thermal excitation and ionization for the study of arc discharge plasma yields extremely important and interesting data on the nature of and laws governing the processes in the arc discharge channel.

The theory of thermal excitation and thermal ionization is based on relations found by Bol'tsman and Sakha (1, 2, 6).

The plasma composition can be determined proceeding from the well-known method of thermo-chemical computations. To do so it is necessary to know the values for the constants of ionization equilibrium given by Sakha's formula (15).

As an example, let us examine the computation of the plasma composition of water vapor (15).

If we confine ourselves to the triple ionization degree of oxygen atoms, then the calculated system of equations will take the following form

$$\begin{gathered} p = p_e + p_{HI} + p_{HII} + p_{OI} + p_{OII} + p_{OIII} + p_{OIV}; \\ p_e = p_{HII} + p_{OII} + 2p_{OIII} + 3p_{OIV}; \\ \frac{p_{HI} + p_{HII}}{p_{OI} + p_{OII} + p_{OIII} + p_{OIV}} = 2{,}0; \\ K_{p_{HII}}(T) = \frac{p_{HII} p_e}{p_{HI}}; \end{gathered} \qquad (1)$$

(1)

$$K'_{P_{OII}}(T)=\frac{P_{OII}P_e}{P_{OI}};$$

$$K'_{P_{OIII}}(T)=\frac{P_{OIII}P_e}{P_{OII}};$$

$$K'_{P_{OIV}}(T)=\frac{P_{OIV}P_e}{P_{OIII}},$$

where

$P_e, P_{HI}, P_{HII}, P_{OI}$ etc., are partial pressures of electrons, hydrogen atoms, protons, oxygen atoms, singly charged oxygen ions, etc.;

$K'_{P_{HII}}(T), K'_{P_{OII}}(T)$ etc., are the so-called corrected constants of ionization equilibrium.

The ionization equilibrium constants are computed according to Sakha's formula

$$K_{P_{n+1}}(T)=\frac{P_{n+1}P_e}{P_n}=2\frac{B_{n+1}(T)}{B_n(T)}\frac{(2\pi m_e)^{3/2}}{h^3}(kT)^{3/2}e^{-\frac{I_{n+1}}{kT}}. \qquad (2)$$

where $B_{n+1}(T)$, $B_n(T)$ are the sums for n + 1 and n x ionized atoms;

m_e is the electron mass;

h is the Planck constant;

k is the Bol'tsman constant;

I_{n+1} is the ionization energy for n + 1 ionization degree.

The sum by states is computed according to formula

$$B_{n+1}(T)=\sum_s g_{n+1,s}e^{-\frac{\chi_{n+1,s}}{kT}},$$

where $g_{n+1,s}$ is the statistic weight;

$\chi_{n+1,s}$ is the excitation energy of the s-th level of a (n + 1)-times ionized atom.

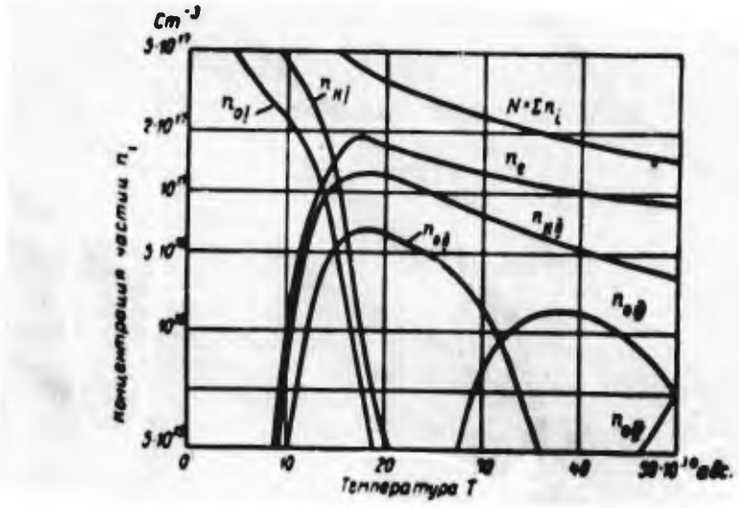

Fig. 7. Variation in the composition of water vapor plasma depending on the temperature at a pressure of 1 atmosphere. a) Concentration of particles n_i, b) temperature T, c) abs.

The presence in the plasma of charged particles leads to the generation of microfields and to a decrease of the actual quantity of ionization energy by the quantity ΔI, for the computation of which

A. Unsold (15) proposes the following formula:

$$\Delta I = 7 \cdot 10^{-7} \sqrt[3]{n_e}, \text{ ev}, \qquad (3)$$

where n_e is the concentration of electrons in cm^3.

In this case, the corrected ionization equilibrium constants have to be computed according to the expression

$$K_{p_{s+1}}(T) = K_{p_{s+1}}(T)\, e^{\frac{\Delta I}{kT}}. \qquad (4)$$

It is obvious that here, when carrying out computations, it is necessary to utilize the method successive approximations.

Figure 7 shows a diagram which characterizes the variation in the composition of water vapor up to a temperature of 50,000° abs at a pressure of 1 atmosphere (15).

With the aid of the above method we can calculate the plasma composition of any substance.

Let us now examine some relationships used in the computation of processes occurring in arc discharge plasmas.

An arc discharge plasma possesses the property of quasi-neutrality. This means that in any sufficiently small elementary volume of arc discharge plasma the total electric electron charge equals the total charge of positive atoms ions (13, 14, 23).

The electric field imparts to the free electrons and atom ions

a directional motion. We shall henceforth take into consideration only the flow of electrons since atom ions have a great mass and, hence, react faintly to the influence of the electric field (2, 14, 23).

The electric field accelerates the motion of electrons. When in motion, the electrons collide with ions and neutral particles. As a result of these collisons, the electrons impart to the ions or atoms that part of the energy which, though numerically small, can on account of the large overall number of collisons engender excitation of the atom or ion or generate ionization processes (the so-called first-order inelastic impact).

In order to compute electron mobility, we used the Langevin formula (2, 12, 23)

$$b_e = \alpha \frac{e\lambda}{m_e V_{heat}}, \qquad (5)$$

where α is the correction coefficient changing from 0.75 to 1.38;

e is the electron charge;

λ is the mean length of a free range of an electron;

m_e is the electron mass;

V_{heat} is the mean thermal electron velocity.

The mean thermal (quadratic) velocity of a particle in its general form is computed by the formula

$$V_{mean} = \sqrt{\frac{3kT}{m}}, \qquad (6)$$

where m is the mass of the particle.

The mean length of the free range of an electron equals

$$\lambda = \frac{1}{\sum_k n_k Q_{ek}}, \qquad (7)$$

where n_k is the concentration of heavy particles with which an electron can collide;

Q_{ek} are the corresponding effective sections of the heavy particles for colliding with the electrons.

The numerical values for n_k are found from thermodynamic computation of the plasma composition.

The values for the effective sections Q_{ek} in the plasma can be substantially greater than the usual gas-kinetic sections of particles.

In the case of collision between electrons and neutral particles, we utilized the so-called Ramsauer section Q_{e0}, which depends upon the energy of the moving electron (2).

The great extension of the Coulomb field causes a sharp increase in the effective section Q_{ei} of ions under the impact of

electrons (23).

In this case the size of the effective section is computed according to ~~ferrum~~ formula

$$Q_{ei} = \frac{Z^2 e^4}{(kT)^2} \ln \frac{kT}{Ze^2 n_i^{1/3}}, \qquad (8)$$

where Z is the atomic number;

and n_i is the ion concentration.

Proceeding from what was mentioned above we can find the current densities

$$j = en_e b_e E, \qquad (9)$$

where E is the field intensity.

Accordingly, the magnitude of specific electric conductivity equals

$$\sigma = en_e b_e. \qquad (10)$$

Figure 8 shows the dependence of specific electric conductivity of water vapor plasma on temperature (12).

Alongside the great production of quantities of ionization energy, the high mobility of electrons leads to a sharp increase in the heat conductivity of plasma.

The coefficient of thermal conductivity of plasma $\varkappa$ is computed according to the molecular-kinetic theory of gases taking

account of an additional energy transfer effect on account of ambipolar diffusion (12).

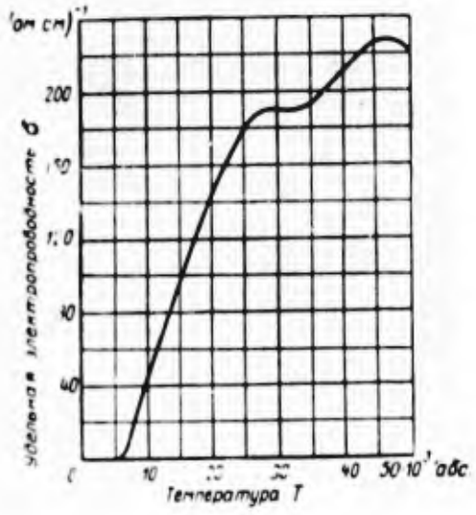

Fig. 8. Dependence of specific electric conductivity of water vapor plasma on temperature. a) specific electric conductivity b) temperature T c) abs.

A good idea about the character of the change in the coefficient of thermal conductivity of the air with changing temperatures can be gathered from Fig. 9.

Arc discharge plasma has a great radiation capacity, hence at high temperatures it is necessary to take account of heat transfer by means of radiation.

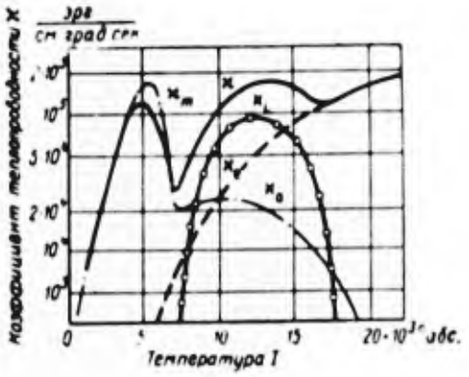

Fig. 9. Variation of the coefficient of thermal conductivity of the air as a function of temperature variation. a) coefficient of thermal conductivity b) erg/cm degree sec c) temperature T d) abs.

In the radiation spectrum of a plasma, alongside lines correspond-

ing to discrete energy levels of atoms or their ions, there are regions of continuous radiation (20, 23, 25).

Continous radiation results from the presence of free electrons whose distribution is governed by Maxwell's law (1, 6).

When a free electron hits the electric field of an ion it radiates a light quantum. If, in so doing, the electron remains free, i.e., there occurs a so-called free-free transition, this radiation is called bremsstrahlung (1, 6, 18).

Yet, after emitting a light quantum, the electron may be captured by the ion. In this case there takes place a free-fixed transition accompanied by a so-called recombined radiation.

Free-free and free-fixed transitions are numerically characterized by the appropriate coefficients of absorption or radiation. When computing plasma radiation processes, induced (forced) radiations (1, 20) are taken into consideration.

The computation of plasma radiation was undertaken in a series of experimental and theoretical researches.

As is known from (4, 14, 18, 19,20), the radiation factor of a spectral line in the absence of reabsorption is determined by

[redacted]

formula

$$\varepsilon(T,p)=\frac{1}{4\pi}A_n^m h\nu\frac{g_m}{B(T)}n(T)e^{-\frac{\chi_m}{RT}}, \qquad (11)$$

where A_n^m is the Einstein probability factor of spontaneous transition of an electron from the m-th excitation level to the n-th;

g_m is the statistic weight of the m-th excitation level;

$B(T)$ is the sum by states;

$n(T)$ is the concentration of particles;

χ_m is the excitation energy of the m-th level.

With increasing temperature (maintaing a constant pressure p) the number of particles n (T) decreases on account of both a decreasing density and thermal ionization.

At the same time, the exponential co-factor in formula (11) increases monotonely with temperature.

Thus, with increasing temperature the variation of $\varepsilon(T,p)$ is affected in mutually opposite directions by two factors, as a result of which the curve $\varepsilon(T,p)$ at a given temperature which can be denoted by $\tilde{T}$ reaches a peak.

Certain conveniences are afforded by the introduction of a so-called standard radiation factor (18, 19, 20)

$$\varepsilon^*(T,p)=\frac{\varepsilon(T,p)}{\varepsilon(\tilde{T},p)}, \qquad (12)$$

where $\varepsilon(\tilde{T},p)$ is the maximum value of the radiation factor.

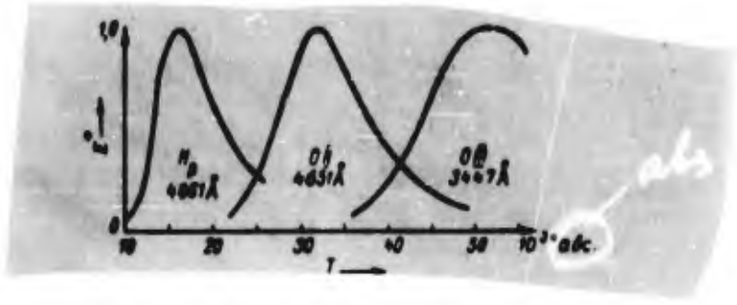

Fig. 10. Dependence of the standard radiation factor $\varepsilon^*(T,p)$ for the lines H_β (λ = 4,861 Å), O II (λ = 4,651 Å) and O III (λ = 3,447 Å) on temperature.

Figure 10 shows the curves of the variation of $\varepsilon^*(T,p)$ with temperature at p = 1 tm for the lines

H_β (λ=4861 Å), OII (λ=4651 Å) и OIII (λ=3447 Å) [15]. A 56

With the aid of the appropriate formula it is also possible to compute the standard values of the radiation factor for the region of continuous radiation $\varepsilon^*_\nu(T, p)$.

One of the methods of spectrographic determination of high temperature temperatures in arc discharge plasmas (18, 19, 20) is based the utilization of the computed values for $\varepsilon^*(T, p)$ or $\varepsilon^*_\nu(T, p)$.

3. TAKING SPECTROGRAMS OF THE RADIATION OF THE CHANNEL AND THE HIGH-TEMPERATURE JET OF AN ELECTRIC ARC PLASMOTRON.

The test was carried out with a d-c electric arc plasmotron built in the laboratory of the AD-2 MAI chair. Figure 11 shows the general view of the testing installation taken from the stabilizing assembly.

The high temperatures developed in the channel and the jet of electric arc plasmotrons make it impossible to measure temperatures by introducing any kind of contact receivers into the investigated zone.

The temperatures of the channel and the jet of electric arc plasmotrons have to be thus measured by astrophysical methods.

As a basis of methods of spectral analysis for the measurement of high temperatures we can take the temperature dependence of the radiation factors of individual spectrum lines or the continuous spectrum, as well as the broadening effect of spectrum lines (for example, the doppler broadening, the broadening on account of the Stark effect, etc.).

Fig. 11. General view of an experimental electric arc plasmotron.

We shall not dwell upon the description of all of these methods inasmuch as the theoretical assumptions and the procedure of such measurements are described in sufficient detail in the appropriate literature (10, 12, 15, 17, 18, 19, 20, 23, 24).

The interpretation of radiation spectra makes it possible to get an idea not only about the qualitative composition of plasma but also to determine the local concentration of particles and the temperature prevailing in various zones of the electric discharge channel and the high-temperature jet.

The intensity values, measured by the spectrum height, for the case of optically thin radiating lathes are scaled following the Abel integral equation (17, 20). In order to simplify the reduction, a simpler method of concentric zones has been proposed which was utilized for measuring the temperature of the flame and also in the practice of spectral analysis (9).

In order to facilitate the spectrographic investigation of arc discharge channels, the central part of the stabilizing assembly of an electric arc plasmotron is made entirely of quartz tubes or provided with small observation ports (15, 25).

In this case, the optical axis of the spectral apparatus is

placed perpendicularly to the axis of the arc ~~x~~ discharge channel.

Figure 12 shows the operation of an electric arc plasmotron. On the right, a highly luminescent high-temperature jet.

The test spectrograms of the radiation of a stabilized arc dicharge channel and a high-temperature jet of an electric arc plasmotron were taken with a medium-dispersion ISP-28 quartz spectrograph with an operating range of 2,000 to 6,000 Å.

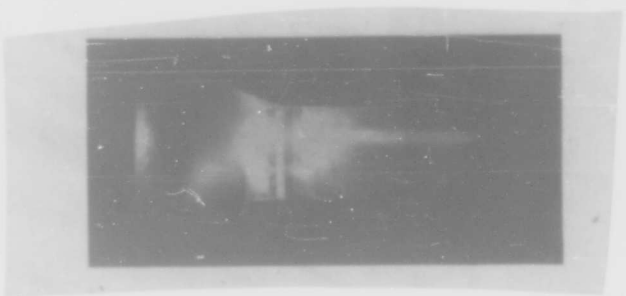

Fig. 12. Operation of an electric arc test plasmotron.

The illuminating system consisted of an achromatic quartz lens with a focal length F = 150 mm and a quartz condenser with a focal length F = 275 mm slipped onto the spectrograph's slit. The total diameter (in light) of the achromatic quartz lens equalled 15 mm.

To elimate the "vignette" effect and increase the depth of sharpness we used diaphragms made in the form of detachable annular sleeves with aperture diameters of 6, 8 and 10 mm. The achromatic quartz lens was placed at such a distance from the spectrograph that a sharp image of the section under investigation was projected on the spectrograph collimator slit. Prior to testing, the optical axis of the achromatic quartz lens and the spectrogrpah were made to coincide with the aid of an electric bulb with a scale thread.

The focusing sharpness of the image in the plane of the spectrograph collimator slit was checked with the aid of a small movable electric bulb placed on the axis of the arc channel. The diaphragm with a figure slit placed in front of the spectrograph collimator slit limited the height of the spectrum.

In order to excite the iron line, we used a DG-2 generator

which operated under arc conditions. A steady illumination of the spectrograph collimator slit was achieved by utilizing an [redacted] system consisting of three quartz condensers (the so-called system with intermediate reflection) (4).

*

At the instant of starting the electric arc plasmotron, owing to the melting of the igniting wire, there takes place an ejection of a large quantity of small metal drops. In order to preserve the surface of the optical lens from damages by the drops of molten metal, in front of the achromatic, focusing quartz lens, a rotating metalic shield was inststalled on a holder.

In order to obtain a specific exposure, in front of the spectrograph collimator slit a shutter was placed. During the first series of tests we used a common GOMZ photographic shutter, central-type. In further tests this shutter was replaced by an electric shutter with a rotating exposure disc especially designed for this purpose. This device is shown in Fig. 13. A contact data unit set up on the shutter was switched into the circuit of a loop oscillograph. This made it possible to determine for each test the actual exposure as well as the electric data for the operation of the electric arc plasmotron (voltage and current).

As photosensitive material for the photography of spectra we used photographic plates for scientific purposes (spectral type II, spectral type III and panchromatic). After photographing the spectrum under investigating, each plate was subjected to exposure

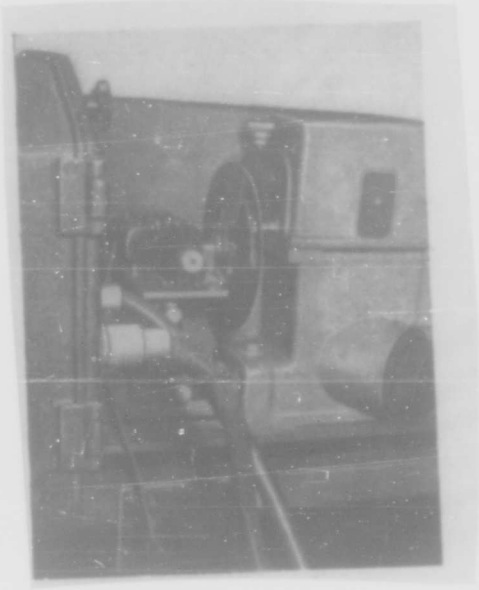

Fig. 13. Electric shutter with rotating exposure disc.

in a spectrosensitrometer ISP-73 in order to obtain a series of characteristic curves for various wave lengths. The plates were processed in the recommended photographic solutions with a strict maintenance of time and temperature conditions (4).

The radiation spectrograms were taken in the stabilized electric arc channel of the plasmotron and in the outflowing high-temperature jet.

The analysis of the spectrograms shows that, as a rule, they contain

[redacted] cyanogen bands, lines of hydrogen and oxygen atoms, and lines of oxygen ions. On the short-wave part of the spectrum taken in the channel and in the high-temperature jet, the line of atomic carbon C I is particularly intensive. This line has a wave length of ~~xxxx~~ 2,478.57 Å and an excitation energy of 7.69 [redacted] electron volts.

Optical blackening densities along the height of spectral lines were measured by means of a MF-2 ~~xxxxxxxxxxxxxxxxxxxxxxxx~~ non-recording photoelectric microphotometer. To read the transverse displacement of the microphotometer table, we used an indicating instrument (indicator watch).

The experimental data were processed on the basis of a method described in (18) and (19).

As a result of mathematical processing of the data from the spectrographic investigation we obtained the radial [redacted] distribution of temperatures in the transverse jet section shown in Fig. 14.

In order to check the reliability of the results obtained, the radial temperature distribution was determined by spectral lines with various wave lengths.

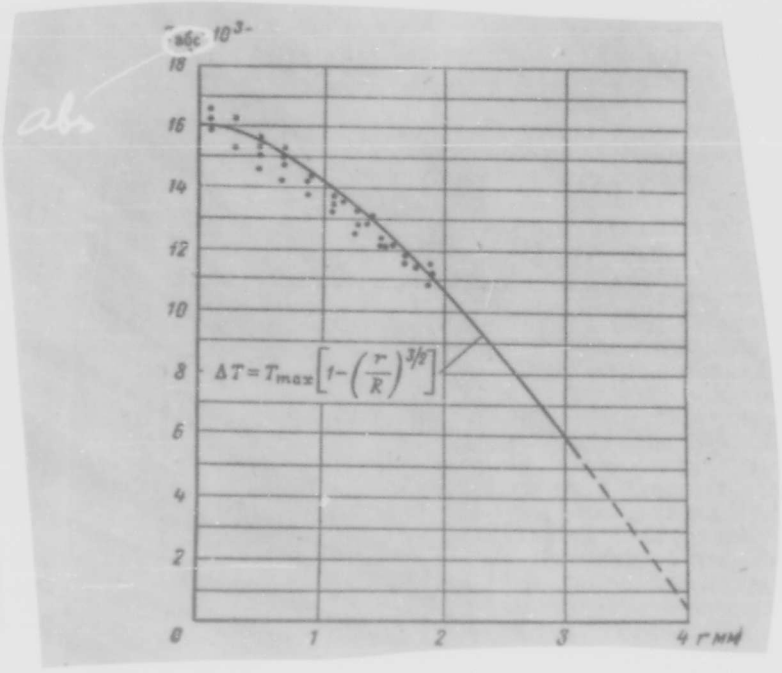

Fig. 14. Radial temperatures distribution of a high-temperature jet.

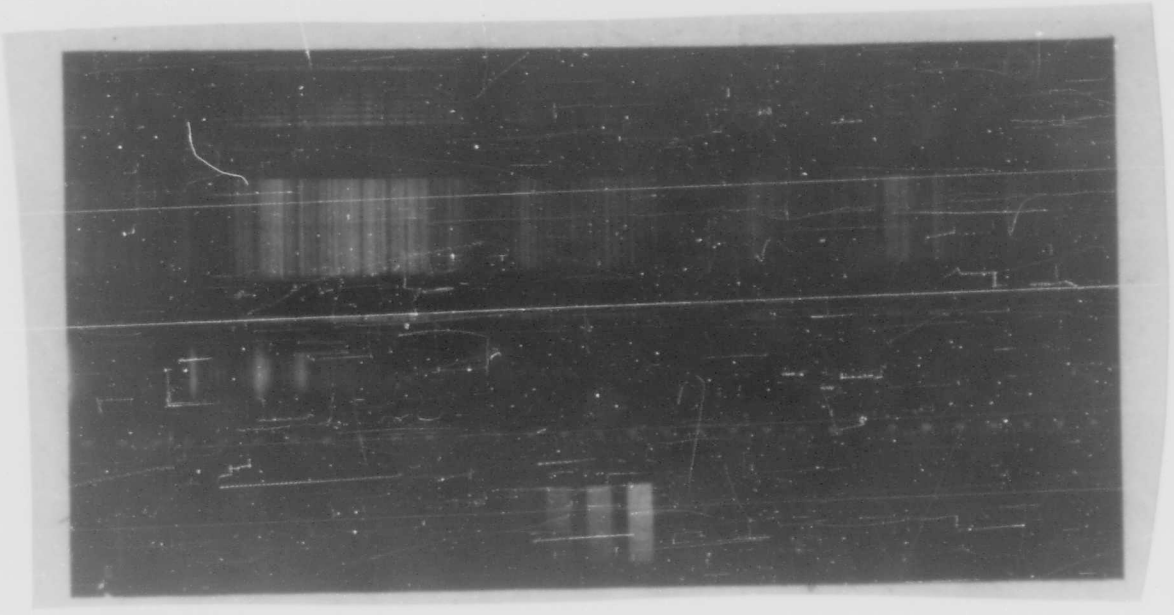

Fig. 15. Radiation spectrum of a stabilized channel of an [redacted] electric arc plasmotron.

Figure 15 shows the radiation spectrum of a stabilized channel taken through the quartz windows in the body of a stabilizing assembly of the plasmotron. The radiation spectrum of a high-temperature jet is shown in Fig. 16.

4. EFFECT OF THE ELECTROMAGNETIC FIELD ON [redacted] PLASMA MOTION INSIDE THE ARC DISCHARGE CHANNEL

When examining the motion of plasma in a plasmo-

tron channel it is necessary to evaluate the effect of the electric field and [redacted] proper magnetic field induced by [redacted] transmission of current through the channel on the electrons and ions.

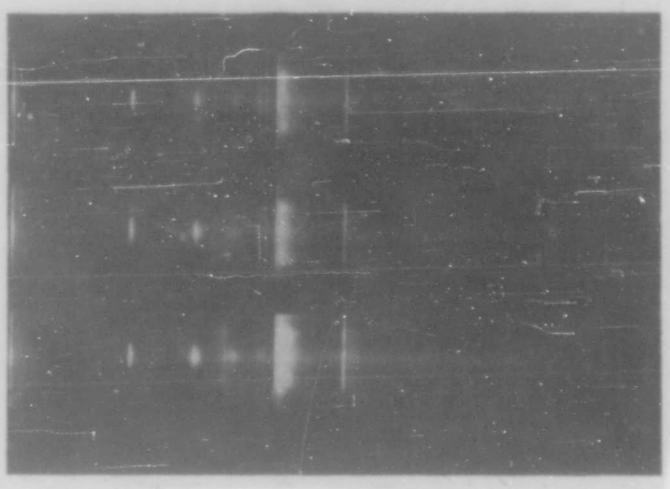

Fig. 16. Radiation Spectrum of a high-temperature jet.

The particular case of a stationary motion of a thermally ionized, quasi-neutral plasma of great density ($p \gg 1$ absolute atmospheres) is described by a system of equations consisting of

Maxwell equations for the electromagnetic field, and conventional hydrodynamic equations computing the interaction of the electromagnetic field with the moving medium.

Maxwell Equations

$$\operatorname{rot}\vec{H}=\frac{4\pi}{c}\vec{j}, \tag{13}$$

$$\operatorname{rot}\vec{E}=0, \tag{14}$$

$$\operatorname{div}\vec{H}=0, \tag{15}$$

$$\operatorname{div}\vec{E}=0, \tag{16}$$

where $\vec{H}$ and $\vec{E}$ are the magnetic and electric field intensities;

$\vec{j}$ is the current density;

c is the velocity of light in the vacuum.

Inasmuch as for conductive media magnetic inductivity is close to unity, it is assumed that magnetic field intensity and magnetic inductivity are equal to one another, i.e., $\vec{H} = \vec{B}$.

Current density j is the sum of conduction current and convective current:

$$\vec{j}=\rho_e\vec{V}+\sigma\left(\vec{E}+\frac{1}{c}\left[\vec{V}\vec{H}\right]\right). \tag{17}$$

The convective current component $\rho_e\vec{V}$, which depends on the motion

of the charges ~~ex the ex temperature~~ of total density ρ_e at a velocity $\vec{V}$, may be regarded as small both in the case of greater conductivity σ and of quasi-neutral plasma ($\rho_e = 0$).

The second component of current density consists of conduction current $\sigma\vec{E}$, which depends on the external electric field $\vec{E}$, and induction current generated by the motion of the conductive medium (plasma) in the proper magnetic field of the arc discharge at a velocity of $\vec{V}$.

Conductivity σ is considered homogeneous and isotropic for the entire medium, i.e., it is regarded as conforming to Ohm's law $j = \sigma E$.

The conditions for the isotropic conductivity is determined by the relation

$$\omega_H \tau \ll 1, \tag{A 63}$$

where ω_H is the Larmor electron frequency;

τ is the mean time of a free electron path.

In the case of ~~ini~~ anisotropic conductivity, Ohm's anisotropic law (7) should be used.

From equation (13) and (17) it ensues that

$$\operatorname{rot}\vec{H} = \frac{4\pi\sigma}{c}\left(\vec{E} + \frac{1}{c}\left[\vec{V}\vec{H}\right]\right). \tag{18}$$

Taking operations rot from both sides of the equation and keeping in mind that rot $\vec{E} = 0$ from condition (14), while grad div $\vec{H} \equiv 0$ according to condition (15), we obtain equation

$$\operatorname{rot}\left[\vec{V}\vec{H}\right] + \frac{c^2}{4\pi\sigma}\nabla^2\vec{H} = 0. \tag{19}$$

Equations (15) and (19) which characterize the interaction of the electromagnetic field with the moving conductive medium, must be completed by the equations of hydrodynamics, energy conservation and state. Such a system of equations enables us to determine completely the motion of the continuum in the electromagnetic fields.

Equations of hydrodynamics

Equation of motion (Navier-Stokes)

$$(\vec{V}\nabla)\vec{V} = -\frac{1}{\rho}\nabla p + \frac{\eta}{\rho}\nabla^2\vec{V} + f + \left(\xi + \frac{\eta}{3}\right)\nabla \operatorname{div}\vec{V}. \tag{20}$$

Equation of continuity

$$\operatorname{div}\rho\vec{V} = 0, \tag{21}$$

where V is the velocity;

ρ is the density;

p is the pressure;

η is the ~~first~~ 1st viscosity coefficient;

ξ is the 2nd viscosity coefficent;

f is the total electrodynamic force.

force f is determined by the interaction of the charge and the current of the medium with the electromagnetic field:

$$\vec{f}=\rho_e\vec{E}+\frac{1}{c}[\vec{j}\vec{H}]. \qquad \text{A 64}$$

In the case of great conductivity σ and small microscopic velocity of the medium as compared to the velocity of light $V/c \ll 1$, the first term, as compared to the second one, may be disregarded (16).

In the case under investigation, the mean conductivity of the medium is small (with I=300a and E=60v/cm σ=5 x 1/ohm x cm $\approx$ 5 x 10^{12} ed. CGSF) and the first condition is not satisfied.

If we assume that at any time instant the total density of charges in the arc channel equals zero (ρ_e = 0, i.e., the plasma is quasi-neutral), then with some approximation we can assume that

$$\vec{f}=\frac{1}{c}[\vec{j}\vec{H}]. \qquad \text{B 64}$$

this condition is usually assumed when studying plasma dynamics in heavy-current stabilized arcs (23).

Using equation (13) we obtain

$$\vec{f}=\frac{1}{4\pi}[\vec{H}\,\mathrm{rot}\,\vec{H}]. \qquad (22)$$

Thus, the equation of stationary plasma motion in an

electromagnetic field takes the following form;

$$(\vec{V}\nabla)\vec{V} = -\frac{\nabla p}{\rho} - \frac{1}{4\pi\rho}\left[\vec{H}\,\mathrm{rot}\,\vec{H}\right] + \frac{\eta}{\rho}\nabla^2\vec{V} + \\ + \frac{1}{\rho}\left(\varepsilon + \frac{\eta}{3}\right)\mathrm{grad}\,\mathrm{div}\,\vec{V}. \qquad (23)$$

Equation of Energy Conservation

This equation can be written in two ways (3):

a) $$\mathrm{div}\,\vec{q} = 0, \qquad (24)$$

where

$$q = \rho\vec{V}\left(\frac{V^2}{2} + W\right) + \frac{c}{4\pi}\left[\vec{E}\vec{H}\right] - (\vec{V}\sigma') - \varkappa\nabla T \qquad \text{A 65}$$

is the density of energy flow.

Here $W = \varepsilon + p/\rho$ is the thermal function of a mass unit (1g) of the medium;

ε is the intrinsic energy;

$$\frac{c}{4\pi}\left[\vec{E}\vec{H}\right] = \frac{1}{4\pi}\left[\vec{H}\left[\vec{V}\vec{H}\right]\right] - \frac{c^2}{16\pi^2\sigma}\left[\vec{H}\,\mathrm{rot}\,\vec{H}\right] \qquad \text{B 65}$$

is the Umov-[redacted] Pointing vector.

b) $$\vec{V}\rho T\,\Delta S = \sigma'_{ik}\frac{\partial V_i}{\partial x_k} + \mathrm{div}\,(\varkappa\nabla T) + \frac{c^2}{16\pi\sigma}(\mathrm{rot}\,\vec{H})^2, \qquad (25)$$

where S is the entropy of the mass unit of the medium;

$\varkappa$ is the heat-conductivity coefficient;

σ'_{ik} is the tensor of viscous voltage, whereby

$$\sigma'_{ik} = \eta\left(\frac{\partial V_i}{\partial x_k} + \frac{\partial V_k}{\partial x_i} - \frac{2}{3}\delta_{ik}\frac{\partial V_e}{\partial x_e}\right) + \xi\delta_{ik}\frac{\partial V_e}{\partial x_e}. \qquad \text{C 65}$$

the terms on the right side of equation (25) characterize the energy

dissipation in one volume unit during 1 sec on account on viscosity, thermoconductivity and Joule heat.

In the problem under investigation, energy is transmitted on account of Joule heat released in the arc channel. For this reason, in the case of small losses to the outer medium, the process may be considered isentropic, i.e., the equation of energy transfer may be written as

$$\frac{c^2}{16\pi^2\sigma}(\operatorname{rot}\vec{H})^2=\sigma'_{ik}\frac{\partial V_i}{\partial x_k}+\operatorname{div}(\varkappa\nabla T). \tag{26}$$

Equation of State

$$p=p(\rho, T). \tag{27}$$

Thus, the complete system of equations has the following form:

$$\operatorname{rot}[\vec{V}\vec{H}]+\nu_m\nabla^2\vec{H}=0; \tag{28}$$

$$\operatorname{div}\vec{H}=0; \tag{29}$$

$$(\vec{V}\nabla)\vec{V}=-\frac{\nabla p}{\rho}-\frac{1}{4\pi\rho}[\vec{H}\operatorname{rot}\vec{H}]+\frac{1}{\rho}\nabla^2\vec{V}+\frac{1}{\rho}\left(\xi+\frac{1}{3}\right)\operatorname{grad}\operatorname{div}\vec{V}; \tag{30}$$

$$\operatorname{div}(\rho\vec{V})=0; \tag{31}$$

$$\frac{c^2}{16\pi^2\sigma}(\operatorname{rot}\vec{H})^2=\sigma'_{ik}\frac{\partial V_i}{\partial x_k}+\operatorname{div}(\varkappa\nabla T); \tag{32}$$

$$p=p(\rho, T). \tag{33}$$

The diffusion of the magnetic field owing to small conductivity may be evaluated according to the value of the magneto-hydrodynamic

Reynolds number

$$Re_m = \frac{VL}{\nu_m},$$

A 66

where V and L are the characteristic velocity and linear dimension, respectively;

$\nu_m = c^2/4\pi\sigma$ is the magnetic viscosity.

If $Re_m \gg 1$, the medium can be regarded as ideal, i.e., nonviscous, with a small diffusion of the magnetic field and small Joule losses.

Let us evaluate the value of Re_m for the calculated conductivity $\sigma = 5 \times 10^{12}$ ed. CGSE. With $V \approx 5{,}000$ m/sec, L = 1 cm and

B 66

we obtain

$$\nu_m = \frac{c^2}{4\pi\sigma} = \frac{9 \cdot 10^{20}}{4\pi 5 \cdot 10^{12}} \approx 10^7$$

$$Re_m = \frac{5 \cdot 10^6 \cdot 1}{10^7} = 5 \cdot 10^{-1}.$$

C 66

With such a small magneto-hydrodynamic Reynolds number we can assume that the first term rot $[\vec{V}\vec{H}]$ of equation (28) is small in comparison with the second. This statement is equivalent to a denial of the magneto-hydrodynamic effect, i.e., for the assigned conditions the problem amounts to a conventional problem of gas dynamics with a hypothetical error in the results obtained of about 5 to 10%.

Thus, the above system of equations (28) to (33) can be sim-

plified and written as

$$(\vec{V}\nabla)\vec{V} = -\frac{\nabla p}{\rho} + \frac{\eta}{\rho}\nabla^2\vec{V};$$

$$\operatorname{div}(\rho\vec{V}) = 0;$$

$$\frac{p}{\rho} = \sigma'_{ik}\frac{\partial V_i}{\partial x_k} + \operatorname{div}(\varkappa\nabla T);$$

$$p = p(\rho, T).$$

A 67

an identical evaluation can be effected if we investigate the mobility of particles in the electric and magnetic fields of the arc discharge.

Inasmuch as in a partially ionized plasma there exists a mixture of neutral and charged particles with various sizes and masses, it is necessary to study the motion of the most mobile ones, i.e., the electrons. By examining the motion of electrons during the time interval between two collisions with atoms and ions we can assume the mean electron velocity to be

$$V_{cp} = \frac{V_{max} + V_{min}}{2}.$$

B 67

The effect of the proper magnetic field of the channel arc is small, hence, for a steady-state problem we can assume that plasma is governed by Ohm's law and regard it as a metalic conductor.

We disregard the initial velocity and express the mean electron velocity by electric quantities on the basis of the classic approxima-

tion:

$$V_{ср}=\frac{1}{2}V_{max}=\frac{1}{2}\frac{eE}{m}\frac{\lambda}{V_{heat}+V_{trans}}, \qquad \text{C 67}$$

where e is the electron charge;

E is the electric field strength;

m is the electron mass;

λ is the mean free electron path;

V_{heat} is the mean velocity of the thermal motion of electrons

V_{trans} is the transfer velocity of the directed motion of electrons under the effect of the electric field;

$$V_{trans}=\frac{j}{en_e}. \qquad \text{D 67}$$

where $j = I/S$ is the current density;

n_e is the concentration of electrons in a volume unit.

With a current of 300 a and a section of 0.01 cm^2, which corresponds approximately to an ionized column of the channel arc 3 mm in diameter and a temperature of the channel axis equaling 30,000° abs, $n_e = 10^{17}$ cm^{-3}.

Hence, current density

$$j=\frac{300\cdot 3\cdot 10^{6}}{0{,}01}=9\cdot 10^{10} \qquad \text{A 68}$$

and

$$V_{\text{пере}} = \frac{9 \cdot 10^{13}}{10^{17} \cdot 4{,}8 \cdot 10^{-10}} = 2 \cdot 10^{1} \text{ см/сек.}$$

B 68

the mean velocity of the thermal motion of electrons

$$V_{\text{тепл}} = \sqrt{\frac{3kT}{m_e}},$$

C 68

where $k = 1.38 \times 10^{-16}$ erg/degrees--- the Bol'tsman constant;

$T = 30{,}000°$ abs -- maximum plasma temperature;

$m_e = 9.1 \times 10^{-28}$ g -- the electron mass.

Hence $$V_{\text{тепл}} = \frac{3 \cdot 1{,}38 \cdot 10^{-16} \cdot 3 \cdot 10^{4}}{9{,}1 \cdot 10^{-28}} \approx 1{,}2 \cdot 10^{8} \text{ см/сек.}$$

D 68

Let us note that the velocity of the most mobile particles of the channel arc plasma is quite small in comparison with the velocity of light and that the plasma motion can be regarded as nonrelative.

V_{trans} / V_{heat} equals approximately 0.1 to 0.2, i.e., V_{trans} is about 10 to 20% of V_{heat}.

For this reason, when solving the problem of plasma flow by means of gas dynamics equations without taking into consideration the electromagnetic forces, it is possible to obtain the first approximation with an accuracy of about 10%.

Inasmuch as V_{heat} exceeds V_{trans} by one order, it is possible,

when computing the values for the mean velocity, to disregard V_{trans} in favor of V_{heat}. Then

$$V_{ср}=\frac{1}{2}\frac{eE}{m}\frac{\lambda}{V_{тепл}},$$

$$\lambda=\frac{1}{\sigma_{эфф}n_e}, \qquad \text{E 68}$$

where $\sigma_{эфф}$ is the effective section of collision between an electron and an ion;

n_e is the concentration of electrons in a volume unit.

As is known from (5)

$$\sigma_{эфф}=\pi\left(\frac{Z_1Z_2e^2}{mV^2_{тепл}}\right)^2\ln\Lambda, \qquad \text{F 68}$$

where Z_1 and Z_2 are the particle charges;

$\ln\Lambda$ is the term for the computation of remote collisions with coulomb interaction of charged particles.

Under the conditions of the investigated problem, the electron concentration exceeds by one to two orders the concentration of twice-ionized oxygen where the value of $\ln\Lambda$ is close to unit (1). Then for $Z_1 = Z_2 = 1$ we obtain (1)

$$\sigma_{эфф}=\pi\left(\frac{1\cdot1\cdot4{,}8^2\cdot10^{-20}}{9{,}1\cdot10^{-28}\cdot1{,}2\cdot10^{16}}\right)^2\ln\Lambda\approx10^{-15}\ см^2. \qquad \text{A 69}$$

(1) The quantity Λ can be determined more accurately according to formula $\Lambda=\frac{3}{2Z_1Z_2e^2}\left(\frac{k^3T^3}{\pi n_e}\right)^{1/2}$, which yields sufficiently reliable results with $T \ll 4 \times 10^5$.

The mean length of the free electron path will equal

$$\lambda = \frac{1}{\sigma n_e} = \frac{1}{10^{-15} \cdot 10^{17}} \approx 10^{-2} \text{ см}, \qquad \text{B 69}$$

i.e., by one order less than the characteristic dimension assumed when investigating the problem.

By determining V_{heat} and λ we obtain with the ~~index~~ electric field strength being of the order of ~ 60 v/cm

$$V_{ср} = \frac{1}{2} \cdot \frac{4{,}8 \cdot 10^{-10} \cdot 60 \cdot 10^{-2}}{300 \cdot 9{,}1 \cdot 10^{-28} \cdot 1{,}2 \cdot 10^{-8}} \approx 5 \cdot 10^{8} \text{ см/сек}. \qquad \text{C 69}$$

This confirms the condition assumed earlier whereby the motion of electrons in the channel arc plasma is determined basically by the thermal electron velocity.

Utilization of equations of gas dynamics without taking into consideration the electromagnetic forces (Maxwell equations) is expedient only if we want to obtain a preliminary approximate solution.

The effect of magnetic forces with an operating current I = 300 a and the radius of the ionized column r = 0.1 cm can be disregarded. In fact, the field strength around the cylindrical conductor equals

$$H = \frac{2I}{cr} = \frac{2 \cdot 300 \cdot 3 \cdot 10^{9}}{3 \cdot 10^{10} \cdot 10^{-1}} \approx 600 \text{ эрст}. \qquad \text{D 69}$$

The drift speed of charged particles (electrons) under the effect of the magnetic field $V_H = eHr/m$, where r in the given case cannot

be greater than the mean length of the free electron path;

$$r \leqslant \lambda \leqslant 10^{-2}\ см. \qquad D'\ 69$$

whence

$$V_H = \frac{1{,}6 \cdot 10^{-20} \cdot 600 \cdot 10^{-2}}{9{,}1 \cdot 10^{-28}} \approx 10^4\ см/сек. \qquad E\ 69$$

i.e., $V_H \ll V_{trans} \ll V_{heat}$.

Proceeding from the given evaluation of the effect of various factors on the plasma motion, the solution of the problem in the first approximation can be found by utilizing conventional equations of gas dynamics providing that no particular claim is placed on an excessive accuracy of the results.

For the stabilization of arc channels in plasmotrons, one may use not only water or other fluids but also various gases (hydrogen, nitrogen, argon, atmospheric air, etc.).

When utilizing electric arc plasmotrons for practical purposes of [redacted] technical and physical investigations, an extreme importance is acquired by problems regarding the determination of such plasma parameters as composition, temperature, velocity, etc. The solution of these problems is connected with the overcoming of a series of supreme [redacted] difficulties of methodical and technical nature.

The construction of electric arc plasmotrons and a thorough investigation of their working properties as well as the study of plasma parameters is of great significance for the progress of modern science and technology.

REFERENCES

1. Aller L., Astrofizika, (Astrophysics)) translation from the English, vol. 1, IL, 1955.

2. Kaptsov N. A., Elektronika, Gosudarst Gostekhizdat (Gosubarstvennoye Tekhnicheskoye Izdatel'stvo) (Electronics, State Technical Press) 1956.

3. Landau L. D., Livshits E. M., Elektrodinamika Sploshnykh Srd (Electrodynamics of Continuous Media), Gostekhizdat, 1957.

4. Mandel'shtam S. L., Vvedenie V Spektral'nyy Analiz (Introduction into Spectroanalysis), Gostekhizdat, 1946.

5. Spittser L., Fizika Polnost'yu Ionizovannogo Gaza (Physics of a Fully Ionized Gas, translation from the English), IL, 1957.

6. Unzol'd A., Fizika Zvezdnykh Atmosfer (Physics of Stellar Atmospheres, translation from the German), IL, 1949.

7. Gershman B. N., Ginzburg V. L., O Vliyanii Magnitnogo Polya Na Konvektivnuyu Neustoychivost' v Atmosferakh Zvezd I v Zemnoy

Ionosfere, "Astronomicheskiy Zhurnal" (On the effect of magnetic fields on convective instability in Stellar Atmospheres and the Earth's Ionosphere, " Astronomic Journal"), 1955, vol. 32, No. 3.

8. Dzhiannini Gm., Palazmennaye Struya. Atomnaya Tekhnika Za Rubezhom (Plasma Jets. Atomic Technology Abroad), No. 2, Atomizdat, 1958.

9. Dubrovskaya O. N., Opredeleniye Poley Temperatury Plameni Bez Primeneniya Mestnogo Okrashivaniya , Sbornik " Izmereniye Temperatur Plamen" (Determination of the Temperature Fields of the Flame without ousing Local Coloring, Collection "Measuring Temperatures of Flames" edited by A. E. Kadyshevich , Oborongiz, 1954.

10. Prayning O., Polucheniye Vysokikh Temperatur (do 55,000° C) v Laboratornykh Usloviyakh, "Uspekhi Fizicheskikh Nauk" (Obtaining High Temperatures (up to 55,000° C) under Laboratory Conditions, "Progress of Physcial Sciences"), 1955, Vol. 55, No. 4.

11.Weiss R., Untersuchung des Plasmastrahles, der aus einem Hochleistungsbogen austriet, Zeitschift für Physik, Bd. 138, 1954.

12. Maecker H., Der elektrische Lichtbogen, Ergebnisse der exakten Naturiwssenschaften, Bd. 25, 1951.

13. Rompe R. und Steenbeck M., Der Plasmazustand der Gase, Ergebnisse der exakten Naturwissenschaften, Bd. 18, 1939.

14. Weizel W. und Rompe, R., Theorie elektrischer Lichtbögen und Funken, Leipzig, 1949.

15. Burhorn F., Maecker H. und Peters T., Temperaturmessungen am Wasserstabilisierten Hochleistungsbogen, Zeitschriff für Physik, Bd. 131: 1951.

16. Elsasser W., Dimensional Relations in Magnetohydrodynamics, The Physical Review, 1954, vol. 95, No.1.

17. Hörmann H., Temperaturverteilung und Elektronendichte in frei brennenden Lichtbögen, Zeitschrift für Physik, Bd. 97. Heft 9-10, 1935

18. Larenz R. und Bartels H., Die Temperatur in der Säule des Gerdien-Bogens, Die Naturwissenschaften, Jgng.37 Heft 7, 1950.

19. Larenz, R., Uber ein Verfahren zur Messung sehr hoher Temperaturen in nahezu durchlässigen Bogensäulen, Zeitschriff für Physik, Bd. 129, 1951.

20. Larenz, R., Temperaturmessungen in der Säule eines Gerdien-Bogens, Zeitschrift für Physik, Bd. 129, 1951.

21. Lochte-Holtgreven W., Erzeugung und Anwendung höchster Temperaturen, VDJ-Zeitschrift, Bd. 97, No.23, 1955.

22. Maecker H., Ein Lichtbogen für hohe Leistungen, Zeitschrift für Physik, Bd. 129, Heft 1, 1951.

23. Maecker, H.,Plasmaphysik, Internationale Tagung über Strausstrahlen und Raketen, Freudenstadt, 1956.

24. Peters T., Plasmaströmungen, Internationale Tagung über Strausstrahlen und Raketen, Freudenstadt, 1956.

25. Jürgens G., Temperatur und Elektronendichte in einem wasserstabilisierten Lichtbogen, Zeitschrift für Physik, Bd. 134, 1952.

DISTRIBUTION OF LIQUID IN A SPRAY WITH IMPINGING JETS

By

I. G. Panevin

Sprayers with impinging jets are utilized in various fields of technology, from fire-fighting devices to liquid-fuel jet engines. With the latter, their use has been most widespread. Up to the present time, however, the particular operational features of such nozzles have not been sufficiently studied. The present paper exposes briefly the results of theoretical and experimental investigations of the distribution of the liquid flow in the spray of a nozzle with two as well as three impinging jets. This research was undertaken from 1954 to 1955.

REVIEW OF THE WORKS INVESTIGATING IMPINGING JETS

The process of spreading of a liquid resulting from the collision of two axially symmetric jets intersecting at an arbitrary angle has been inadequately investigated both from the theoretical and experimental points of view.

An accurate theoretical investigation of the above process is rendered extremely difficult by the three-dimensionality of motion.

For this reason, the methods of conformal transformation are inapplicable here. A simpler, though less accurate, way consists in simplyfing the physical effect model. Indeed, this was the system adopted by Wittenbauer (1). He is the only author who attempted a theoretical study of the given problem. Considering the fluid nonviscous, he investigated the spreading over the surface of the sheet of a jet colliding with the sheet at an arbitrary angle, and found the law for the spreading of the liquid proceeding from the investigation of flow conditions in the jet and in the liquid film at considerable distances from the point of collison. The solutions found by Wittenbauer are of a particular nature. Among the basic propositions advanced by him there is one lacking any solid foundations. In fact, he admits the presence in the film of a component flow velocity which exceeds the velocity in the jet. This assumption interferes with the Bernoulli equation. For this reason, Wittenbauer's formula requires a more reliable evidence.

(1) Wittenbauer's work is described in the book by F. Forkhgeymer (2).

The experimental investigations of this subject are also extremely scarce.

Let us dwell upon the following three most important works. Bond (3), in studying the surface tension of fluids, measured the diameter of a round liquid film forming by a coaxial collison of two water jets. He showed that the velocity of the liquid in the film is practically equal to that in the jets and that energy losses resulting from the collison of the jets can be disregarded. Although it refers to the case of small flow velocities (up to 10 m/sec), this conclusion is extremely important. D. Li (1) measured the distribution of fuel in the spray of a twin-jet diesel sprayer. He found that "the transverse section of the jet injected from the nozzle with two intersecting jets has a near-elliptic shape, the shorter ellipse axis lying in the plane crossing the axis of the channels." The increase in counterpressure in the test chamber affected but slightly the fuel distribution in the spray. Kertschmar and Wedaa (4) devised an optical method for the study of the mixing properties of two liquid components in the spray of twin-jet spray nozzles with impinging jets. They established that the quality of intermixing increases with higher velocities of the liquid, but that at the same time the extension of the mixing area grows too.

In order all the above experimental investigations, the authors examined only individual particular problems relating to the collison of jets. General regularities governing this process were not found. No attempts were made to generalize theroetically the results obtained, or to check experimentally the Wittenbauer formula.

2. THEORETICAL INVESTIGATION OF THE SPREADING [redacted] OF A LIQUID RESULTING FROM TWO IMPINGING JETS

Below we investigate the problem relating to the spreading of a liquid resulting from two jets impinging at an arbitrary angle. The liquid is assumed nonviscous and incompressible. Two jets of identical diameter d impinge at an angle $2\alpha_1$. From the intersection point the liquid spreads radially forming a sheet lying in the symmetry plane which passes across the bisector of the angle of collision. This plane will henceforth be called the main plane of the jet. Since both jets spread identically, we may confine ourselves to examining one jet only, regarding the main plane as an impenetrable surface (1). We take the bisector of the angle of collision of the jets as the main jet axis and assume that it is directed in the same sense as the projection of the velocity vector of the jets in the

main plane.

From point 0 where the flow is totally retarded, the liquid spreads radially in all directions, forming a film. Thus, point 0 is the pressure center and the water divide. The direction of the radial motion is coordinated at the angle φ read from the main jet axis. We also assume that the tangential flow of the liquid is absent, i.e., $\delta V/\delta\varphi = 0$.

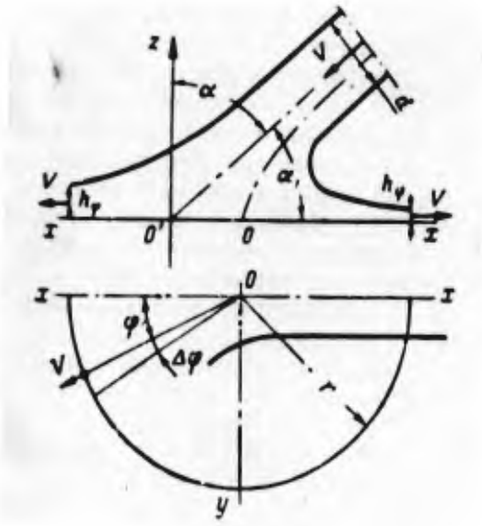

Fig. 1. Schematic Diagram of The Spreading of a Jet in the Main Stream Plane.

At some sufficiently great distance r from the point of collision the curvature of the flow lines in the film can be disregarded, and the pressure of the liquid over the film thickness can be considered constant, equaling the surrounding pressure. Then, from the Bernoulli equation it ensues that the velocities in the jet and the film must be identical inasmuch as the surrounding pressure is constant.

In the arbitrary elementary sector $\Delta\varphi$ the liquid flow equals $\Delta G_\varphi = \rho V h_\varphi r \Delta\varphi$, where ρ and V are respectively the density and velocity of the liquid, r is the radius of the cylindrical section under investigation, h_φ is the variable thickness of the film in this section. It can be readily be seen that with constant velocity the law of variation $h_\varphi = f(r)$ is hyperbolic.

Let us require that in the jet and the cylindrical film section under investigation, besides the law of energy conservation (Bernoulli's equation), the laws of flow conservation and conservation of the quantity of motion also be satisfied. On the basis of the first requirement, after simplification, we obtain

$$\int_0^{2\pi} h_\varphi \, d\varphi = \frac{\pi d^2}{4r}, \quad (1)$$

while on the basis of the second requirement, also after simpli-

fications, we obtain

and

$$\left.\begin{aligned}\int_0^{2\pi} h_\varphi \cos\varphi\, d\varphi &= \frac{\pi a^2}{4r}\sin\alpha\\ \int_0^{2\pi} h_\varphi \sin\varphi\, d\varphi &= 0.\end{aligned}\right\} \quad (2)$$

The first equation is obtained by projecting on the main axis, while the second results from projecting on a line perpendicular to this axis. The second equation expresses the condition that spreading takes place symmetrically to the main axis.

With the aid of the system of integral equations (1) and (2), it is possible to find the law of the variation of film thickness in the cylindrical section selected. Let us note that a number of particular solutions correspond to this system. Let us look for one of these solutions in the form

$$h_\varphi = \frac{h_1}{1-\sin^n\alpha\cos\varphi}, \quad (3)$$

where h_1 and n are functions of the angle α (see Fig. 1) subject to determination.

Since equation (3) represents the equation of an ellipse with polar coordinates, it has been assumed beforehand that the change in the thickness of the film in the cylindrical section is elliptic in character.

By substituting expression (3) in equations (1) and (2), and carrying out the required transformations we obtain

$$h_1 = h_0 k_c;$$
$$h_0 = \frac{d^2}{8r};$$
$$k_c = \frac{\cos^2 \alpha}{1 + \sin^2 \alpha};$$
$$n = \frac{\ln \frac{2 \sin \alpha}{\sin^2 \alpha + 1}}{\ln \sin \alpha}.$$

A 75

then, substituting the expressions obtained for h_1 and n in expression (3) we obtain finally

$$h_\varphi = \frac{h_0 \cos^2 \alpha}{1 + \sin^2 \alpha - 2 \sin \alpha \cos \varphi}. \qquad (4)$$

Formula (4) is almost analogous to Wittenbauer's formula (the only difference being the selection of the angle α), this formula being obtained with sufficient accuracy.

The analysis of this formula shows that the film thickness in any cylindrical section does not depend on the flow velocity of the liquid, but that it is a function of the diameter and the angle of collision of the jets (it ensues from Fig. 1 that the angle of collision $\alpha = \pi/2 - \alpha_1$).

In the direction of the central axis ($\varphi = 0$) the film attains the maximum thickness

$$h_{max} = \frac{h_0 \cos^2 \alpha}{1 + \sin^2 \alpha - 2 \sin \alpha}. \qquad (5)$$

The film thickness referred to the maximum thickness equals

$$\bar{h}_\varphi = \frac{h_\varphi}{h_{max}} = \frac{1+\sin^2\alpha-2\sin\alpha}{1+\sin^2\alpha-2\sin\alpha\cos\varphi}. \qquad (6)$$

The absolute film thickness, in the case of two impinging jets, will be twice as great as the quantity h_φ obtained from formula (4).

3. TEST EQUIPMENT AND METHOD FOR INVESTIGATING THE PROCESS OF SPREADING AND MIXING OF THE LIQUID RESULTING FROM TWO IMPINGING JETS.

It was the purpose of this experimental investigation to study the process of spreading and mixing of the liquid in the stream of a sprayer nozzle with impinging jets and follow the effect borne on this process by the basic injection parameters: velocity, diameter, angle of collision and length of jets, non-coaxiality of their collision and counterpressure of the surrounding medium.

The tests were carried out in two experimental chambers. The first was designed for operation under atmospheric counterpressure. For the convenience of visual observation, its walls were made of organic glass. The second chamber was designed for operation under increased counterpressure (up to 5 gauge atmospheres) and was welded of sheet steel.

In the top part of the chamber an atomizer cone(a general-

purpose jet nozzle) was installed. This device is designed to obtain the required combination of jets lying in the same plane and intersecting at one point. With its aid it was possible to change the number of jets, the angle of collision (from 40 to 180°), the nozzle diameter (1) (from 1 to 2 mm), the length of the jet from (2 to 50 mm) and the non-coaxiality of the jets (from 0 to 2 mm).

As working components we used water and kerosene fed into the atomizer cone from tanks under the pressure of compressed air. The test equipment made it possible to feed through each of the two or three nozzles any of the components mentioned above, thus creating the required pressure differential at the sprayer nozzle Δp in the range of 1 to 15 atmospheres.

The flow tension in the transverse section of the stream was measured by means of two jet intakes. Each of them had a set of

(1) In the test described the jet diameter amounts to approximately 0.8 of the nozzle diameter (d_c).

cells connected by pipes with graduated cylinders. Each graduated cylinder had a capacity of 10 cm^3 and a scale with 100 divisions. The intake cells covered an area of 49 mm^2, the inlet edges of the cell being pointed. From the top the intake cells could be closed by hinged covers. The first jet intake had 169 cells arranged in a group on a plane surface which had the shape of a sector of a circle with a radius of 100 mm and a central angle of 90°. The device was placed in the chamber at a distance of 130 mm from the point of collison of the jets. After effecting four measurements it was possible to measure the flow tension on an area limited by a circumference 200 mm in diameter. The second jet intake had 13 cells arranged in a single row. It was placed at 100 mm from the point of collison in the investigated radial stream section crossing the point of intersection and perpendicular to the main stream plane. Unlike the first jet intake, the second one did practically not cause any turbulence in the secondary air stream entrained by the liquid jet. Comparison of the results obtained by both devices shows that turbulence generated by the first jet intake did not result in any noticeable changes in the distribution of the liquid in the jets.

The flow tension j_F (the liquid rate of flow per one unit of the area of the intake cell) was measured in the following way. The jet intake was installed in the chamber and the nozzle (atomizer cone) was set into the assigned operating conditions (the assigned pressure differential Δp). Then, the cover of the device was opened for a given period of time measured by means of a timing device. The liquid fed into the intake cells flowed from there into the measuring cylinders. After switching off the equipment, the graduated cylinders were removed from the device and the level of the liquid was read in each of them. By knowing the measuring time and the area of the intake cell, the flow tension could be readily computed at the corresponding point of the transverse section of the jet. In our case it was more convenient to refer the flow rate not to an area unit but to a solid angle unit. The flow tension j thus obtained had the dimension g/sec steradian.

The weight ration of the components of k was measured with the aid of the same jet intakes. After measuring the level of the liquid, the graduated cylinders were placed into a special centrifuge and the mixture was centrifugated until water separated completely from kerosene. The quantity k was computed according to

the formula

$$k = \frac{(h\gamma)_{\text{mean}}}{(h\gamma)_{\text{experiment}}},$$

A 77

where γ and h are, respectively, the specific gravity and the level of the liquid in the graduated cylinder. In most tests the relative error of measuring flow tension did not exceed 2%, attaining ± 5 to 10% only in individual cases. The relative error when measuring the weight ratio of components did not exceed 10%.

4. TEST RESULTS

Twin-Jet Nozzle

a) Distribution of liquid in the main plane of the stream.

Figure 2 shows the result of measurements of the relative flow tension in the various radial stream sections obtained with the aid of the second jet intake. Relative flow tension is intended here as the ratio of the liquid flow through the total area of intake cells at any radial stream section to the corresponding flow in the central radial section ($\varphi = 0$). The test curves (dotted lines) correspond to various jet diameters and lengths (d = 1 to 2 mm, l = 3 to 7 mm) as well as various pressure differentials at the nozzle (Δp = .2 to 5 atmospheres) at a constant counterpressure of 1 absolute atmosphere. Solid lines show the results of theoretical

computations according to formula (6). Let us note that in each radial stream section the relative flow tension, according to the definition given above, must equal the relative film thickness inasmuch as the flow rate of the liquid in the film is assumed to be constant at all of the radial sections, and to be equal to the rate of flow in the jets.

Analysis of Fig. 2 shows that changes in the velocity, diameter and length of the jet do not affect the law of distribution of the liquid in the main stream plane of a twin-jet nozzle. However, experimental functions $\lambda_\varphi = f(\varphi, \alpha)$ do not coincide with sufficient accuracy with the theoretical ones. This discrepancy is systematic in character, and the difference increases as the angle of collision of the jets ($\alpha_1 = 90° - \alpha$) decreases. This suggests that the assumption of the absence of tangential flows in the liquid advanced earlier does not correspond to actual conditions.

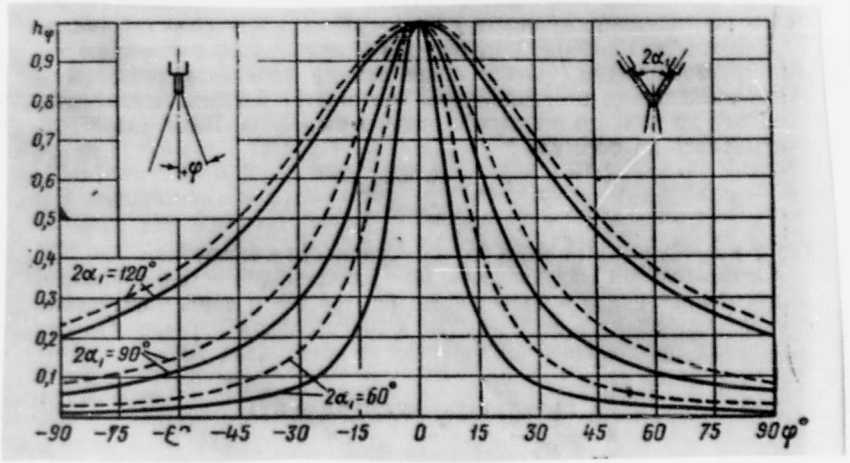

Fig. 2.. Variation in the relative flow tension j (or relative film thickness h_φ) of the liquid in the main jet plane of a twin-jet nozzle.

Actually, the study of the curves in Fig. 2 shows that as the angle of collision decreases, the film thickness increases in the direction of the central axis where a sharply outlined peak appears. The curvature of the flow lines in the peak, as well as the surface tension of the liquid, must lead to increased pressure

inside the liquid as a result of which there must arise tangential flows from the peak. Hence [redacted], the flow rate in the direction of the central axis decreases, while it increases in the peripheral jet areas. This must lead to an excess of the experimental values of $\bar{h}_\varphi$ over the theoretical ones.

The experimental dependences $\bar{h}_\varphi = f(\varphi, \alpha)$ are adequately determined by the equation

$$\bar{h}_{\varphi_2} = \frac{1 + \sin^2\alpha - 2\sin\alpha}{1 + \sin^2\alpha - 2\sin\alpha\cos(\alpha\varphi)}, \qquad (7)$$

where $\bar{h}_{\varphi_t}$ is the true relative film thickness;

$\alpha = \cos^{-1}\alpha$ is the experimental factor.

Relation (7) is true with $0° \leqslant \alpha \leqslant 60°$ and loses its significance with $\alpha \to 90°$.

The absolute value for the actual film thickness can be expressed x by the following relation:

$$h_{\varphi_2} = \frac{h_0 h_\varphi \cos^2\alpha}{1 + \sin^2\alpha - 2\sin\alpha\cos(\alpha\varphi)}, \qquad (8)$$

where the coefficient k_0 determined by the condition of equality between the flow in the jets and the film is

$$k_0 = \frac{\pi\alpha}{2}\left\{\operatorname{arctg}\left[\frac{(1+\sin\alpha)^2}{\cos^2\alpha}\operatorname{tg}\frac{\pi\alpha}{2}\right]\right\}^{-1}. \qquad (9)$$

The relative flow rate in an arbitrary sector determined by the angle $\pm\varphi$ can be computed with the aid of the formula

$$\Delta\bar{G}_1 = \frac{4\varphi^2}{\pi\alpha}\operatorname{arctg}\left[\frac{(1+\sin\alpha)^2}{\cos^2\alpha}\operatorname{tg}\frac{\pi\alpha}{2}\right]. \qquad (10)$$

It is interesting to compute the relative liquid flow $\Delta\bar{G}_{180}$ assigned to the back half plane of the jet. Taking into account formula (9), we obtain from formula (10):

$2\alpha_1$	60°	90°	120°
$\Delta\bar{G}_{180°}$	0,07	0,12	0,21

(A 79)

Thus, an increasing angle of collision of the jets contributes to a more uniformly distributed rate of flow of the liquid in the main stream plane. At the same time, however, it leads to an increased flow of the liquid in the direction of the rear half plane of the jet.

b) Distribution of the liquid in the radial jet section.

The theoretical investigation of the problem relating to the distribution of the liquid in the radial jet section is considerably more complex inasmuch as in this case we have to study the process of disintengration of the liquid film forming by collison of jets, as a result of its interaction with the surrounding gaseous medium.

In another paper (1), this author investigated the problem relating to the disintegration of plane liquid films flowing in a motionless gaseous medium. He found that these films can disintegrate under the effect of so-called symmetrical and non-symmetrical fluctuations, the latter having a greater effect on the distribution of the liquid in the radial stream section of a twin-jet nozzle. Moreover, the distribution of the liquid in the radial stream section is strongly affected by the instability of its flow in the jets near the point of their collison. Yet, the data available proved to be insufficient for obtaining the appropriated references dependences.

Experimental investigations of the problem have also shown that the only factor which affects substantially the distribution of the liquid in the radial stream section is the angle of collision of the jets. Thus, with an increasing angle of collision the dispersion of the liquid to the peripheral stream section increases,

(1) See the second paper by this author in the present collection of articles.

whereas [redacted] the curve of the flow rate distribution acquires a smoother character. This is seen in Fig. 3 which shows [redacted] the curves of relative flow tension distribution [redacted] corresponding to three different values of the angle of collision: 60, 90 and 100°. In Fig. 3 on the abscissa are plotted the distances determining the position of the intake with regard to the main plane, while the relative tension is plotted on the ordinate. The intake is placed at 120 mm from the collision point of the jets. The test conditions were as follows: d_c = 1.5 mm; Δp = 5 atmospheres.

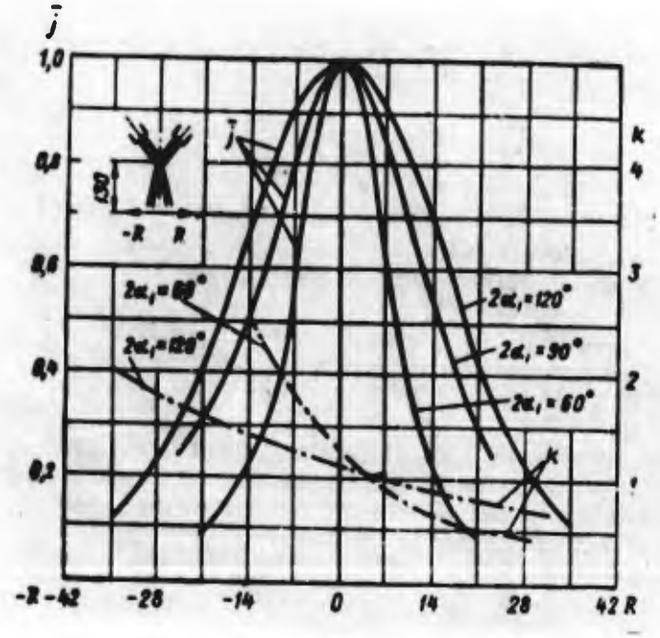

Fig. 3. Variation of relative flow tension $\bar{j}$ and coefficient k of relation of components in the central radial stream section of a twin-jet nozzle as a function of the angle $2\alpha_1$ of collision of the jets (R in mm).

The increase in the velocity and diameter of jets leads to a small decrease in the dispersion of the liquid in the radial stream section. As we move away from the nozzle, uniformity in the distribution of the liquid increases.

It should be noted that application of the normal law of distribution of errors (with the aim of obtaining) the approximation of the curves of the distribution of the liquid in the radial stream section does not yield positive results.

c) Relation of Components in the Stream

A typical picutre of flow tension distribution and the relation of components in the transverse stream section is shown in Fig. 4. Here are traced the curves of equal flow tension (solid lines) and curves of equal coefficients k (dotted lines) which correspond to the collision of water and kerosene jets (d_c = 1.5 mm, Δp = = 5 atmospheres, 2α = 60°). The calculated value for k = 1.1. It can readily be seen that the curves of equal k are virtually parallel to the trace of the main stream plane. As to the radial section, the coefficients k are so distributed as if the jets had been mutually "shot through". Yet, such a "shooting through" did actually not take place, inasmuch as the jets collided long before

their disintegration. This character of the distribution of the coefficients k is likely to be associated with the instability of the jet flow near the point of collision mentioned above.

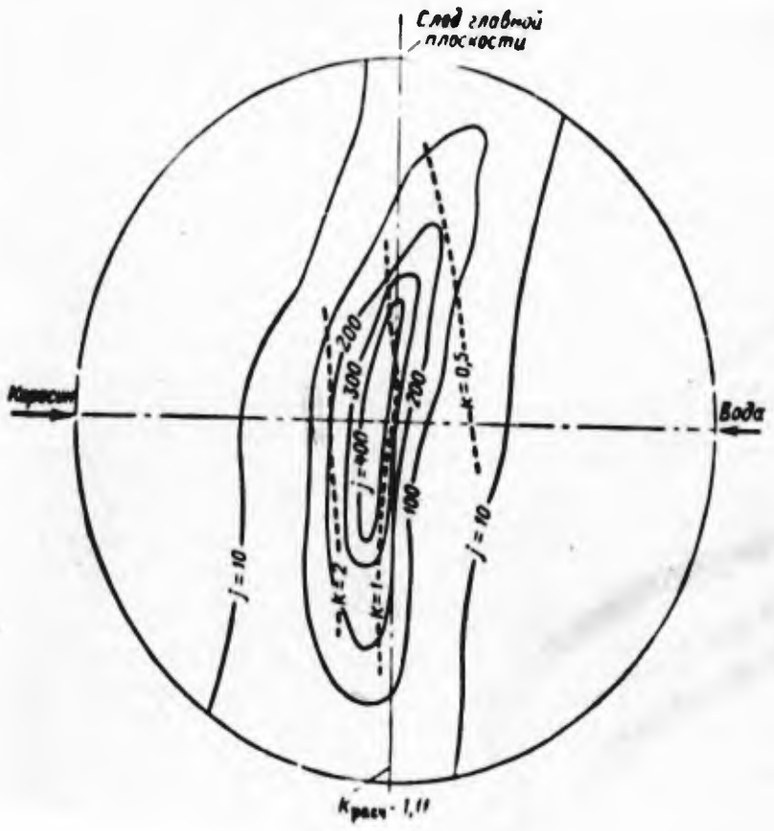

Fig. 4. Distribution of flow tension j and the component relation coefficient k in the transversal stream section of a twin-jet nozzle with Δp = 5 atmospheres, d = 1.5 mm and $\gamma\alpha$ = 60°. a) kerosene b) trace of main plane c) water d) small k_{ref}.

An increase in the angle of impinging jets promotes a more uniform distribution of the relation of components in the radial stream section. This is seen from Fig. 3 where the dotted lines indicate the distribution curves of coefficients k for $2\alpha_1 = 60$ and 120°.

An increase in [redacted] jet velocity also somewhat improves the mixing of the components, while changes in the jet diameters have virtually no effect on it.

d) Effect of Individual Injection Parameters on the Distribution of Liquids and the Relation of Components in the Stream.

The effect of the angle of collision, of the velocity and diameter of jets has been examined above. In the following it remains to be noted that the difference in velocities can be of considerable importance in the interaction of jets. Thus, if the velocity of one of them,[1] [redacted] exceeds the velocity of the other [redacted] by more than 20% ,then, as a result, the first jet will shoot through

---

(1) If the liquid densities are different, then we have to compare the normalized velocities $V\sqrt{\rho}$ inasmuch as pressure at the water divide point is determined by the kinetic energy of the liquid .

the second one. This xxxi impairs substantially the intermixing of liquids? On the contrary, a difference in the diameters at identical velocities does not substantially impair the intermixing of liquids. The lengths of jets does virtually not affect the character of their interaction provided coaxiality of collision is insured. Exx

Eccentricities of jets (non-coaxiality of collision) has a substantial effect on their interaction. Increases in eccentricity lead to a rotation of the main stream plane around the central axis. At the same time we observe a redistribution of the flow rate of the liquid in the transverse stream section, and intermixing of the components deteriorates. The magnitude of the eccentricity of jets can best be evaluated by the rotation angle of the main stream plane. Rotation by an angle of more than 30° can lead to a considerable deterioration of intermixing. Insofar as increases in the jet length promote increases in linear eccentricity, they should be limited to 1 to 5 calibers.

Counterpressure does generally affect but slightly the character of the distribution of flow rate and relation of components in the stream.

There are two known systems of outflow of jets from single-jet

nozzles: a continuous one and a broken-up one. In the first case, the jet diameter is equal to that of the sprayer nozzle while the velocity in the jet is 20% less than the theoretical one; in the second case, the jet diameter is smaller than the nozzle diameter by a quantity depending on the angle of the inlet edge, while the velocity in it is virtually equal to the theoretical one. Moreover, in the case of broken-up outflow conditions, the jet after leaving the nozzle disintegrates more rapidly. The preferable among the operating conditions of sprayers with impinging jets is the broken-up one.

A serious drawback of twin-jet sprayers is the rejection of the liquid toward the rear half-plane of the stream. Three-jet sprayers with three jets lying in one plane and impining in one point are free from this drawback. The importance of the central jet consists in that it diverts the rear film towards the front half-plane of the stream while interacting with the former. In so doing, the central jet itself splits up into arms which are placed symmetrically in the peripheral areas of the mean stream plane. As to the rest, the distribution of the rate of flow in the front sector of the main stream plane is identical with that of the twin-jet sprayer, as is

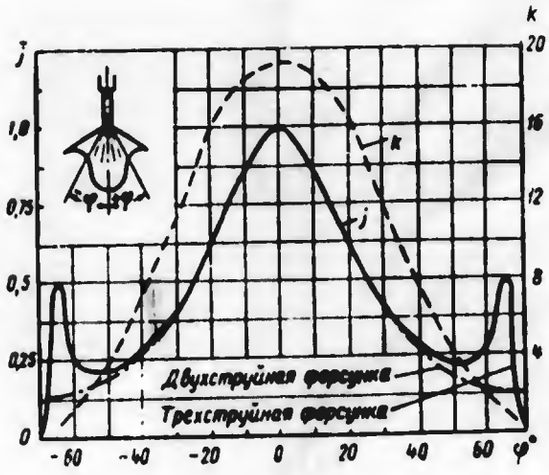

Fig. 5. Distribution of relative flow tension $\bar{J}$ and the coefficient of component relationship k in the main plane of the jet of a three-jet sprayer nozzle. a) Twin-jet sprayer nozzle b) Three-jet sprayer nozzle.

seen in Fig. 5, which shows the dependence of relative flow tension on the angle φ (solid line). The broken line shows the distribution of the relation of components in the main stream plane corresponding to the case where water is fed through lateral nozzles and kerosene through the central ones. The excess of water in the core of the jet and the excess of kerosene in the peripheral areas corroborate the statement made above concerning the breaking up of the central jet. This is the situation if the reduced jet velocities are approximately identical. Yet, the increase in the reduced velocity of the central kerosene jet by 1.35 times with respect to the lateral water jets made it possible to obtain a virtually uniform distribution of the relation of components in thetransverse jet section.

In other respects, the effect of the angle of collision, jet velocity and diameter on the distribution of the liquid in the stream of three-jet sprayers is identical with that of twin-jet sprayers.

Thus, in a number of cases, three-jet sprayers can be considerably better mixing devices than twin-jet ones.

REFERENCES

1. Li D., Issledovaniye Raspredeleniya Topliva v Strue, kn. "Dvigateli

Vnutrennego Sgoraniya", (Investigation of Fuel Distribution in Jets, "Internal Combustion Engines"), Vol. V, ONTI NKTP, 1936.

2. Forkhgeymer F., Gidravlika "Hydraulics", Vol. V, ONTI NKTP, 1935

3. Bond, W., The surface tension of a moving water sheet. "The procedings of the physical society", 1935, vol.47, No.2_1.

4. Kretschmar, G., Wedaa H., An optical method for the study of impinging jets in a liquid stream. "Journal of the Optical Society of America", 1953, vol.43, No.6

ON ATOMIZING LIQUIDS BY SPRAYERS WITH IMPINGING JETS

By

I.G. Panevin

In the present article are briefly set forth the results of an experimental and theoretical investigation of the spraying of liquids mainly by means of twin-jet sprayers with impinging jets.

The process of spraying of liquids by means of sprayers with impinging jets has never been studied theoretically, and very little experimental work has been done on this subject.

In experimentally investigating the operation of various types of diesel sprayers, D. Li (3) established that sprayers with impinging jets produce sprays of lower quality than single-jet nozzles (the homogeneity of spraying deteriorates and the size of drops increases). Heidmann and Humphrey (9) studied the collision process of liquid jets with the aid of spark photography and photoelectric devices. They found that as a result of the disintegration of a liquid film forming at the point of collision of jets there occurred the formation of a group of drops recalling in its form concentric waves. According to the authors, the frequency of these

waves grows proportionally with the velocity of the jets, decreases slightly with an increasing angle of collision and depends but slightly on the diameter of the jets. Fry and Thomas (7) studied the collision of two water jets in order to obtain a fire-fighting sprayer. They measured the fineness of spraying by capturing the drops in castor oil. Inasmuch as in this medium the drops tend towards intensive coalescence we may assume that the quantitative data obtained by the authors are somewhat too high. They obtained an experimental dependence of the median drop diameter x_m on jet velocity V and the angle of collision $2\alpha_1$:

$$x_m = 0{,}775 - 0{,}005V\cos\alpha_1 \text{ mm.} \qquad \text{A 85}$$

This dependence was obtained for a jet 1.5 mm in diameter. Its linear character is worth noting. There appear to be no sufficient reasons for the introduction in the formula of the angle of collision inasmuch as the data of the authors are determined with the same degree of accuracy by the dependence $x_m = a - bV$. The effect of the angle of collision and of the jet diameter on the quantity x_m was not sufficiently apparent.

Although many theoretical works have been devoted to the study of the spraying process of liquid jets, a common point of view on

this subject has not been elaborated as yet. At the present time, there are three theories of spraying which are based on a different understanding of the nature of this phenomenon. The first theory associates this process with fluctuations on the surface of liquid jets, the second connects it with the effect of the surrounding gaseous medium on the jet and the third with turbulent pulsations in the jet. The two latter theories have meaning only in the case of high velocities of the liquid (50 to 100 m/sec and more), whereas the first theory is valid in the case of low velocities (up to 10 to 15 m/sec). When investigating the intermediate range of velocities (15 to 50 m/sec) which frequently occur in practice, it is necessary to take into account both the fluctuations of the jet surfaces and the effect of the surrounding gas.

The conditions of disintegration of a motionless cylindrical circular jet under the action of surface tension forces were investigated for the first time by D. Reley (5). He showed that axially symmetric turbulences whose length is 4.44 times that of the jet diameter are the most unsteady ones. Reley's theory is also valid in the case of low jet velocities (up to 15 m/sec). Oka (10) examined the disintegration of a ring of liquid under similar conditions and found that it breaks

up under the action of the same axially symmetrical fluctuations. V. N. Blinov (1) attempted to apply Reley's theory to high velocities (up to 30 m/sec) . In so doing, he showed, proceeding from A. S. Predvoditelev's hypothesis on the possibility of resonance of the jet and the drop, that also non-spherical cylindrical jets can disintegrate, which, as is known, does not ensue from Reley's theory. The experimental results obtained by V. N. Blinov have adequately corroborated his theoretcial conclusions. K. Veber (2) developed Reley's theory of disingtegration of spherical cylindrical jets by introducing into the investigation the effect of the liquid viscosity and then also the effect of the gaseous medium. The calculating formulas, however, permitting to calculate the viscosity of the liquid, were obtained by him only for the simplest cases.

York, Stubbs and Tek (6) have investigated from a theoretical point of view the stability of a film of a nonviscous liquid flowing on a plane wall, taking into consideration inertia forces, surface tension and aerodynamic forces. The problem was solved by the method of small fluctuations. The substantial drawback of this work consists in that the authors did not obtain an expression for

the optimal determination of the optimal wave length in analytic form. Squire (11) undertook a theoretical investigation of the problem relating to the stability of a plane liquid film moving in a gaseous medium. In so doing, he studied only the case of nonsymmetrical fluctuations and also confined himself to the assumption that the relative length of waves arising on the surface of the film is great.

After terminating the present work, the author became acquainted with the paper by Haggerty and Shea (8) published in December 1955. While investigating in this paper the same problem as in (11), the authors analized both nonsymmetrical and symmetrical turbulences on the surface of the liquid film. On the basis of the same simplifying assumptions on great relative wave lengths, the authors solved the problem relating to the boundary of film stability by the fluctuation frequency of surface waves. Expressions for the determination of optimal wave lengths were not obtained. Thus, the above theoretical works have failed to solve completely the problem relating to the stability of a plane liquid film moving in a surrounding gaseous medium. The basic drawback to these works consists in that they do not consider the case of short waves prevail-

ing in the velocity range under investigation, and also do not provide an expression for the analitical determination of optimal wave lengths.

1. THEORETICAL INVESTIGATION

In his preceding paper "On the Distribution of Liquid in the Spray of a Nozzle with Impinging Jets" (1), the author investigated the problem relating to the spreading of a liquid film forming by two impinging jets. Below we examine the breaking-up of this film into drops. This problem is solved in the following three stages: first we study the conditions of film stability, then we examine the breaking up of the film into individual streaks and, finally, we investigate the disintegration of streaks and the formation of drops. In order to simplify our task, we assume that the film is plane and unlimited in the plane xz, and that its motion is progressive. The liquid and the gas surrounding it are considered to be nonviscous and noncompressible.

(1) See page 72 to 84.

Stability of Films

Let the film with the thickness 2h (Fig. 1) move in a stationary gas medium at a velocity V. On the interface between the liquid and the gas, surface tension forces and inertial forces are acting. This may lead to the loss of stability in the film. Let us apply the method of small fluctuations. This method consists in that on the interface surfaces we assume the existence of small harmonic fluctuations with a wide spectrum of frequencies, which, in the course of time, and under the action of the above forces, may either damp or remain harmonic or, finally, increase in their amplitude, which must lead to the disintegration of the film. The problem consists in finding the stability boundaries for the film by the frequency of oscillations and by determining an optimal wave length, i.e., the length of the wave of that perturbation which grows fastest in time.

The mathematical problem amounts to a simultaneous solution of the equation of the basic film motion and the small oscillations of the liquid and gas, and to checking the solution obtained for stability. We assume that the motion of the film and gas are bidimensional (in the plane xy). The equations of interface motion can be written as follows:

written as follows:

$$y = h + \eta; \quad \eta = \eta_0 e^{i(\sigma\tau + kx)}, \tag{1}$$

where y is the ordinate of the interface point investigated;

η_0 is the initial amplitude of a small perturbation;

τ is the time ;

$\sigma = 2\pi / T_B$

$k = 2\pi / \lambda$

λ is the wave length;

T_B is the oscillation period.

The oscillations of the upper and lower boundaries of the film must agree with one another (A). There can be two cases of such agreement: nonsymmetrical oscillations, when the surfaces oscillate in the phase ($\eta_1 = \eta_2$), and symmetrical oscillations when $\eta_1 = -\eta_2$. Here and below, the indices "1" and "2" denote the parameters referring to, respectively, the upper and lower half-planes (see Fig. 1).

Since the motion of the liquid and gas are considered potential, the continuity equation may be written as a Laplace equation

$$\frac{\partial^2 \varphi}{\partial x^2} + \frac{\partial^2 \varphi}{\partial y^2} = 0, \tag{2}$$

where φ is the potential of the liquid or gas.

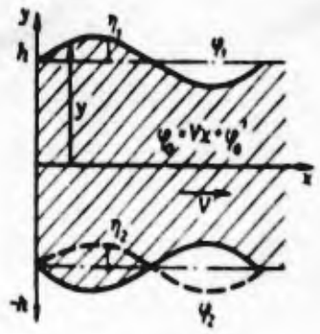

Fig. 1. Wave-like perturbations on the surface of a liquid film.

By solving equation (2) in its general form by taking into consideration equation (1) we find the expression for the determination of the potential of the liquid velocity

$$\varphi_0 = Vx + [A\,\mathrm{ch}\,(ky) + B\,\mathrm{sh}\,(ky)]\,e^{i(\sigma t + kx)}. \qquad (3)$$

Likewise, we obtain for the gas

$$\varphi_s = (M_s e^{ky} + N_s e^{-ky})\,e^{i(\sigma t + kx)}, \qquad (4)$$

Where s = 1.2.

The values of the coefficients in (3) and (4) can be determined by means of examining the boundary conditions (4):

$$1)\left[\frac{\partial\varphi_s}{\partial y}\right]_{y=+\infty}=0;\quad 2)\left[\frac{\partial\varphi_1}{\partial y}\right]_{y=h}=\pm\left[\frac{\partial\varphi_2}{\partial y}\right]_{y=-h};$$

$$3)\left[\frac{\partial\varphi_0}{\partial y}\right]_{y=h}=\pm\left[\frac{\partial\varphi_2}{\partial y}\right]_{y=-h}. \qquad \text{A 88}$$

In the given case, the fourth, kinematic boundary condition takes the form:

$$4)\left[\frac{\partial\varphi_s}{\partial y}\right]_{y=h}=\frac{\partial\eta_s}{\partial t}\quad\text{и}\quad\left[\frac{\partial\varphi_0}{\partial y}\right]_{y=h}=\frac{\partial\eta_0}{\partial t}+V\frac{\partial\eta_0}{\partial x}. \qquad \text{B 88}$$

The fifth dynamic boundary condition can be written as

$$5)\ p_0-p_s+T\frac{\partial^2\eta_0}{\partial x^2}=0, \qquad \text{A 89}$$

where T is the coefficient of surface tension;

p is the pressure.

For a non-stabilized motion which takes place in the case under investigation, the energy equation can be written as a Lagrange equation;

$$\frac{\partial\varphi}{\partial t}+\frac{V^2}{2}+\frac{p}{\rho}=\text{const}, \qquad (5)$$

where ρ is the density of the corresponding medium.

The rate of the flow of the liquid or gas are determined by formula

$$V=\sqrt{\left(\frac{\partial\varphi}{\partial x}\right)^2+\left(\frac{\partial\varphi}{\partial y}\right)^2}. \qquad (6)$$

By utilizing the five boundary conditions as well as equations (1), (5), and (6), we can determine all the unknown coefficients in the expressions (3) and (4) excepting the initial amplitude η_0. By dropping the intermediate operations we obtain for the case of symmetrical and nonsymmetrical oscillations

$$\sigma_c = \alpha_c \pm i\beta_c \text{ и } \sigma_n = \alpha_n \pm i\beta_n, \tag{7}$$

where

(8)

$$\alpha_c = -\frac{kV \operatorname{cth}(kh)}{\bar{\rho} + \operatorname{cth}(kh)}, \quad \beta_c = k\sqrt{\frac{\bar{\rho}\operatorname{cth}(kh)V^2}{|\bar{\rho} + \operatorname{cth}(kh)|^2} - \frac{Tk}{\rho_0|\bar{\rho} + \operatorname{cth}(kh)|}};$$

$$\alpha_n = -\frac{kV \operatorname{th}(kh)}{\bar{\rho} + \operatorname{th}(kh)}, \quad \beta_n = k\sqrt{\frac{\bar{\rho}\operatorname{th}(kh)V^2}{|\bar{\rho} + \operatorname{th}(kh)|^2} - \frac{Tk}{\rho_0|\bar{\rho} + \operatorname{th}(kh)|}}. \tag{9}$$

Here $\bar{\rho} = \rho_1/\rho_0$ is the relative density of the gas which, in most cases, does not exceed 0.1.

Taking into consideration (1), expression (7) takes the following form:

$$\eta = \eta_0 e^{-\beta t} e^{i(\omega t + kx)},$$

B 89

whence it is seen that depending on the value for β, three cases of oscillations are possible: damped ($\beta > 0$), harmonic ($\beta = 0$) and rising ($\beta < 0$) oscillations when the amplitude grows with time according to the exponential law ($\eta = \eta_0 e^{\beta t}$).

From expression (7) it is seen that with symmetrical and non-

symmetrical oscillations $\beta < 0$ is possible. Thus, both these oscillations of 2 types can lead to the disintegration of the film.

Figure 2 shows the increment dependence of the growth of oscillations β on the relative wave length $\bar{\lambda} = \lambda/h$ obtained by computation. This computation was performed for the case of a water film 0.2 mm thick moving in an air medium at atmospheric counterpressure and normal temperature ($\bar{q} = 0.0012$, T = 74 dyn/cm). The rate of flow of the film corresponds to four values for the pressure differential at the nozzle (Δp = 1; 3; 5 and 10 atmospheres). It is seen in Fig. 2 that at any flow rate on the film surface there must exist both damped (short) and growing (long) waves. Waves with the length λ_0 determine the boundary of stability. β = 0 corresponds to these waves, while the maximum values for β corresponds to waves with an optimal length λ_{opt}. In the general case, the value for β is greater for nonsymmetrical oscillations, although with a growing film velocity the difference between $\beta_н$ and β_c decreases. At the same time λ_0 and λ_{opt} also ~~xorx~~ grows smaller.

Fig. 2. Dependence

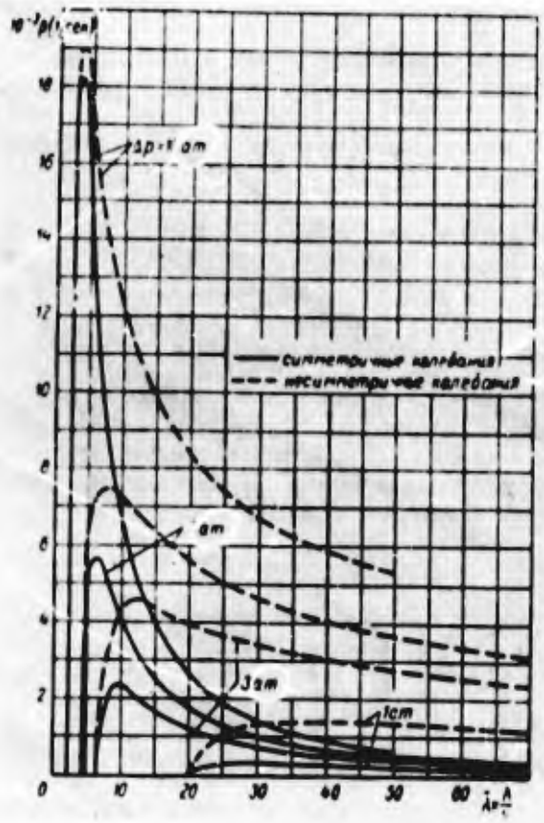

Fig. 2. Dependence of the Increment in the Growth of Oscillations β on the Relative Wave Length $\bar{\lambda}$ at Varying Pressure Differentials at the Nozzle. a) Symmetrical oscillations b) nonsymmetrical oscillations.

Tmx

In order to determine the values for λ_{opt} let us investigate the expressions (8) and (9) for the extremum. For this purpose we differentiate them with λ and set them equal to zero. We disregard the terms containing $\bar{\varrho}^{-2}$ and obtain for the symmetrical and nonsymmetrical oscillations, respectively:

$$W_c = a\varphi_1(a) + \frac{1}{\rho} a\varphi_2(a) \tag{10}$$

and

$$W_n = a\psi_1(a) + \frac{1}{\rho} a\psi_2(a). \tag{11}$$

where $W = V^2 \varrho_0 h/T$ is the Weber criterion;
$\alpha = 2\pi/\bar{\lambda}$.

The first terms of expression (10) and (11) can be neglected, the permitted error with $\varrho \leqslant 0.01$ not exceeding 1%. Then, from (10) and (11) We obtain the value for the optimal wave length for symmetrical ani nonsymmetrical oscillations:

$$(\lambda_{opt})_c = 2\pi \frac{T}{\rho_1 V^2} \varphi_2(a) \tag{12}$$

and

$$(\lambda_{opt})_n = 2\pi \frac{T}{\rho_1 V^2} \psi_2(a). \tag{13}$$

The coefficients

$$\varphi_2(a) = \frac{\operatorname{cth}^3 a + \frac{3}{a}\operatorname{cth}^2 a + \operatorname{cth} a}{\operatorname{cth}^3 a + \frac{2}{a}\operatorname{cth}^2 a + \operatorname{cth} a} \tag{14}$$

and

$$\psi_2(a) = \frac{\operatorname{th}^3 a + \frac{3}{a}\operatorname{th}^2 a - \operatorname{th} a}{\operatorname{th}^3 a + \frac{2}{a}\operatorname{th}^2 a - \operatorname{th} a} \tag{15}$$

remain virtually constant over the entire range of wave lengths ($\bar{\lambda} > 10$), where $\varphi_r \approx 1.3$ and $\psi_r \approx 2.0$. If $\bar{\lambda}$ drops to 5, the value for φ_r and ψ_r decreases by 10 to 15 %. With a further decrease in $\bar{\lambda}$, the decrease in φ_r and ψ_r is even more abrupt.

We find the boundary of stability from the stipulation $\beta = 0$. From (8) and (9), neglecting the quantity $\bar{\varsigma}$, we obtain for both types of oscillations

$$\lambda_0 \approx 2\pi \frac{T}{\rho_1 V^2}. \qquad (16)$$

It is ~~xxcc~~ interesting to note that λ_{opt} and λ_0 do not depend on the film thickness, at least in the field of long waves.

Breaking-Up of the Film in Individual Streaks

It is obvious that the waves with $\lambda = \lambda_{opt}$, with the greatest increment in the growth of oscillations, will grow more rapidly with time, hence it may be expected that it is this turbulence which will lead to a breaking-up of the film. In the problem of impinging jets under investigation, film thickness changes according to the hyperbolic law hr = const rather than remaining constant. This was already noticed earlier. In spite of this, however, owing to the fact that λ_{opt} does not depend on the film thickness, we may assume that the annular streaks which broke off from the film will have an

initial width equalling λ_{opt} . Hence it ensues that the radius of the cylindrical section of the ring must equal

$$R_0 = \sqrt{\frac{2\lambda_{opt}}{\pi}}. \qquad (17)$$

Let us assume that the film disintegrates under the effect of symmetrical oscillations. We also assume that the growth in the amplitude begins at a certain small distance r_1 from the point of collision and that at a distance r the amplitude of turbulence becomes equal to half the film thickness as a result of which the latter breaks up and a ring separates from it. Considering β constant and equalling a certain mean quantity β_{mean} in the section where the film is disrupted, we obtain the following expression for the determination of the film thickness at the point of rupture:

$$\ln\left(\frac{h}{h_0}\right) = \frac{r\beta_{mean}}{V}\left(\frac{h_1}{h} - 1\right). \qquad (18)$$

where V is the rate of film motion.

It is convenient to solve equation (18) graphically by assigning the quantity r_1 and determining the quantity η_0 experimentally (it can be readily computed with the aid of formula (18) itself by changing preliminarily the length of the continuous film r).

Breaking-Up Of Rings into Drops

The ring which broke off from the film has initially a non-

circular section (the shape of this section is something inbetween a rectangle and an ellipse). For this reason, when analyzing the stability of the ring, Reley's and Oka's conclusions may not be applied. Let us use Blinov's method for this purpose. It is true, that in this case, the aerodynamic forces influencing the ring will not be taken into account, yet, in the range of velocities under investigation, they may be disregarded in the first approximation, especially since it is extremely difficult to obtain a precise solution of the given problem owing to the fact that the formation and disintegration process of rings is actually much more complex than the simplified picture described above.

Following Blinov (1) we determine the oscillation period of a noncircular cylindrical liquid column

$$T_c = 2\pi \sqrt{\frac{\rho_0 R_0^3}{T} \frac{1}{n_1(n_1^2-1)}}; \qquad \text{A 92}$$

here, the factor n_1 characterizes the shape of the transverse ring section ($n_1 = 2$ is an ellipse; $n_1 = 4$ is a square, etc.). The oscillation period for a drop

$$T_c = 2\pi \sqrt{\frac{r_{drop}^3 \rho_0}{Tn(n-1)(n+2)}}, \qquad \text{B 92}$$

where r_{drop} is the radius of the drop and n characterizes the order

of oscillation frequency of the drop. Basic frequency corresponds to $n = 2$.

Proceeding from Predvoditelev's hypothesis on the resonance of jets and drops ($T_j = T_d$), owing to which there may occur the disintegration of a noncircular jet, assuming $n = 2$ and $n_1 = 3$ (x) (the mean between $n_1 = 2$ and $n_1 = 4$) and using formulas (12) and (17), we obtain the unknown drop diameter

$$d_k = \pi \sqrt{\frac{Th}{\rho_1 V^2}}. \qquad (19)$$

2. THE TEST

The investigation was carried out with an installation described above. (xx) We studied the effect of the basic injection parameters on the process of spraying in a twin-jet nozzle. As a working liquid we used water. The diameter of the nozzles ranged from 1 to 2 mm, the angle of collision from 40 to 160° and the pressure differential at the nozzle from 1 to 15 atmospheres. The drops were caught on a smoke-stained plate with the aid of a special device. This device

(x) The selection of $n_1 = 3$ is formal. Nevertheless, the numerical coefficient obtained in formula (19) as a result of such a selection comes very close in its magnitude to the experimental one.
(xx) See page 72 to 84.

made it possible to place the plate at any point of the jet and open it for a determined, extremely short period of time. Virtually, this device did not cause any turbulence in the jet of the nozzle. It was placed at a distance of 150 to 250 mm from the point of collision of the jets. The layer of carbon black exceeded by 1.5 and more times the diameter of the largest drops (for this reason the diameter of the drop impression was assumed to equal the actual drop diameter). The drop impressions were measured under the microscope with a 80-fold magnification. Spark photography of these spray jets was effected according to the shadow method in a camera obscura with the flare of a spark discharge. For this purpose we utilized a condenser with a capacity of 0.02 microfarad and a working voltage of 10 to 20 kv.

The measuring results of drop impressions were processed in the usual manner: we determined the dependence of the distribution of the relative drop weight G along the diameter x. As is known, the distribution curves are satisfactorily described by the equation

$$1-G=e^{-\left(\frac{x}{\bar{x}}\right)^n}, \qquad \text{A 93}$$

where $\bar{x}$ is the dimension constant;

n is the distribution constant.

For this reason the experimental functions obtained were plotted on a diagram with the coordinates log log 1/1 - G, log x, where they were approximated with the straight lines log log 1/1 - G = n log x + const. The distribution constant n was determined as the tangent of the inclination angle of the above straight line to the axis x. As the characteristic dimension of drops we took the median diameter x_m corresponding to G = 0.5. The scattering of experimental points around the approximating straight line was small since in order to determine one value for x_m we measured from two to five thousand drops.

As a result of spark photography of the spray jet of a twin-jet nozzle we established that the liquid film forming at the point of collision of two jets can disintegrate under the action of both symmetrical and nonsymmetrical oscillations. The development of symmetrical oscillations is shown in Fig. 3 a and b , that of non-symmetrical oscillations in Fig. 3 c. In all three cases the out-flow conditions of the jet were abrupt. It should be noted that only in the case of broken up jet outflows does one observe in pure form both types of film oscillations which alternate continuously; continuous

outflow results in a mixed type of film oscillations, as shown in Fig. 3 d and e (excepting the outflow system, the test conditions for all five spark photographs were identical; nozzle diameter 1.5 mm, angle of impinging jets 100°, pressure differential at the nozzle 1 atmospheres). Generally, the wave length corresponds satisfactorily to the theoretical values of λ_{opt}. Yet, with increasing film rates the actual wave length begins to somewhat exceed the theoretical one, while in the range of $V > 25$ m/sec there begin to appear intensive turbulences with great wave lengths.

Let us investigate the effect of the basic injection parameters on the spraying of the liquid by a twin-jet nozzle.

The film rate has a sizeable effect on the fineness of the spray as is seen in Fig. 4, which shows the experimental dependence of the median drop diameters x_m on the film rate V (it is assumed that the film rate equals the theoretical jet outflow velocity). Outflow conditions were abrupt. The experimental points corresponding to the five pressure differentials at the nozzle (Δp = 1, 5, 10 and 15 atmospheres) are well approximated with the straight line

$$x_m = 0{,}320 - 0{,}0028V \text{ мм},$$

where V is the velocity in m/sec .

Comparison of this function with Fry's and Thomas' formula shows that from a qualitative point of view they describe the spraying process in the same way. Yet, the latter yields a slightly excessive value for x_m as compared with the former. This is likely to be explained by the forthcoming shortcomings in the measuring procedure of the fineness of the spray utilized by the above authors, as we pointed out earlier. Figure 4 shows also the theoretical function $x_m = f(V)$ obtained with formulas (18) and (19).

The film thickness was determined by the following formulas

$$h_1 = \frac{d_c^2}{4r} \frac{\cos^2 \alpha}{1 + \sin^2 \alpha - 2 \sin \alpha \cos \varphi}, \qquad \text{B 94}$$

where $\alpha = 90° - \alpha_1$;

φ is the angle in the main spray plane read from the central axis.

In all of the computations the quantity $\eta_0 = 0.11$ mm, determined by the method described above, was considered constant. The correspondence of experimental and theoretical results was found to be sufficiently adequate.

The linear character obtained for the function $x_m = f(V)$ does in no way contradict the fact that the quantity η_{opt} with growing

film velocities decreases in an inversely proportional way to V^2 since at the same time the film thickness increases at the disruption point (owing to increasing β the length of the continuous film decreases).

The ditribution constant n for the above values of Δp was found to equal respectively 2.53; 2.28; 2.12; 2.0 and 1.98. In the case of continuous jet outflow (Δp = 1 atmosphere) n = 2.4.

The jet diameter also exerts a rather strong effect on the fineness of spray. This is seen in Fig. 5 which shows the experimental and theoretical dependence of x_m on the nozzle diameter d_n at Δp = 5 atmospheres. In the case of abrupt outflow conditions, the jet diameter amounted to 0.8 d_n. The correspondence between theory and test was found to be satisfactory. The quasi-linear character of these functions is explained by the fact that according to formula (19) the drop diameter grows proportionally with the jet diameter provided $h \sim d_n^2$. At the same time, however, the film thickness somewhat increases at the rupture point (owing to increasing β). The distribution constant n for d_n = 1.0; 1.5 and 2.0 mm turned out to be equal to 2.6; 2.12 and 2.01.

The angle of collision is the third factor which strongly

affects the fineness of spray. Figure 6 shows the experimental and theoretical dependence of x_m on the angle of collision of jets 2α. As in all the tests mentioned above, also here the fineness of spray was measured in the jet core or, more exactly, in the central radial section. The increase in the drop diameter with a decreasing angle of impinging jets is explained by the fact that the film thickness grows in the section under investigation. In the present tests the nozzle diameter amounted to 1.5 mm, jet outflow conditions were abrupt, Δp = 5 atmospheres. A slight excess of the experimental data as compared to the corresponding theoretical values in the case of large angles of collision may be evidence of the fact that with increasing angles of collision the film velocity somewhat decreases, as compared with jet velocities, owing to losses of energy from collision. This difference, however, is small.

The collision constant n for the angles of collision of 60, 80, 120 and 140° equalled respectively 1.68; 2.08; 2.12 and 2.14.

Figure 7 shows the results of measuring x_m in various radial jet sections within sector limits $\varphi = \pm 30°$. As was to be expected, the drop dimensions diminish as they move away from the central

jet axis, provided this corresponds to a decrease in the film thickness. The experimental points fall satisfactorily on the theoretical curve. Counterpressure has a slight effect on the fineness of spray. Thus, an increase in counterpressure from 1 to 6 absolute atmospheres caused to decrease x_m only by 5 to 7%. A decrease in λ_{opt} with increasing g, is accompanied simultaneously by an increase in the film thickness at the rupture point owing to an increase in . As a result, the second process neutralizes to a considerable degree the first process.

Non-coaxiality of impinging jets affects spraying only in those cases where, under its influence, there takes place a substantial change in the film thickness. A slight non-coaxiality has hardly any effect on the fineness of spray.

Jet length has virtually no bearing on the fineness of spray. When disintegrated jets impinge, the diameter of drops somewhat increases.

With a nonintermittent jet outflow the quantity x_m increases by 12 to 14% as compared with intermittent jet outflow at the same pressure differentials at the nozzle (see Fig. 3). This is connected with a decrease in the velocity and an increase in the jet diameter

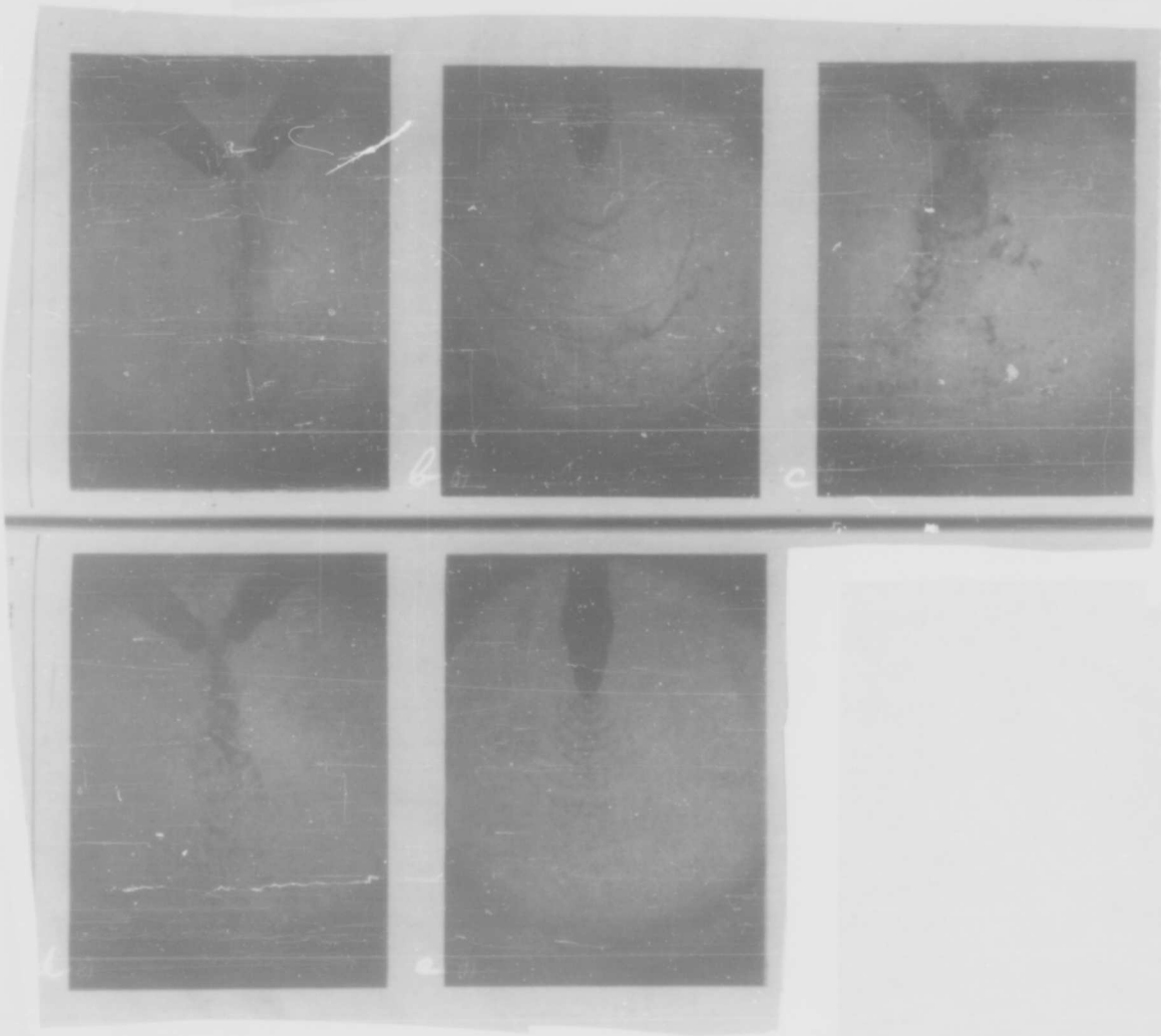

Fig. 3. Photograph of the spray jet of a twin-jet nozzle, obtained by means of spark photography. a),b) intermittent jet outflow conditions, symmetrical waves. c) intermittent jet outflow conditions, nonsymmetrical waves d),e)nonintermittent jet outflow conditions.

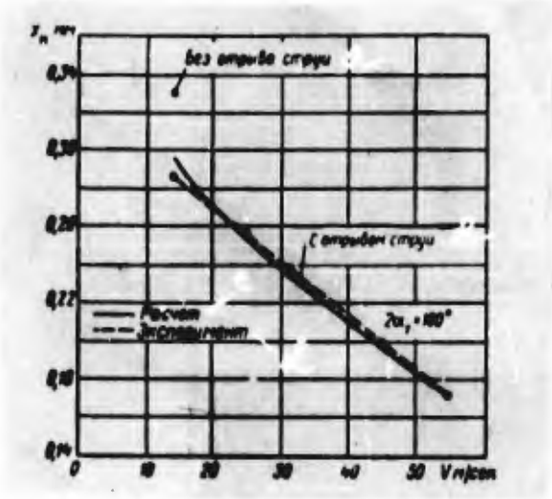

Fig. 4. Dependence of median drop diameter on jet velocity.
a) without breaking-up of the jet b) with breaking-up of the jet.
c) computation d) test.

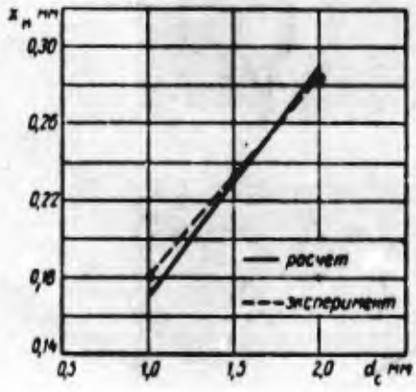

Fig. 5. Dependence of median drop diameter on the nozzle diameter.
a) computation b) test.

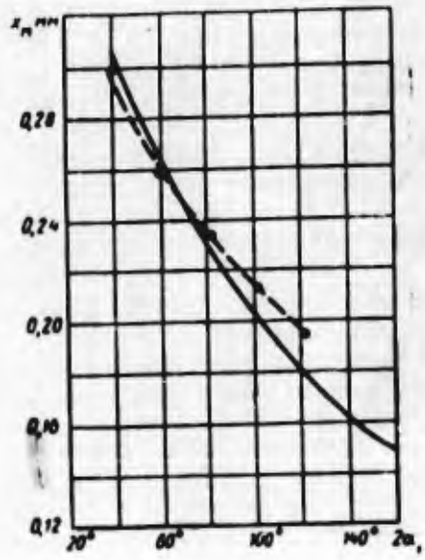

Fig. 6. Dependecne of median drop diameter on the angle of impinging jets.

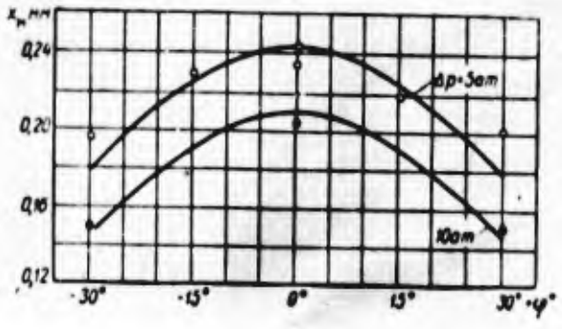

Fig. 7. Variation of the median jet diameter in the main jet plane.

as well as with an earlier disintegration of the film.

Variations in the film thickness in the main jet plane of twin-jet nozzles with impinging jets results in a deterioration of the homogeneity of spray, as was noted by D. Li (3). It is obvious that a single centrifugal nozzle can produce a more homogeneous spray since the thickness of the sheet flowing out of such a nozzle has an approxiamtely constant thickness over its entire perimeter. Nevertheless, in those cases where a lesser homogeneity of spray is desirable (for example, in order to increase the thickness of the combustion front in ZhRD, etc.), nozzles with impinging jets are to be preferred.

The effect of the basic injection parameters on the spray of the liquid of a three-jet nozzle with jets lying in the same plane and intersecting at one point, is virtually the same as that of a twin-jet nozzle.

As a result of the investigation of spraying of liquids by nozzles with impinging jets, we obtained reference dependences which make it possible to compute the median drop diameter in the jet of a twin-jet nozzle. For a more exhaustive check of the conclusions obtained, however, it is necessary to study experimentally

the effect of surface tension, as well as other physical properties of the liquid, on the fineness of spray.

REFERENCES

1. Blinov V. N., O. Dispepsnosti Tekhnicheski Razdroblennoy Vody, Izd. VTI (On the Dispersity of Technically Disintegrated Water, VTI Press), 1931.

2. Veber K., Raspad Strui Zhidkosti, "Dvigateli Vnutrennego Sgoraniya" (Breaking-up of a Liquid Jet, "Internal combustion engines"), vol. 1 ONTI NKTP, 1936.

3. Li D., Vliyaniye Konstruktsii Sopla i Usloviy Raboty Na Raspylivaniye i Raspredeleniye Topliva, "Dvigateli Vnutrennego Sgoraniya" (Effect of Nozzle Design and Operating Conditions on the Spraying and Distribution of Fuel, "Internal combustion engines"), vol. 1, ONTI NKTP, 1936.

4. Lamb G., Gidrodinamika (Hydrodynamics), GITTL 1947.

5. Reley D., Teoriya Zvuka (The Theory of Sound), vol. 1, OGIZ 1944.

6. York Y., Stubbs H., Tek M., The Mechanism of disintegration of liquid sheets, Trans. ASME, 1953, vol. 75 No. 7.

7. Fry J., Thomas P., The production of fire-fighting sprays by

impinging jets, Engineering, 1953, vol. 179. No.7

8. Hagerty W., Shea J., A Study of the Stability of plane fluid sheets. Journ. Appl. Mech?, 1955, vol. 22, No. 4

9. Heidmann M., Humphrey J., Fluctuation in a spray forming by two impinging jets, Journ. Amer. Rock. Soc. 1952, vol. 22, No.3

10. Oka S., On the stability and breaking up of ring of liquid into small drops, Proc. Phys-Math. Soc. of Japan, 1936,vol.18 ser.3 No.9.

11. Squire H., Investigation of the instability of moving liquid film.Brit. Journ. Apll. Phys., 1953, vol.4, p. 167-169.

INVESTIGATION OF THE SPREADING OVER A WALL OF AN AXIALLY SYMMETRICAL JET

By

Candidate of Technical Sciences V. A. Kurochkin

The diagram of the spreading over a wall of a liquid jet is shown in Fig. 1.

An axially symmetrical steady jet of a noncompressible non-viscous liquid collides with a horizontal plane x, y which represents a solid unlimited wall, and spreads over it as a continuous sheet. The angle of collision between the jet axis and the plane is α. In a section I-I, which is sufficiently remote from the spreading plane, the velocity of the jet is equal to v_0. The rate of flow of the liquid in the jet equals Q.

At the contact point of the jet with the wall there forms a center of pressure from where the liquid in the form of a film spreads over the surface of the wall. The spreading process of this film can be descrbied by functions connecting the thickness h and the spreading velocity of the film v with the coordinates of the spreading plane.

In the literature hydrodynamics there are available some attempts to solve similar problems for an ideal liquid (4, 7) but the results of these investigations have been applied only to flows in the vicinity of a critical point (pressure center) with a perpendicularly falling jet.

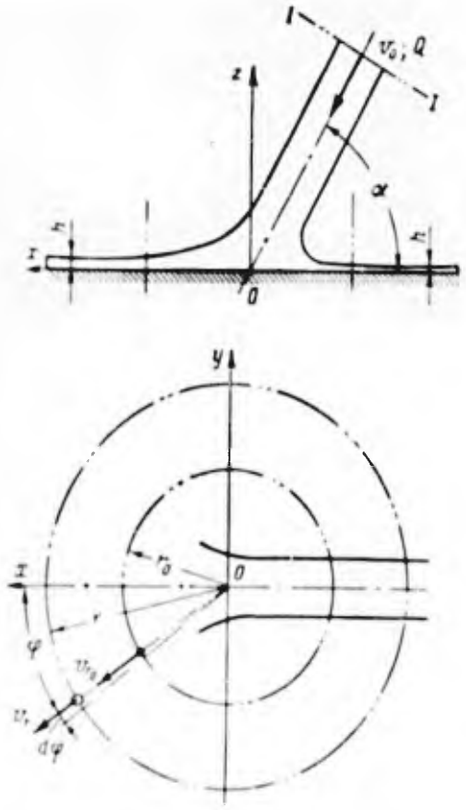

Fig. 1. Diagram of the spreading of a jet over a wall.

F. Wittenbauer (6) obtained a particular solution of the problem relating to the spreading of an axially symmetrical jet of an ideal liquid over a plane placed at an arbitrary angle with regard to the jet axis. This solution was purely theoretical, experimentally it remained unchecked.

For the realx case of the spreading of a jet over a wall there are known a few experimental data which bear evidence of the fact that the picture of the spreading of a jet of real liquid is substantially different from that of the spreading of a jet of ideal liquid.

The data available do not make it possible to determine by computation the film parameters with sufficient accuracy. In connection therewith we conducted an investigation of the above problem with the nrw purpose of obtaining the required experimentak and theoretical data for the computation of the film parameters.

1. CALCULATED DEPENDENCES

Theoretical investigations of the spreading of a liquid film beyond the boundaries of a cylindrical section with a radius r_0, sufficiently removed from the point of impact of the jet with the wall, have shown that in this field of flow the curvature of the

free surfaces is small while the flow lines are almost parallel to the spreading surface. If we lead aside the problem of the distribution of velocities of liquid particles over the film thickness and examine for each vertical on the plane of spreading only one value of velocity, which is a mean in size and direction, then for the above film flow area the basic assumptions of the [redacted] problem of [redacted] hydraulics of flows with free surfaces (3, 5) will be true. Moreover, the gas-hydraulic analogy between such flows and flows of compressible gas will also be true. The existence of such an analogy was for the first time pointed out by N. E. Zhukovsky (1).

Analysis shows that in the case of an impact of a jet with a wall, there occurs in the beginning a "turbulent" film flow similar to the supersonic gas flow, and that in the area of "turbulent" flow the spreading of the film from the point of impact of the jet with the wall at any angle of incidence of the jet must be radial. In this case the continuity equation and the equation of film motion written for the assigned flow scheme in a cylindrical system of coordinates take the following form:

$$v_r \frac{\partial v_r}{\partial r} = -g \frac{\partial h}{\partial r} + F_r, \tag{1}$$

$$\frac{\partial}{\partial r}(v_r h r) = 0, \tag{2}$$

Where g is the acceleration of gravity;

F_r is the projection of friction on the direction of the radius-vector r.

Integration of equations (1) and (2) enabled us to obtain the following analytical expressions for the determination of the velocity and thickness of the film

$$v_r h r = q, \tag{3}$$

$$v_r = \frac{\sqrt{n} q^{1-n} (2-n)}{4} \frac{v_0}{r_0 (r^{2-n} - r_0^{2-n}) + 1}, \tag{4}$$

where ν is the coefficient of kinematic viscosity;

q is the function of the distribution of the rate of flow during the impact of the jet with the wall,

which is numerically equal to the quantity of the total rate of flow of the liquid in the direction of the given radius-vector referred to the unit of the central angle. Below, this function will be called flow tension.

Losses of pressure head in order to overcome friction force were computed according to the conventional formula used in hydraulics for the determination of pressure head losses in conduits and pipes of non circular sections (3), written for elementary displacement as

A 104

$$dh_{tp} = -\frac{F_t}{g}\,dr = \lambda \frac{dr}{4R}\,\frac{v_r^2}{2g},$$

where R is the hydraulic radius which for flows with free surfaces and small depth equals the thickness of the flow h;

λ is the coefficient of hydraulic losses, represented by the power function $\lambda = A\,Re^{n}$ of the Reynolds number expressed by the velocity and thickness of the film;

$$Re = \frac{v_r h}{\nu}. \qquad \text{B 104}$$

The results of tests for the investigation of collision phenomena of two jets and of a jet with a wall show that energy losses from the impact of a jet with a wall are relatively small. This made it possible to take the velocity of the film v_{r0} in the initial cylindrical sections r_0 of the flow area investigated as approximately equalling the outflow velocity v_0 of the jet.

Formulas (3) and (4) make it possible to determine by computation the velocity and thickness of the film at any point of the plane of spreading. For these computations, however, it is necessary to know the value for the flow tension $q = q(\alpha, \varphi)$ and the coefficient of hydraulic losses $\lambda = f(Re)$.

The dependence for the determination of flow tension can be

obtained from the equation of continuity and the equation of quantity of motion written for the volume of liquid, comprised between the sections I-I and r as:

$$Q = \int_0^{2\pi} v_0 h_0 r_0 \, d\varphi. \tag{5}$$

$$Q v_0 \cos\alpha = \alpha_0 \int_0^{2\pi} v_0^2 h_0 r_0 \cos\varphi \, d\varphi + T_{fr} + T_{pr}. \tag{6}$$

Here T_{fr} is the projection of friction forces on the axis x;

T_{pr} is the projection of pressure forces on the axis x;

α_0 is the coefficient of the quantity of motion,

which characterizes the ratio of the actual quantity of motion in the section r_0 to the quantity of motion computed according to the mean film velocity in this section equalling v_0.

The projection of pressure forces on the axis x equals the projection of the resultant of these forces in the section r_0 but, keeping in mind the negligible film thickness, the value of this projection can be disregarded.

For an ideal liquid $\alpha_0 = 1$, $T_{fr} = 0$, hence, in this case, the system of integral equations (5) and (6) is in agreement with the particular solution

$$C_{id} = \frac{Q}{2\pi} \frac{\sin^2\alpha}{1 + \cos^2\alpha - 2\cos\alpha\cos\varphi}. \tag{7}$$

This function expresses the distribution of the rate of flow when a jet of ideal liquid collides with the wall. For an actual liquid the distribution of the rate of flow ~~with~~ will differ considerably from the ideal one, although the nature of the distribution will basically be determined by ~~the~~ a function of the form of (7), whence we may assume that for an actual case the function of the distribution of the rate of flow has the form

$$q = \frac{Q}{2\pi} \frac{k_0 \sin^2 a}{1 + \cos^2 a - 2 \cos a \cos a\varphi}. \qquad (8)$$

Here, we introduced an additional multiplier a taking into account the real conditions of interaction of the jet with the wall.

The value of factor k_0 is determined by the equation of continuity (5):

$$k_0 = \frac{\pi}{\sin^2 a} \frac{1}{\int_0^{\pi} \frac{d\varphi}{1 + \cos^2 a - 2 \cos a \cos a\varphi}}. \qquad (9)$$

Equality (8) must ~~be~~ also satisfy equation (6), whence we could also determine the additional multipliers a. Yet, to do this, it is necessary to know the value of the factor a_0 and ~~the~~ of ~~the~~ friction T_{fr} when the jet collides with the wall. Since it appears impossible to determine theoretically these values, mulitiplier a must be determined experimentally.

2. RESULTS OF EXPERIMENTAL INVESTIGATIONS

The distribution of the rate of flow when a jet collides with a wall was studied with the aid of jet gauges. The design of these devices made it possible to measure the flow in cylindrical film sections whose radius amounted to 15, 30, 50, 80, 125 and 175 mm. We effected a large number of pourings at angles of incidence of the jet α equalling 90, 75, 60, 45, 30 and 20°. The tests were carried out with jets of water and kerosene outflowing from openings 1; 1.5; 2 and 3 mm in diameter. The rate of outflow was determined according to the pressure differential at the nozzle which ranged from 3 to 15 atmospheres. The length of the jet prior to its impact with the wall amounted usually to about 10 mm, but in some tests it changed from 5 to 30 mm. On the basis of the results of measurements we computedthe values for the relative flow tension $\bar{q} = q/Q$ for the corresponding angles of spreading φ.

The test results show that the character of the flow distribution during the spreading of the jet along the wall does not change with an increasing radius of the cymindrical section in which the measurements are effected, and that the value for the relative flow tension $\bar{q}$ along the given radius-rector remains constant. This fact

is evidence of the radial spreading of the film and also represents an experimental confirmation of the fundamental assumption on which the derivation of the flux calculated functions is based.

The test results have also shown that the distribution of relative flow tension $\bar{q}$ by the angle φ is determined only by the angle of incidence of the jet and the physical properties of the liquid, and does not depend on the velocity and the diameter of the jet. This made it possible to utilize dependence (8) when processing the experimental data. Computations carried out with this function in mind have shown that the value of the additional multiplier a is well determined by the equation

$$a = \sin^m\alpha + \frac{1-\sin^m\alpha}{\pi}\varphi. \qquad (10)$$

The exponent m was found to be equal to 3.0 for water and 3.7 for kerosene. The factor k_0, computed according to formula (9), is well determined by the following expressions:

For water

$$k_0 = \sin^{1.4}\alpha, \qquad (11)$$

For kerosene

$$k_0 = \sin^{1.5}\alpha. \qquad (12)$$

Thus, flow tension q for the spreading of water and kerosene jets can be computed analytically according to formula (8) taking into accound dependences (10), (11) and (12). The mean error for the computation of flow tension does not exceed 6 to 8%.

Figure 2 brings the results of these computations. (solid lines) for water jets and experimental data for mean arithmetical values of all the measurements of flow tension obtained by tests for the given angle φ at a specific angle of incidence of the jet α. Similar results were also obtained for kerosene jets. On the basis of the functions obtained it is possible to compute by approximation the flow tension for the spreading of other liquids.

Besides measurements of flow tension, we carried out tests for the determination of the thickness of films forming by the spreading of water and kerosene jets. In these tests, the angle of incidence of the jets, the outflow rate of the jets and the diameter of the openings varied within the limits mentioned above. For the measurement of film thickness we applied a method based on the absorption by a sheet of liquid of a directed beam of radioactive rays. As a radiation source we chose a preparation of the radioactive strontium isotope Sr^{90} yielding a pure β-radiation.

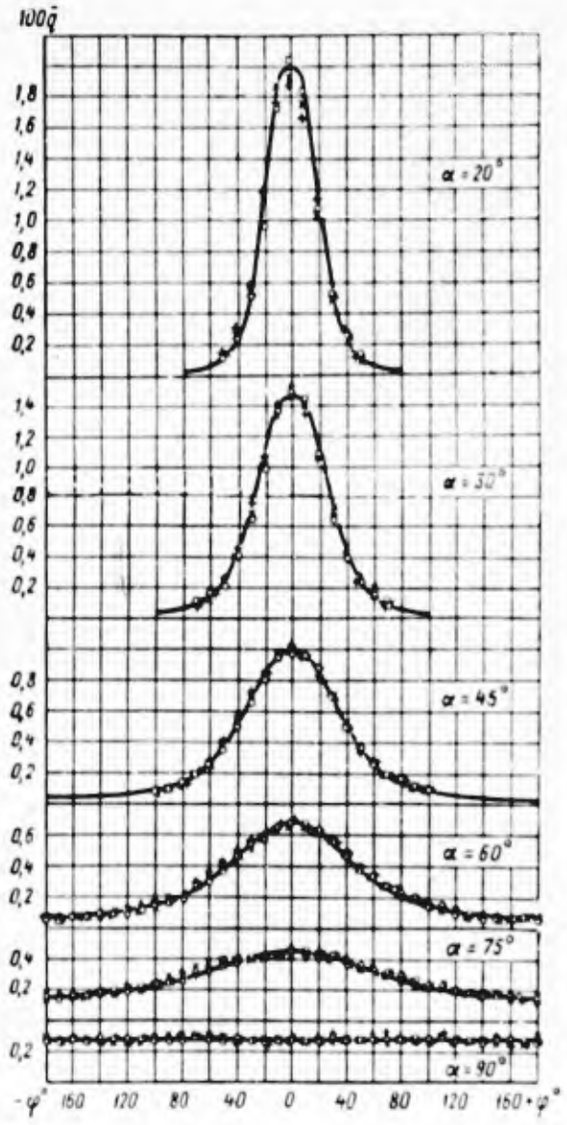

Fig. 2. Relative flow tension for the spreading of a water jet along a wall. Experimental data: a) O spreading on organic glass; b) X spreading on stainless steel; c) ▽ spreading on stainless steel d) — theoretical curve.

Radiation intensity was measured with the aid of a radiometric device of the B type. The absolute error of film thickness measurements did not exceed 0.02 to 0.03 mm.

Figure 3 shows the results of certain film thickness measurement tests. The comparison of experimental results with film thickness variation curves during the spreading of a jet of ideal liquid (dotted lines on the diagrams) are evidence of the fact that when a real liquid spreads, the film velocity continuously decreases and, hence, there takex place losses of pressure head required to overcome hydraulic resistances.

If we know the thickness h and flow tension q in the given radial section of the liquid film it is possible to compute the value for the coefficient of hydraulic losses λ. The results of such computations are shown in Fig. 4 (the diagram is plotted in logarithmic coordinates). As is seen in the diagram, the experimental values for λ fit quite satisfactorily into one strip which has a sharply expressed minimum at Re = 500 to 600. This is evidence of the fact that the Reynolds number expressed by the mean velocity and thickness of the film represents the criterion of the motion conditions of the liquid during the spreading of the jet over a wall.

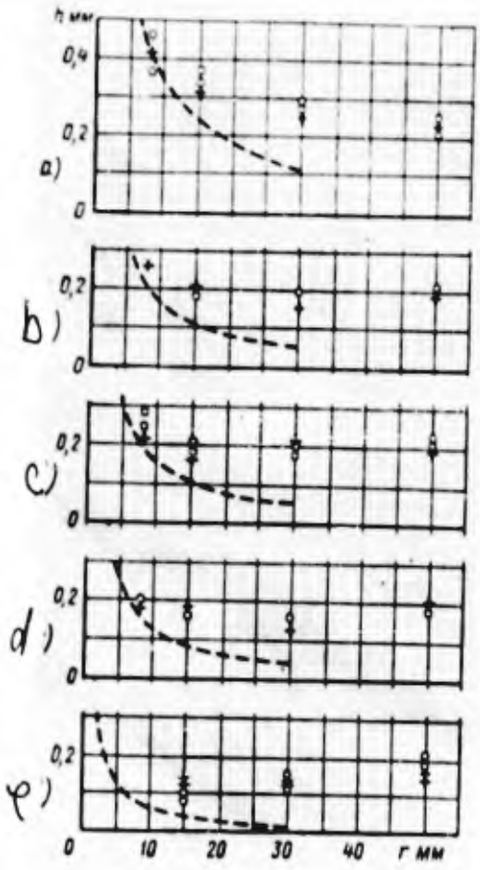

Fig. 3. Thickness of a film spreading over the wall of a water jet with Δp = 10 atmospheres and d = 3 mm.

1. [illegible]	ϑ°	φ°	q cm³/sec rad → 2
3	30	0	141,7
	30	30	72,2
	60	0	66,0
	60	30	51,9
	90	—	27,0

1) diagram 2) q cm³/sec rad 3) experimental data 4) spreading over organic glass 5) spreading over stainless steel.

Like other cases of the motion of liquids (in pipes, open channels, etc.), the critical Reynolds number during the spreading of a jet along a wall can be set at 575.

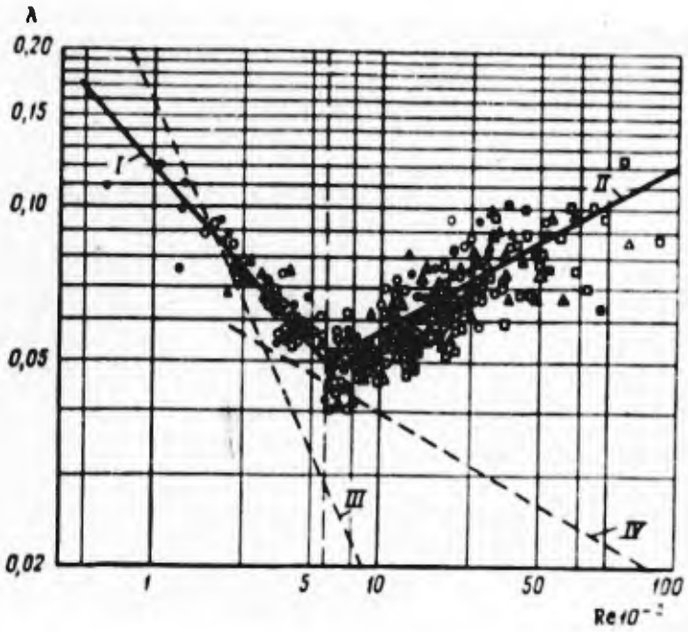

Fig. 4. Dependence of the coefficient of hydraulic losses λ on the Reynolds number. a) for water jets b) for kerosene jets.

a) ○ – Δp = 3 am; △ – Δp = 5 am; □ – Δp = 10 am.

b) ● – Δp = 3 am; ▲ – Δp = 5 am; ■ – Δp = 10 am.

am = atm

We note in the diagram (Fig. 4) the scattering of the experimental values for the coefffident λ within the range of 0.02 to 0.03. The analysis of test results showed that this scattering depends greatly upon errors in the determination of the film thickness h

and flow tension q for the given radial section. In connection therewith it became possible to substitute the area of λ values computed on the basis of test results with a certain averaging curve and approximate this curve to the analytical functions of $\lambda = f(Re)$.

As a result, we obtained the following exponential formulas for the coefficient of hydraulic losses:

a) With

$$50 < Re \leqslant 575 \qquad \text{A 109}$$

$$\lambda = 1{,}2Re^{-0.5} \text{ (curve I in Fig. 4)} \qquad (13)$$

b) With

$$575 \leqslant Re < 2 \cdot 10^4 \qquad \text{B 109}$$

$$\lambda = 1{,}021 \cdot 10^{-2} Re^{0.25} \text{ (curve II in Fig. 4)} \qquad (14)$$

For comparison, the dependences of the friction factor during the motions of liquids in smooth pipes on the Re number (curves III and IV) are also plotted in Fig. 4.

The computations of film thickness carried out to formulas (3), (4), (8) taking account of functions (10), (11), (12), (13) and (14) are shown in Fig. 4 in the form of solid curves. These computations have shown that the absolute value of the radius r_0

has no substantial bearing on the computations of the film parameters and that a certain arbitrariness in their selection is fully permissible. Owing to this, the value for the radius r_0 for jets with diameters from 1 to 3 mm can be assumed to be equally 5 mm.

In conclusion let us note that theoretical analysis and the results of additional tests have made it possible to determine the lowest boundary of the film flow region, within the limits of which the calculated functions mentioned above are true. For a horizontal wall the boundary value of the radius-rector up to which the computed data will be reliable was found to be approximately equal to 0.6 r_k where r_k is that value of the radius-rector with which the design velocity of the film v_k equals $\sqrt{gh_k}$.

For an inclined wall the values of the boundary radius must be diminished by 30 to 50%.

CONCLUSIONS

When a jet collides with a wall, the distribution of the rate of flow is determined only by the angle of inclination of the jet and the physical properties of the liquid. It does not depend on the velocity and diameter of the jet if the latter change within

the range under investigation (v_0 = 20 to 50 m/sec, d = 1 to 3 mm). For the investigated interval of jet parameters the Reynolds number expressed by ~~the~~ velocity and thickness of the film, is the criterion which determines the motion of the liquid when a jet spreads over a wall.

The experimental and theoretical dependences obtained make it possible to determine by means of computation the velocity and thickness of the film (within specific limits). The results of the investigation are true only for the case of spreading of axially symmetrical, sufficiently steady jets forming by the outflow from carefully worked openings.

REFERENCES

1. Zhukovskiy N. E., Analogiya Mezhdu Dvizheniyem Tyazheloy Zhidkosti v Uzkom Kanale i Dvizheniyem Vaza v Trube s Bol'shoy Skorost(yu (Analogies between the motions of heavy liquids in a narrow duct and the motion of gases in pipes at high velocities), op. compl., vol. 7, ONTI 1937.

2. Latyshenkov A. M. and Lobachev V. G., Gidravlika (Hydraulics), GILSA, 1956.

3. Meleshchenko N. T. , Planovaya Zadacha Gidravliki,Otkrytykh Vodotokov (Systematic hydraulical problem of open water ducts), "News of NIIG", vol. 34, 1948.

4. Prandtl' L. Gidroaeromekhanika (Hydro-aeromechanics), IL, 1951.

5. Prokof'yev Yu. F. and Novotvortsev V. I., Osnovy Teoreticheskogo Metoda.Postroyeniya Tranzitnykh Potokov (Fundamentals of the theoretical method for plotting transient flows), "News of NIIG", vol.17, 1935.

6. Forkhgeymer F. , Gidravlika (Hydraulics) ONTI NKTP, 1935.

7. Shlikhting G, Teoriya Pogranichnogo Sloya (Theory of Boundary Films) , IL, 1956.

EXPERIMENTAL INVESTIGATION OF THE EFFECT OF VIBRATION OF PIPES ON THE PARAMETERS OF THE LIQUID FLOWING IN THEM

By

Candidates of Technical Sciences L. A. Latyshev, N. B. Rutovskiy, V. B. Tikhonov

The problem of unsteady operation of aircraft engines has received a constantly growing attention in recent times. One of the causes for unsteady engine operation is to be sought in the interaction between the vibration of pipes and the variation of the parameters of the liquid flowing in them. Comparatively few investigations have been devoted to this problem. To some extent, we may refer to the study of this phenomenom the works of Zlotnik (1), Housner (2), Miordson (3), and Ushakov. (6).

Among these, Housner's (2) study on the bending vibration of pipes containing flowing fluids is of the greatest interest. The basic results obtained by this author are the following:

1) The parameters of the fluid flowing in a vibrating pipe are substantially affected by internal and external forces.

2) Dynamic unsteadiness of pipe lines can arise at great flow velocities of the fluid.

Recent investigations by Handelman (4) and Long (5) have improved Housner's from the point of view of accuracy by taking into consideration additional equation terms depending on inertial forces.

That part of the problem which determines the effect of mechanical factors on the hydrodynamics of fluid flows in a pipe line has not been studied in the above papers although this phenomenon may indeed exert a substantial effect on the normal operation of aircraft engines.

In computing the external and internal forces affecting a vibrating pipe line and the fluid flowing in it, the solution can take the form of a system of equations each of which represents one of the sides of the phenomenom. Utilizing Housner's transformation, the equation for forced vibrations of the pipe line can be written as follows:

$$EJ\frac{\partial^4 y}{\partial x^4}+\rho w^2\frac{\partial^2 y}{\partial x^2}+2\rho w\frac{\partial^2 y}{\partial \tau\,\partial x}+(\rho+\rho_{1p})\frac{\partial^2 y}{\partial \tau^2}\frac{1}{\sqrt{1+\left(\frac{\partial y}{\partial x}\right)^2}}-$$
$$-(\rho+\rho_{1p})y_0\omega^2\frac{1}{\sqrt{1+\left(\frac{\partial y}{\partial x}\right)^2}}\sin\omega\tau=0, \qquad (1)$$

where τ is the time in sec;

x is the coordinate along the pipe line axis, in m;

y is the vibration amplitude of the pipe line, in m;

y_0 is the vibration amplitude of the pipe line end (sealing), in m;

ρ is the density of fluid, in kg x sec^2/m^4;

ρ_p is the density of the pipe line material, in kg x sec^2/m^4;

ω is the radian vibration frequency, in rad/sec;

ν is the vibration frequency, in cycles per second;

E is the elastic modulus of the pipe line material, in kg/m^2;

J is the inertia moment during bending of the pipe line, in m^4;

w is the rate of flow of the fluid, in m/sec.

Unlike the other authors, we have taken the inertia overload force $(\rho+\rho_p)\frac{\partial^2 y}{\partial t^2}$ in its projection on the normal to the elastic curve of the pipe line. This improvement may be of fundamental importance in the case of strong deflection and high pipe line vibration frequencies.

On the other hand, it is necessary to compute the unsteady flow of the fluid in the pipe line. This can be done with the aid of a specific system of equations (7)which are true for small vibrations but can, with some approximatioh, be applied to actual engineering problems:

y is the vibration amplitude of the pipe line, in m;

y_0 is the vibration amplitude of the pipe line end (sealing), in m;

ρ is the density of fluid, in kg x sec^2/m^4;

ρ_p is the density of the pipe line material, in kg x sec^2/m^4;

ω is the radian vibration frequency, in rad/sec;

ν is the vibration frequency, in cycles per second;

E is the elastic modulus of the pipe line material, in kg/m^2;

J is the inertia moment during bending of the pipe line, in m^4;

w is the rate of flow of the fluid, in m/sec.

Unlike the other authors, we have taken the inertia overload force $(\rho+\rho_p)\frac{\partial^2 y}{\partial t^2}$ in its projection on the normal to the elastic curve of the pipe line. This improvement may be of fundamental importance in the case of strong deflection and high pipe line vibration frequencies.

On the other hand, it is necessary to compute the unsteady flow of the fluid in the pipe line. This can be done with the aid of a specific system of equations (7)which are true for small vibrations but can, with some approximatioh, be applied to actual engineering problems:

$$\frac{\partial w}{\partial \tau} + g\frac{\partial y}{\partial x} + \frac{\partial^2 y}{\partial \tau^2}\frac{\frac{\partial y}{\partial x}}{\sqrt{1+\left(\frac{\partial y}{\partial x}\right)^2}} + 2w\frac{\partial w}{\partial x} = -\frac{1}{\rho}\frac{\partial p}{\partial x}; \quad (2)$$

$$\frac{\partial}{\partial \tau}(\rho w f) + \frac{\partial}{\partial x}(\rho w f) = 0; \quad (3)$$

$$c^2\frac{\partial w}{\partial x} = \frac{1}{\rho}\frac{\partial p}{\partial \tau}, \quad (4)$$

where f is the pipe line section in m^2,

p is the pressure of the fluid in the pipe line, in atmospheres.

In fairly short pipe lines which are characteristic for aircraft engines, friction of the fluid against the walls may be disregarded.

If we take into consideration the formation of waves in the pipe line from forces of turbulence evenly distributed along the length of the vibrating pipe line, the phenomenon of wave reflection from the free ends of the hydraulic system, the change in the diameter of pipe lines, their rigidity, etc., then the simultaneous solution of the system of equations (1) to (4) becomes rather difficult. For this reason, the present paper is devoted to investigating experimentally the effect of vibrations of pipe lines on the flow conditions of fluids. This is particularly important in order to gain a qualitative and physical idea of the phenomenon.

1. TEST EQUIPMENT

This equipment allowed of testing straight pipe lines as well as such with a bend in the center.

Owing to the fact that the available vibration equipment with systematic adjusting was unable to ensure the production of vibrations with frequencies up to 200 cycles per second at overloads up to 180 g, we had to produce an equipment with fixed working frequencies of 25, 50, 75, 100, 125, and 175 cycles per second which are resonance frequencies of cantilever spring beams. Excitation of vibrations was effected by means of a special electric system. The general view of the installation is shown in Fig.1. Its hydraulic part, whose diagram is shown in Fig. 2, allowed of obtaining various rates of flow of the fluid from 1 to 4 m/sec.

From tank 1, the fluid, which has a constant temperature, is fed by a whirl pump 2 into a pressure receiver 3 above the free surface of the fluid contained in it. The receiver is connected with the tested pipe 4 by a rubber canvas hose (5), which ensures free travel of the part under investigation with respect to the receiver.

From the pipe line, the fluid flows as a free jet through another rubber canvas hose 6 into a receiver 7 above the level of the fluid

contained in it, from where it flows back into tank 1. The fact that there are two free fluid surfaces makes it possible to eliminate the effect of vibrations arising in the system, substituting them by vibrations induced in the pipe line under investigation. The assigned rate of fluid through the pipe line is ensured by the selection of a throttle plate installed at the inlet into receiver 7. The pneumatic system of the installation serves for maintaining the assigned pressure in both receivers. The investigated pipe line 4 is fastened to the vibrator heads.

Fig. 1. General View of Installation.

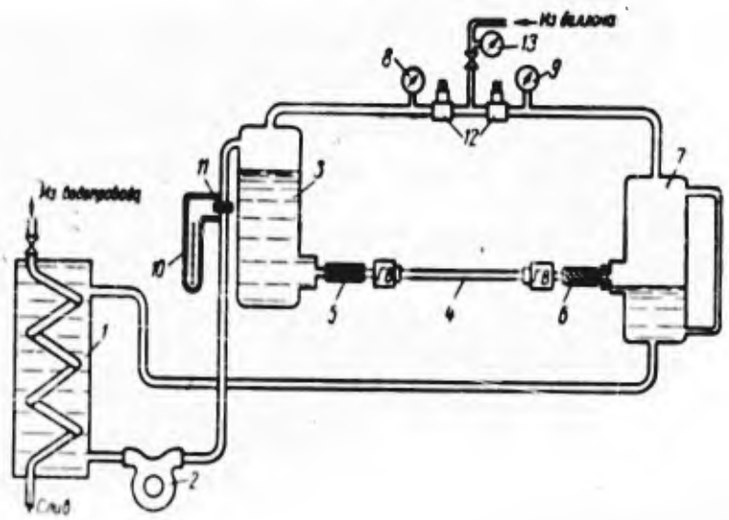

Fig. 2. Schematic diagram of hydraulic system.

1) Delivery tank with cooler 2) whirl pump 3) pressure receiver 4) pipe line under investigation 5) rubber canvas hose 6) rubber canvas outlet hose 7) collecting tank 8) manometer of pressure receiver 9) manometer of free receiver 10) differential manometer 11) measuring plate 12) air reducers of pneumatic system 13) high-pressure manometer; GV-vibrator head. a) from water feed pipe b) from tank c) discharge.

The vibrator heads are represented by the tips of two cone-shaped beam-vibrators which constitute the fundamental part of the mechanical system (Fig. 3). Beam-vibrator 1 is fastened to a

support 2 installed on a base plate 3. The vibrations are generated with the aid of an electromagnetic vibrator consisting of a magnetic circuit 4 secured to the base plate. The vibrator head VH is placed into the cut of the magnetic circuit in such as way as to enable the change of only the horizontal clearance of the magnetic circuit. When the proper vibration frequencies of the beam coincide with the vibration frequencies of the magnetic field, there arise resonance vibrations with the required total amplitude and overload. The apparatus is equipped with six beams having varying proper frequencies. The magnetic circuit of the vibrator has two coils of which one, I, is connected with the a-c generator while the other, II, is connected with the d-c generator.

In order to feed coil I with a-c current of varying frequency we devised a special system of electric engines whose general schematic diagram is shown in Fig. 4. As an a-c generator (1) we used a triphase motor with slip rings, whose anchor windings were connected according to a monophase circuit. The generator is activated by a d-c motor 2. Changes in the direction and speed of rotation of the motor rotor 2 allow of obtaining frequencies higher or lower than those of commercial a-c feeding the generator stator 1.

Fixxx2x

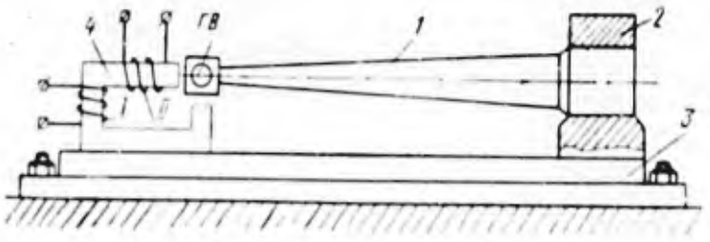

Fig. 2. Schematic diagram of mechanical system. 1) beam-vibrator 2) beam support 3) base plate 4) magnetic circuit; VH-vibrator heads I-a-c coil; II-d-c coil.

The rotating speed of this motor depends on the voltage of the d-c generator 3 run by the a-c motor 4. The power developed by generator 3 is controlled by the excitation current fed from the auxiliary d-c generator 5 connected with the a-c motor 6.

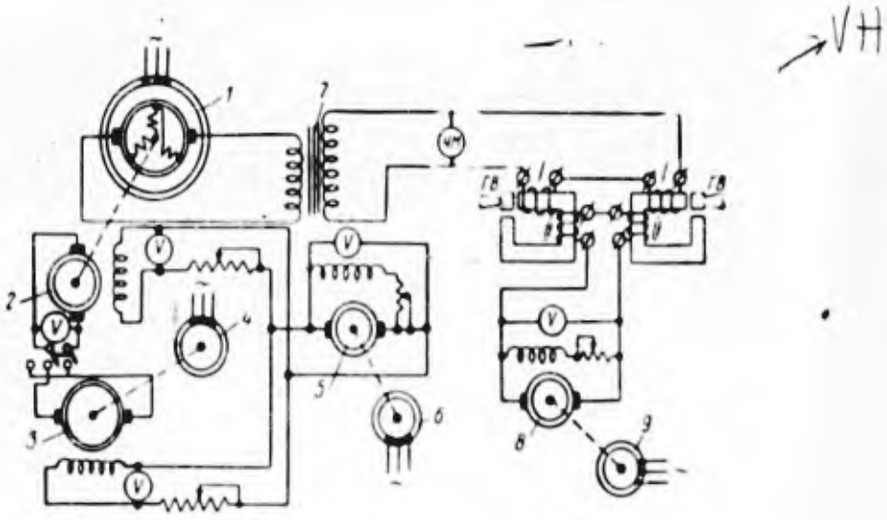

Fig. 4. Schematic Diagram of Electric System. 1) a-c generator 2) d-c electric motor 3) d-c generator 4) a-c electric motor 5) auxiliary d-c generator 6) a-c electric motor 7) special transformer 8) d-c generator 9) a-c electric motor; VH-vibrator heads I - a-c coils; II - d-c coils FM - frequency meter V- volt meters.

Alternating current of assigned frequency is fed into transformer 7 and then into vibrator coils I. Direct current of controlled voltage is fed from generator 8, run by the triphase motor 9, to vibrator coils II. Simultaneous connection of d-c and a-c coils by

superposing magnetic fields allows of increasing the vibration amplitude of the vibrator heads and reduce the frequency of magnetic force by one half as compared with a-c frequency.

During testing, the following quantities were measured:

1) Pressure in the pressure and collecting tanks,

2) rate of the flow of the fluid through the pipe line under investigation,

3) a-c frequency in the vibrators,

4) vibration amplitude of resonance beams,

5) fluctuations of fluid pressure in the vibrating pipe line,

6) fluctuations of the rate of flow of the fluid flowing through the pipe line.

For the fixing of the above quantities we used both standard devices and such which were especially made for the given equipment. Pressure in the collecting and pressure receivers were measured with the aid of class 0.6 manometers. The mean rate of flow of the fluid through the pipe line under investigation was determined by the pressure differential at the measuring plate 11 (see Fig. 2). This pressure differential was measured by the differential manometer 10 only in the case of steady operation of the apparatus

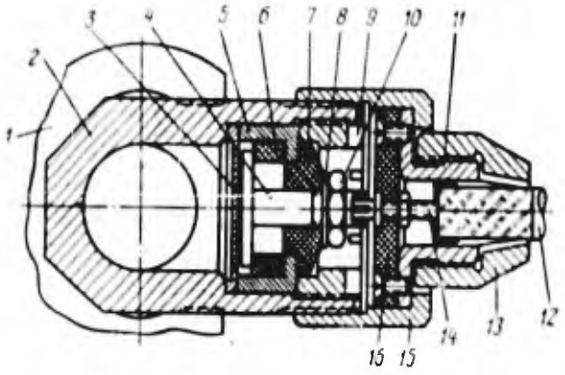

Fig. 5. Capacitance pressure pick-up. 1) door of vibrator head 2) T-piece 3) measuring membrane 4) central electrode 5) distance sleeve 6) insulating sleeve 7) insulating sleeve 8) disc 9) nut of body 10) nut 11) clamping spring collet 12) PK-2 type cable 13) jacket plug of spring collet 14) feed contact 15) jacket plug of body 16) insulating lining.

(the fluid level in the pressure receiver is motionless). The frequency of alternating current fed through to excite the vibrators was measured by a frequency meter with an accuracy up to 0.5 cycles per second.

Inasmuch as the vibration amplitude of the beams is one of the basic parameters, it was measured according to two procedures; with the aid of electric tensiometers glued to the beam surfaces, and by means of a steel needle fastened to the vibrator head.

In spite of preliminary calibration, the electric tensiometers did not yield sufficiently reliable results. For this reason they were basically utilized for orientation purposes during testing.

The fundamental data on the magnitude of the beam vibration amplitude were obtained by means of mechanical recording of the motion of the vibrator head needle on a film traveling during the test on special guides. The width of the recorded track was then measured accurately.

The pressure fluctuations of the fluid at the inlet and outlet of the pipe line under investigation were measured by means of capacitance pick-ups (Fig. 5) installed at the T-pieces of the vibrator heads. The capacitance pick-up was connected with the indicator with frequency modulation whose output signal was fed to a loop oscillograph. The pick-up was secured to the vibrator head in such a way as to prevent the beam vibrations to affect the accuracy of the readings.

The instantaneous rate of flow of the fluid through the pipe-

line under investigation was measured by means of a electro-induction flow meter developped by AD-2 Laboratories (8). The flow meter was switched into the hydraulic system through a cut in the rubber canvas hose 6 (see Fig. 2).

2. TEST RESULTS

Already the first tests showed that in vibrating pipe lines there are fluctuations of the pressure and the velocity with a stationary mean rate of flow (with an accuracy up to 0.5%).

The basic tests relating to the effect of overload on the fluctuation of the fluid were carried out with pipe lines of varying shape, length and diameter at a frequency of 160 cycles per second; some tests were performed at other frequencies. Processing of oscillograms of experiments showed that the amplitude of pressure fluctuations is always directly proportional to the magnitude of overload, the size of the amplitude depending on a number of factors (type of fluctuations, shape of pipe line, etc.).

The tests for the determination of the effect of the rate of flow of the fluid were carried out with pipes 13 x 15 mm in size, having varied shapes and a constant distance between supports amounting to 1.0 to 1.5 m. The pipes vibrated at a frequency of 166

cycles per second under an overload equalling 85 g. Variations in the rate of flow were obtained by changing the throttle plates, so that the pressure in the pipe and, hence, its rigidity remained constant. Figure 6 shows diagrams with typical dependences of the pressure fluctuation amplitudes on the velocity of the fluid flowing in the pipe.

It is seen in Fig. 6 that at a given velocity the fluctuations reach a peak. The position of this peak can shift depending on the shape of the pipe line and the fastening of its ends.

Such a shape of the curve can be explained if we proceed from the solution of equation (1) which can be written as

$$\Delta p = \sum_k a_k w^{b_k} e^{-\varphi_k w}, \qquad \text{A 117}$$

where a_k, b_k and φ_k are the coefficients and characteristic numbers obtained as a result of assigning specific boundary conditions.

A further accumulation of experimental data and integration of the system of equations mentioned above will permit of determining the true values of these quantities.

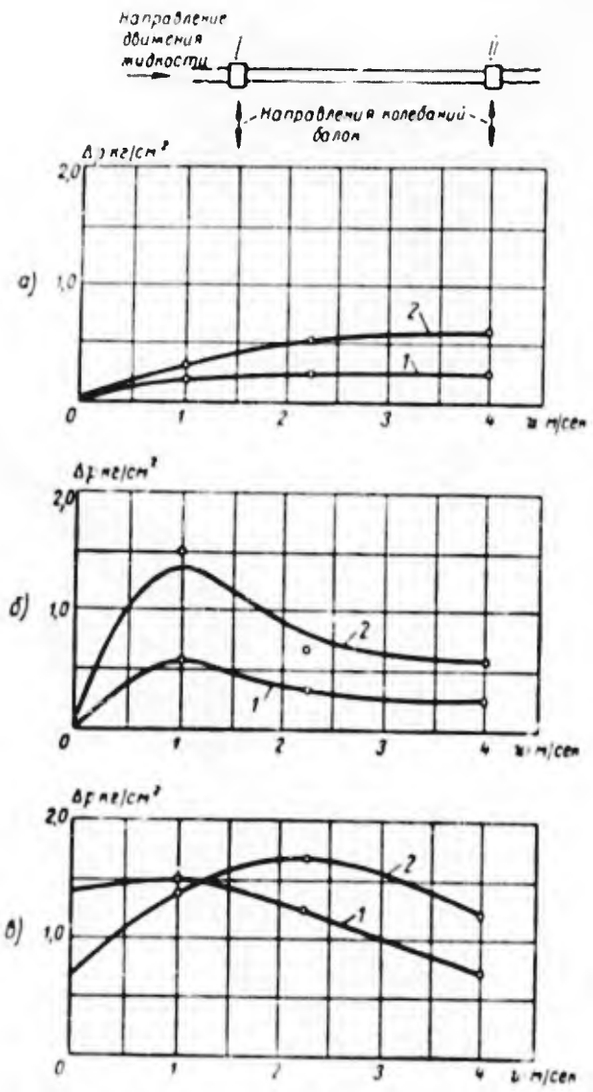

Fig. 6. Effect of the velocity of the fluid flowing in a pipe line on the fluctuation amplitude of internal pressure. 1) pressure fluctuations at point I; 2) pressure fluctuations at point II. a) straight pipe, 13 mm in diameter; l = 1,000 mm; n = 85 g; ϑ = 166 cycles per second. Beam I is vibrating. b) straight pipe, 13 mm in diameter; l = 1,000 mm; n = 85 g; ϑ = 166 cycles per second. Both beams are vibrating. c) Pipe, 13 mm in diameter, with bend 300 mm in diameter; l = 1,000 mm; n = 85 g; ϑ = 166 cycles per second. Beam II is vibrating. 1. flow direction of fluid. 2. Vibration direction of beams.

The curves connecting pressure fluctuations with the diameter and position of the bends in the pipes were found to be extremely interesting. Figure 7 shows the data obtained from tests with aluminum pipes 13 x 15 mm in size. In all the tests, the distance between supports equalled 1,000 mm, both supports vibrated in an identical fashion, the overloads were constant and equalled 85 g.

It is characteristic that the pressure fluctuations attain their greatest amplitude with a fully determined bend diameter for each frequency. Analysis of the set of curves shows that the maximum amplitudes of pressure fluctuations shift with increasing frequencies towards the greater bend diameters.

Apparently, this is due to the effect of two oppposite factors. An increase in the bend diameter leads to an increase in the column of fluid and this, in turn, increases the forming pressure head. At the same time, with a growing bend diameter, the vibrating mass of the pipe and fluid increases, while the rigidity of the entire pipe line decreases. All this results in a decrease in the amplitude of vibrations of the bend proper (taking into account the vibration of supports with constant overload) and, hence, in a corresponding decrease in the amplitude of rigidity pressure fluc-

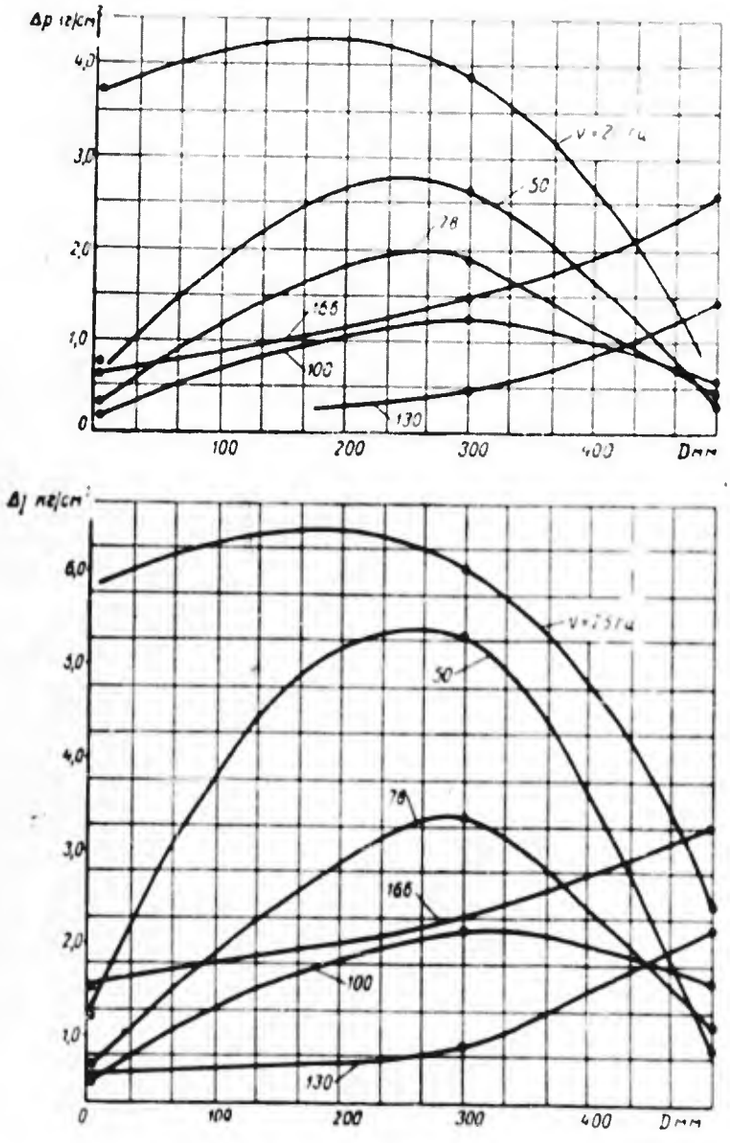

Fig. 7. Effect of diameter of pipe bend on the amplitude of pressure fluctuations. a) kg/cm^2 b) cycles per second.

tuations.

If we assume, as this was done in the tests, that with increasing frequencies the overload stays constant, then, in this case, there occurs a decrease in that portion of energy which is dissipated on account of damping since there is a decrease in the relative displacement of the center of gravity of the pipe bend. Hence, with growing frequencies, the maximum values of Δp connected with the inertness of the fluid column and damping shifts towards greater bend diameters, i.e., towards greater inertial [redacted].

The general picture of vibrations is affected by the geometric parameters of the pipe line, viz., its diameter, length, fastening point, etc. In pipe lines with greater diameters, a larger column of fluid is vibrating, hence it should be expected that the amplitude of pressure fluctuations will be greater there. In fact, tests have shown an increase in the amplitude of pressure p fluctuations when changing from pipes 13mm in diameter to such with a diameter of 20 mm.

In order to confirm this assumption, Fig. 8 gives curves showing the dependence of the amplitude of pressure fluctuations on the pipe diameter and vibration frequency. We carried out tests with pipe lines where the distance between supports equalled 1000 and

1,500 mm. A substantial effect on the character or magnitude of pressure fluctuations was not observed.

Changes in the fixing in of the pipe line (both ends are vibrating, or one of the supports is clamped) promote variations in the frequency or in the amplitude of pressure fluctuations.

Special tests with rubber canvas hoses have shown that the amplitude of pressure fluctuations decreases as absolute pressure in the pipe line increases. This can readily be explained by a decrease in the yielding of the hose walls.

One of the factors which affects greatly the amplitude and shape of the fluctuation of fluid parameters was found to be the vibration frequency of pipe line supports. The harmonic analysis of pressure variation curves revealed a considerable effect of the second and third harmonics, while with increasing overloads an increase in the relative value of the second harmonic was observed. Most of the curves expressing the dependences $\Delta p = f(\nu)$ are cup-shaped with a minimum in the frequency range of 50 to 100 cycles per second. Unfortunately, during the tests, we were unable to expand the range of working frequencies and follow the changes of

Δp at frequencies less than 25 cycles per second and greater than 166 cycles per second while maintaining n = 85 g. Nevertheless, analysis of the system of equations mentioned above allows of discovering the character of the dependences $\Delta p = f(\nu)$.

In the case of vibrating pipes containing flowing fluid, with increasing frequencies the Coriolis forces grow while the kinetic head drops, since the vibration amplitudes decrease with constant overloads. With decreasing frequencies, the inverse phenomenon is observed. At the limit, with zero frequency, kinetic head must yield an increase in pressure equal to the pressure increase from hydraulic impact. In fact, if we extrapolate the test curves to zero, the value for increased pressure will be of the order of 5 to 8 atmospheres, whereas in the case of hydraulic impact at the rate of 1 m/sec, increased pressure amounts to about 10 atmospheres.

As is known, in vibration processes the size of the amplitude depends on the closeness of the frequency of forced vibrations to the frequency of proper vibrations. If we compute the proper frequency of a fluid column contained in a pipe which is open at one end (pressurized receiver) and closed at the other (disc in front of the collecting tank), we obtain the following value:

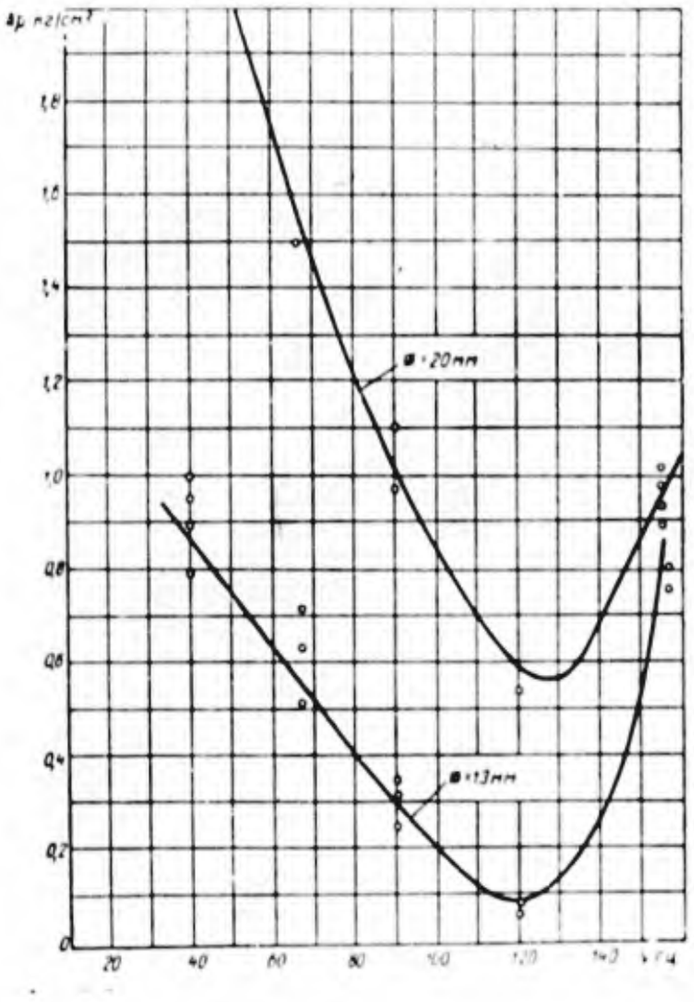

Fig. 8. Dependences of the xpx amplitudes of pressure fluctuations in the fluid on the pipeline diameter and vibration frequency. Straight pipe, l = 1,500 mm. a) kg/cm^2 b) cycles per second.

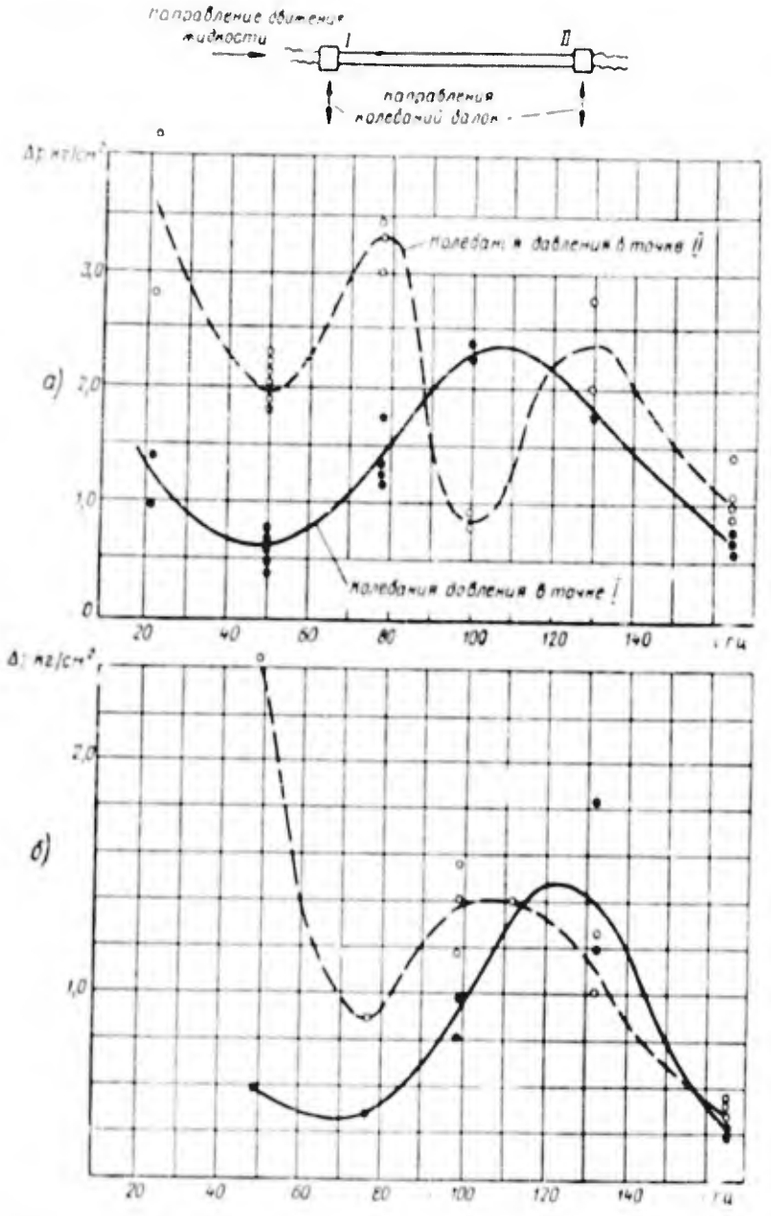

Fig. 9. Effect of pipe vibration frequencies on the amplitude of pressure fluctuations in the fluid. a) Pipe, 13 mm in diameter with bend 500 mm in diameter; l = 1500 mm; n_g = 85. Velocity of flowing fluid W = 2.2 m/sec. Both beams are vibrating. b) Straight pipe, 20 mm in diameter; l = 1500 mm; n_g = 85. Velocity of flowing fluid W = 2.2 m/sec. 1. kg/cm^2 2. flow direction of fluid. 3. vibration direction of beams. 4) pressure fluctuations at point II 5. Pressure fluctuations at point I 6. Cycles per second.

$$\nu = \frac{a}{4l} = \frac{1200}{4 \cdot 10.9} = 27.5 \text{ eu}$$

A 123

where a is the reduced velocity of turbulent expansion in the pipe line;

l is the reduced pipe line length.

It is approximately at this frequency that we observe an increase in Δp recorded experimentally.

It is interesting to note that, when pipes 1.5 m in length vibrated, we observed the appearance of two maximums and two minimums on the curve $\Delta p = f(\nu)$, the frequencies of the maximums and minimums being multiples. Typical curves of this type are shown in Fig. 9.

We undertook special tests where in front of the pipe line we placed a hydraulic pulsator, while the electric vibrators were switched off. These tests showed that when the fluid vibrates, the pipe vibrates too, and that the amplitude of pipe vibrations depends on how closely the frequency of perturbing hydraulic vibrations approaches the proper frequency of the mechanical vibrations of the system consisting of beams and pipes. This seems to indicate that the energy fed into the fluid is dissipated and changes into energy

of mechanical vibrations.

As a result, we can draw the conclusion that there exists an interelation between the pipe line vibrations and pressure fluctuations and the rate of the fluid flowing in this pipe. This phenomenon has to be taken into consideration when analizing the stability of operation of engines.

REFERENCES

1. Zlotnik Sh. L., Dvizhenie Zhidkosti v Vibriruyuchshem Truboprovode (Fluid flows in vibrating pipes), transactions VVIA imeni Zhukovskiy No. 311, 1948.

2. Housner G. W., Bending vibration of a pipe line containing flowing fluid, Journal for appl. Mechanics, 1952, vol. 19, No.2.

3. Niordson F. J. H., Vibrations of a cylindrical tube containing flowing fluid. Transactions of the Roy. inst. of Technology, Stockholm U.D.C. 534, 131, 2, 1953, No.73.

4. Handelman G. H., Bending vibration of a tube containing flowing fluid, Quarterly of appl. Mathematic, 1955, vol. XIII. No.3.

5. Long, R. H. Jr. Experimental and theoretical study of transverse vibration of a tube containing flowing fluid, J. of appl. Mechanics, 1955, voL. 22. No.1.

6. Ushakov V. S., Kolebaniya I Dinamich eskaya Ustoychivost' Truboprovodov Samoletnykh Gidrosistem (Vibrations and dynamic stability of pipes in hydraulic systems of aircrafts), Candidate's dissertation, Leningrad, LKVVIA imeni Mozhayskiy, 1957.

7. Charnyy I. A., Neustanovivsheyesya Dvizheniye Real'noy Zhidkosti v Trubakh (Unsteady flow of a real fluid in pipes), Gostekhizdat (State Technical Press); 1951.

8. Zhilkin B.D. Issledovaniye Elektroindukt ivnogo Raskhodomera Dlya Izmereniya Bystroperemennogo Raskhoda Zhidkosti, "Izvestiya Vysshikh Uchebnykh Zavedeniy MVO SSSR", Seriya "Aviatsionnaya Tekhnika" (Investigation of an electric induction flow meter for the measurement of rapidly changing rate of flow of fluids, "News of Institutes of Higher Learning of the Ministry of Higher Education of the USSR", series " Aviation Technology"), No. 2, 1958.

REGENERATION OF HEAT ~~HEAT RECOVERY~~ IN LIQUID PROPELLANT ROCKET ENGINES

By

A. V. Kvasnikov

1. REGENERATIVE COOLING

Effect of External Cooling on the Parameters of the Cycle

Both during expansion and at the end of it the temperature is noticeably higher in liquid fuel rocket engines than in conventional heat engines utilizing atmospheric air as their working substance. Conversely, the temperature of the working substance receiving heat is found to be considerably lower in liquid fuel rocket engines. Moreover, at the initial stage the working substance of liquid fuel rocket engines is a fluid. Both these circumstances are the reason for the fact that in the thermal cycle of liquid fuel rocket engines the thermodynamic conditions for heat recovery are more favorable than in the cycles of conventional engines where regenerative heat exchange is usually preceded by a process of compression.

Below we shall avail ourselves of the following assumptions:

1. The gaseous phase of the cycle is performed by an ideal gas,

2. There are no heat losses in the chamber, excepting losses

for cooling.

Let us compare the [redacted] parameters cycles of the following three types:

a) Ideal cycle without cooling of the chamber (adiabatic chamber),

b) Cycle with chamber cooling by means of a foreign coolant (chamber with external cooling),

c) Cycle with regenerative cooling of the chamber.

Under the effect of cooling, the gas temperature drops at the end of the chamber and expansion occurs with heat losses. Let us assume that gas expansion takes place polytropically with some constant index of the polytropic curve. The T-S diagram of the gas expansion process in a chamber with external cooling is shown in Fig. 1. In the presence of cooling, to the walls of the chamber, heat heat Q_h is transferred, while Q_n is transferred to the nozzle walls.

We assume henceforth that from an overal heat loss Q_{cool} there takes place a transfer to the head walls

$$Q_h = Q_{cool}$$

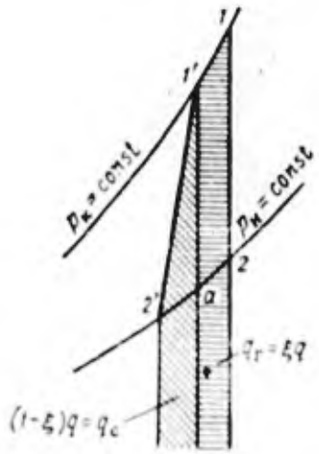

Fig. 1. T-S diagram characterizing heat losses in the case of external cooling of a combustion chamber.

where ξ is the distribution factor of heat losses.

Let us compute the overall value of heat losses to the combustion chamber jacket in portions of the initial gas enthalpy. The absolute value of heat losses can be expressed as follows:

$$Q_{ox} = qI_1 = qC_pT_1 \qquad \text{A 125}$$

where I_1 is the enthalpy of the gas at the beginning of its expansion, for the ideal cycle;

q is the relative loss of heat for cooling.

Figure 1 shows the relative heat losses to the head walls q_h and the nozzle jacket q_n. With identical heat consumption, the work L_{cool} in the cycle with cooling is less than the available work L_{ad}, and the relative efficiency of the cycle can be computed according to the expression

$$\eta_0 = \frac{L_{ox}}{L_{ad}} = \frac{L_{ox}}{L'_{ox}} \frac{L'_{ox}}{L_{ad}}. \qquad \text{B 125}$$

where L'_{ad} is the work in the ideal cycle with identical stages of expansion in a cooled combustion chamber.

The quantity L_{cool} / L'_{ad}, or the ratio of polytropic to adiabatic work at identical stages of expansion and initial gas states, is called polytropic efficiency η_{pol} and is determined by the

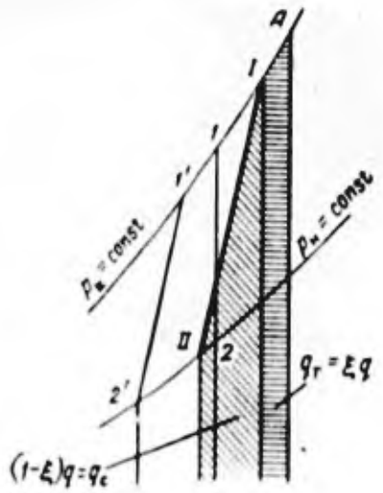

Figure 2. Digaram of the T-S cycle with regenerative heating of the combustion chamber.(Heat transfer quantities are given in fractions of I_1 .

expression

$$\eta_{t\max} = \frac{\frac{n}{n-1}\left(1-\frac{1}{\delta^{a_n}}\right)}{\frac{k}{k-1}\left(1-\frac{1}{\delta^{a}}\right)} = \frac{a\left(1-\frac{1}{\delta^{a_n}}\right)}{a_n\left(1-\frac{1}{\delta^{a}}\right)}, \tag{1}$$

where δ is the expansion ratio, $a = \frac{k-1}{k}$ and $a_n = \frac{n-1}{n}$.

As a result, the efficiency of a cycle with cooling is

$$\eta_{t\max} = \eta_{t\max}\eta_{\Phi} = \eta_{t\max}\eta_{\Phi\max}(1-\xi q). \tag{2}$$

and the specific thrust of the cooled combustion chambers

$$P_{\text{уд}} = \frac{W_{\text{охл}}}{g} = \frac{\sqrt{2gL_{\text{охл}}\eta_{\Phi}}}{g} = \frac{W_{\text{охл}}}{g}\sqrt{\eta_{t\max}} = \frac{W_{\text{охл}}}{g}\sqrt{\eta_{t\max}(1-\xi q)}. \tag{3}$$

where ξ is the distribution factor of heat losses;

$W_{\text{охл}}$, $W_{\text{ад}}$ are the flow rates of gases from the cooled and adiabatic chambers;

g is the acceleration of gravity.

The exponent of the polytropic curve depending on q and found can be found from equation

$$\delta^{\frac{n-1}{n}} - \frac{n-1}{n-k}\frac{1-\xi}{1-\xi q}kg\delta^{\frac{n-1}{n}} - 1 = 0. \tag{4}$$

Parameters of the Cycle with Regenerative Cooling of Combustion Chambers

In Fig. 2, in T-S coordinates are shown the gas expansion lines in various combustion chambers. For adiabatic chambers, the beginning of expansion corresponds to point I. In the case of heat recovery in the cooling nozzle jacket for enthalpy I_k I_i

which determines the heat transferred during condition of combustion, heat Q_n is added. According to the diagram, heat $Q_n = I_I = I_1$ is equidimensional with the area below the polytropic curve I - II or below the section I-1 of the curves p_k = const. Before entering into the combustion chamber, the working heat received already in the combustion chamber jacket, an addition of Q_h calories through the head walls. Prior to the beginning of expansion this quantity of heat is again transferred into the cooling jacket.

In Fig. 2 heat Q_h corresponds to the difference of enthalpies $I_A - I_1$.

The efficiency of regenerative combustion chambers with regard to the initial gas state A (see Fig. 2) is determined according to formula (2). Yet, the heat actually consumed for obtaining work L_{ad} is I_1 rather than I_A i.e., (1 - q)-times less. For this reason, the efficiency of the regenerative cycle is

$$\eta_{iR} = \frac{\eta_{ox}}{1-q}. \tag{5}$$

For specific thrusts of combustion chambers with regenerative and external cooling we obtain the following relationships:

$$\frac{P_{R_{ya}}}{P_{ox_{ya}}} = \sqrt{\frac{1}{1-q}} \tag{6}$$

and

$$P_{R_{ya}} = \frac{W_{aa}}{g}\sqrt{\eta_{ina}}\sqrt{\frac{1-\xi q}{1-q}}. \qquad (7)$$

It can readily be seen from equations (5) to (7) that the heat lost at the head walls is compensated by its reintroduction in the combustion chamber together with the working heat. Consequently, regeneration of heat, which cools the head walls, is useful and raises the efficiency of the cycle, specific work and specific thrust of the combustion chamber with the cooled head to a level corresponding to the ideal cycle.

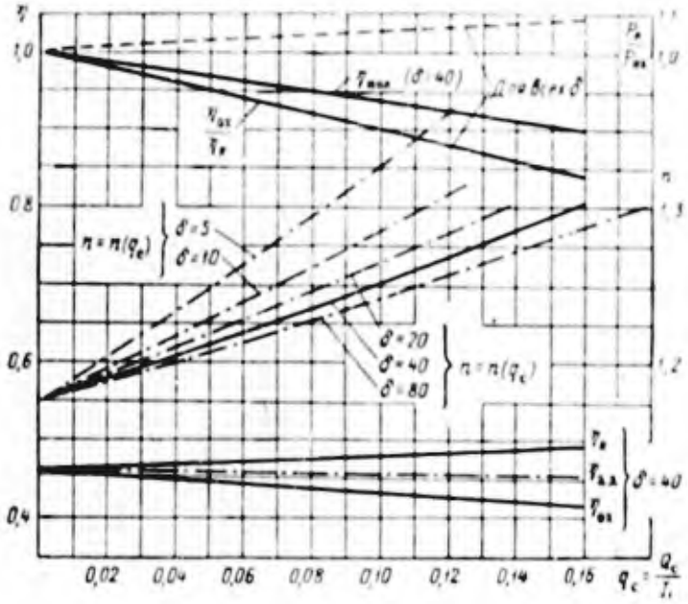

Fig. 3. Effect of heat recovery in the cooling nozzle jacket on the engine parameters.

Assuming the coefficient $\xi = 0$, we thus change to the version consisting of an adiabatic head and cooled nozzle. In this case

$$\eta_R = \frac{a}{a_n}\left(1 - \frac{1}{\beta^{a_n}}\right)\frac{1}{1-q} \qquad \text{A 127}$$

and the regeneration of heat transmitted to the nozzle walls leads to an increase in efficiency and the thrust of the engine. The graphs of Fig. 3 show the changes of the important work parameters of the engine in the presence of heat recovery in a cooled nozzle jacket. When changing from a cooled combustion chamber to a regenerative one, the variations of efficiency and thrust are found to be quite conisderable. For example, when $Q_n = 0.02$, efficiency of the combustion chamber increases, after changing to regenerative cooling, by 2%, and its thrust increases by 1%. These quantities are quite commensurable with those obtained when computing, for example, losses in the nozzle for friction or for the non-parallelity of gas jets at the nozzle outlet.

The magnitude of regenerative heat exchange increases as the dimensions of the combustion chamber decrease and the ratio of the chamber's length to its diameter increases, when in the cooling jacket a relatively greater amount of heat is transferred. With

q = 0.1 the relation $\eta_R/\eta_{cool} = 1.11$ and the thrust of the combustion chamber increase by 5.5%. Regeneration of heat of a system of nozzle cooling improves the efficiency of combustion chambers to such an extent that it exceeds that of adiabatic chambers.

In order to compute the thrust and efficiency of combustion chambers we can utilize simpler empirical dependences than those mentioned above. Thus, with an expansion ratio δ = 5 to 80 and an adiabatic index k differing but slightly from k = 1.2 we obtain

$$\eta_{cool} = 1 - 0{,}6q_c \tag{8}$$

and

$$\frac{P_R}{P_{ad}} = \sqrt{\frac{1-0{,}6q_c}{1-q_c}}. \tag{9}$$

Taking into consideration formula (4), we can determine the exponent of the polytropic curve with the aid of the following expression

$$n = \frac{k(1-0{,}6q_c)}{1-q_c(b+0{,}6)}, \tag{10}$$

where

$$b = \frac{k-1}{\eta_{ad}}.$$

An increase of in expansion ratio δ is bound to reduce the advantages from heat recovery. Within a range of $\delta \to \infty$ the efficiency of an ideal combustion chamber $\eta_{ad} = 1.0$.

The following features of heat recovery in the cooling combustion chamber jackets are worth noting:

1. The relative increase in the efficiency of the combustion chamber becomes even more significant with a lower heat value of the fuel and greater values of k;

2. Heat recovery in the nozzle jacket leads to a more convenient operating cycle than the adiabatic one;

3. Regenerative cooling yields sufficiently noticeable advantages as compared with cooling by means of a foreign agent, especially if the dimensions of the chamber are small;

4. At the modern rate of intensity of external cooling of combustion chambers, heat regeneration yields a negligible improvement in the thrust of the combustion chamber and a small increase in the initial gas temperatures.

2. External Regeneration EXTERNAL REGENERATION

Effect of External Regeneration on the Combustion Chamber Parameters

Heat recovery from the gas after its expansion in the nozzle

ducts will be called external recovery. It is obvious that in this case the regenerator has to be placed behind the nozzle and butt against it.

We shall first examine the heat recovery process under the following conditions:

1. There are no hydraulic losses in the chamber or regenerator.

2. The consumed heat is fed to the working substance from outside.

3. Velocity and pressure of the gas in the regenerator are constant.

Following diagram T-S in Fig. 4, the gas after expanding in section 1-2 enters into the regenerator at the state 2. The heat available for recovery is measured by enthalpy I_2.

Let us call the quantity

$$q_R = \frac{Q_R}{I_2} = \frac{I_3}{I_2} \qquad \text{A 129}$$

the regeneration rate of the cycle.

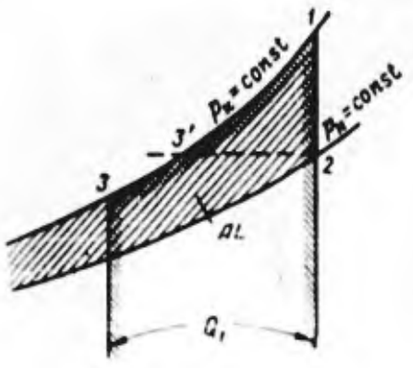

Fig. 4. T-S diagram of the regenerative cycle of a rocket engine.

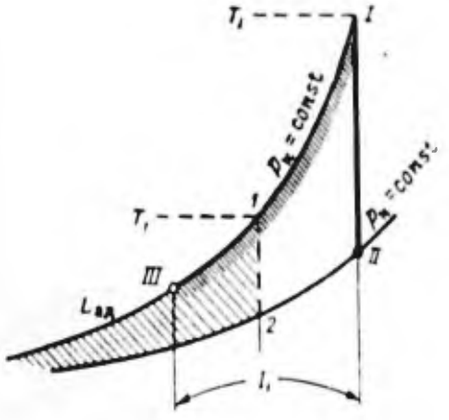

Fig. 5. T-S diagram showing the transition from the adiabatic cycle to the regenerative one, maintaining the calorific value of the charge.

At an identical initial state of the gas in the normal and regenerative cycles, specific work is found to be the same, while the efficiency of cycles varies since

$$\eta_R = \eta_{tt} \frac{l_1}{l_1 - l_3} = \eta_{tt} \frac{T_1}{T_1 - T_3} = \frac{\delta^\varepsilon}{\delta^\varepsilon - q_R} \eta_{tt} \qquad \text{B 129}$$

or

$$\eta_R = \frac{\delta^\varepsilon - 1}{\delta^\varepsilon - q_R}. \qquad (11)$$

Under the above condition the quantity of specific thrust remains unchanged. The same applies to specific fuel consumption.

Let us now change the second of the conditions adopted when examining the regeneration process, in the following way.

Let the quantity of heat fed to the working substance be always one and the same, and let it be determined by its calorific value. In this case, regeneration of heat leads not only to a change in efficiency but also in the specific thrust of the chamber.

In Fig. 5, the normal adiabatic cycle is represented in the T-S diagram by the expansion curve 1-2, the heating capacity $I_1 = C_p T_1$. The inclusion of a regenerator leads to a "speeding up" of the cycle which is expressed by an increase in the initial temperature of expansion and an increase in the useful work and thrust of the chamber. The parameters of the cycle will become steady when

heat production in the chamber and the subsequent gas expansion will lead to such a temperature of the off-gases at which the assigned regeneration rate q_R will be obtained. In Fig. 5, the regenerative cycle corresponds to an expansion in sector I-II where

$$l_I - l_{III} = l_I - q_R l_{II} = l_1 \qquad \text{A 130}$$

and

$$T_I - q_R T_{II} = T_1\left(1 - \frac{q_R}{\varkappa}\right) = T_1. \qquad \text{B 130}$$

From the latter relationship we obtain

$$\frac{T_1}{T_I} = \frac{\varkappa}{\varkappa - q_R}. \qquad \text{C 130}$$

The maximum temperature increases, when changing to the regenerative cycle, all the more, the lower the efficiency of the initial adiabatic cycle.

For [redacted] thrust we obtained the following relationship

$$\frac{P_R}{P_{ad}} = \sqrt{\frac{L_R}{L_{ad}}} = \sqrt{\frac{T_1}{T_I}} = \sqrt{\frac{\varkappa}{\varkappa - q_R}}. \qquad (12)$$

According to the latter expression, [redacted] specific fuel consumption decreases too.

Figure 6 shows the variation of the coefficient η_R and the ratio η_R/η_{ad} with varying δ and q_R. The efficiency ratios represent also the maximum temperatures ratio in the compared cycles.

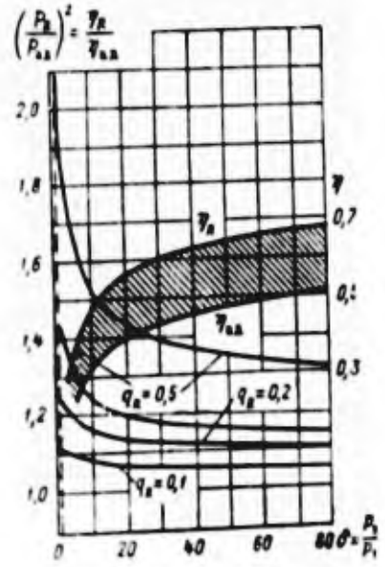

Fig. 6.. Effect of expansion ratio δ on the efficiency of the regenerative cycle of liquid fuel rocket engines at various regeneration rates.

Effect of the " Cold Capacity" of the Fuel on [redacted] Regeneration Rate.

As was shown above, the increase in specific thrust depends on the rate of regeneration. If we take into consideration that the cooling agent has to be the fuel, this means in that the increase in P_{sp} depends on the cooling capacity, or the "cold capacity", of

the fuel.

Let us rate the cooling capacity of the fuel by the ratio of the maximum permissible quantity of heat absorbed by the fuel in the cooling jacket of the regenerator, to the heating capacity of the fuel. According to this determination, the cooling capacity of the fuel

$$\beta = \frac{Q_{ох}}{H} \qquad (13)$$

or

$$\beta = \frac{\alpha}{(1+\alpha)H} Q_{ох.о} + \frac{1}{(1+\alpha)H} Q_{ох.г} \qquad (13)$$

where α is the ratio of the fuel components;

$Q_{cool.ox}$ and $Q_{cool.f}$ are the losses of heat for cooling of the oxidant and the fuel;

H is the heating capacity of the fuel.

We can readily obtain the following formula for the determination of the initial rate of regeneration:

$$q_R = \frac{1}{1-\beta} \delta^a. \qquad (14)$$

Then

$$\frac{T_1}{T_1} = \frac{\eta_R}{\eta_{ох}} = \frac{\delta^a}{\delta^a - q_R} = 1 + \beta \qquad (15)$$

and

$$\frac{p_R}{p_{ох}} = \sqrt{\frac{T_1}{T_1}} = \sqrt{1+\beta}. \qquad (16)$$

Table I gives the value for β_{max}, $(q_R)_{max}$, T_1/T_{ad} and $(P_R - P_{ad})/P_{ad}$ computed from formulas (13) to (16) for three types of fuel.

From these data we can conclude that external regenera regeneration in engines with fuels similar to those mentioned above cannot be considered profitable since the slight gain in thrust is lost to a great extent by the complexity of the installation and the increase in its weight.

TABLE I

Показатели	Кислород и этиловый спирт 70%-ный	Азотная кислота и керосин с испарением в рубашке камеры	Азотная кислота и спирт 96%-ный	
			без испарения	с испарением в рубашке камеры
$(q_R)_{max}$ при степени расширения δ:				
10	10,3	14,5	15,7	19,1
20	11,5	16,3	17,6	21,5
40	12,5	18,3	19,8	24,1
80	14,5	20,6	22,2	27,1
$\frac{T_1}{T_1} = \frac{\gamma_R}{\gamma_{ad}}$	1,075	1,11	1,12	1,15
$\frac{P_R - P_{ad}}{P_{ad}}$ %	3,8	3,5	6,0	7,3
β_{max} %	7,5	11,0	12	15

1. Indices 2. Oxygen and ethyl alchohol, 70% concentration 3) nitric acid and kerosene evaporating in the jacket of the chamber 4) nitric acid and alchohol, 96% concentration 5) without evaporation 6) with evaporation in the chamber jacket 7) $(q_R)_{max}$ with expansion ratio δ:

Utilization in Regenerators of Inert Substances with Great Cooling Capacity Carried by the Fuel

Let us examine the work parameters of a regenerator engine with an addition to the fuel of inert substances with great cooling capacity. Let us then compare this system with the normal one at identical values for maximum temperatures, dimensions of nozzle sections, pressures p_k, expansion ratios and tank capacities for the working substance, assuming that the inert substance, as well as the basic one, has the properties of an ideal gas.

Let there be 1 kg of working substance i.e., a mixture consisting of m' kg of fuel and m'' kg of inert substance designed for heat removal in the regenerator. If I'_1 is the enthalpy of 1 kg of fuel gases in the chamber without regeneration, I_1 is the enthalpy of 1 kg of working substance in the regenerator chamber and Q_R is the heat of regeneration, then the following equation is true

$$I'_1 m' + Q_R = I_1. \qquad \text{A 132}$$

Moreover,

$$Q_R = I_1 q_R = c_p T_1 q_R = c_p T_1 \frac{q_R}{\delta^a}, \qquad I'_1 m' = c'_p m' T_1 \qquad \text{B 132}$$

and

$$I_1 = c_p T_1 = (c'_p m' + c''_p m'') T_1. \qquad \text{C 132}$$

Bearing in mind these relations, the expression for the heat balance can be written in the following form

$$c'_p m' T_1 + c_p \frac{T_1}{\delta^a} q_R = (c'_p m' + c''_p m'') T_1. \qquad \text{D 132}$$

whence

$$m' = \frac{1 - \frac{q_R}{\delta^a}}{1 - \frac{q_R}{\delta^a}\left(1 - \frac{c'_p}{c''_p}\right)} = \frac{1}{1 + \frac{c'_p}{c''_p}\frac{q_R}{\delta^a - q_R}}. \qquad (17)$$

The specific thrusts with identical expansion ratios are determined by the relation

$$\frac{P_R}{P'} = \sqrt{\frac{c_p T_1}{c'_p T_1}} = \sqrt{\frac{c'_p m' + c''_p (1 - m')}{c'_p}}, \qquad \text{A 133}$$

where P' is the specific thrust referred to the sole consumption of fuel.

Utilizing formula (17), we can write this relation as follows:

$$\frac{P_R}{P'} = \sqrt{\frac{1}{1 - \frac{q_R}{\delta^a}\left(1 - \frac{c'_p}{c''_p}\right)}}. \qquad (18)$$

It is seen from this expression that specific thrust P_R can be greater, and also smaller, than the initial/specific thrust P'. Thus, with $c'_p < c''_p$ we find that $P_R > P'$.

Hence, if c'_p is close in magnitude to c''_p, then specific thrust and consumption of the working substance remain almost unchanged and regeneration is justified only in the case where fuel

becomes quite short as compared with the inert substance.

Utilization in Regenerators of External Inert Substances

If the rocket moves in a dense medium, the inert substance for the regenerator may not be contained in the tanks of the rocket but be obtained from outside. In this case, the initial value of enthalpy I_1 in the chamber will be determined from expression

$$I_1'm' + I''m'' + Q_R = I_1 m.$$

B 133

Let us confine ourselves to the case where complete enthalpy of the inert substance when entering the regenerator is small as compared with enthalpy I'_1 and heat Q_R, which will be true in the case of small ratios of velocities V/W. Then, expression (17) determines the connection between the fuel quantity m' and the rate of regeneration q_R.

Let us henceforth take as the basic variable the relative quantity of inert substance determined by expression

$$\lambda = \frac{m''}{m' + m''}.$$

C 133

Utilizing formula (17) we obtain at identical temperatures T_1

$$q_R = \frac{b^a \lambda}{1 - (1-\lambda)\left(1 - \frac{c_{p'}}{c_p}\right)}.$$

(19)

The magnitude of relative thrust will depend also on the velocity of the rocket, i.e.,

$$\bar{P}_R = m\bar{W}' - m''\bar{V}. \qquad \text{D 133}$$

In this expression the outflow rate of gases from the nozzle during regeneration

$$W = W'\sqrt{\frac{\sigma}{\sigma_0}}. \qquad \text{A 134}$$

where W' is the flow rate of λ from the nozzle without regeneration.

After transformation, we obtain for the thrusts the following relation:

$$\frac{P_R}{P'} = \sqrt{1-\lambda\left(1-\frac{\sigma}{\sigma_0}\right)} - \lambda\frac{V}{W'}. \qquad (20)$$

Referring the specific thrusts to a weight unit of the substance consumed by the rocket we find

$$\frac{P_R}{G''} = \frac{P_R}{P'}\frac{1}{1-\lambda} = \frac{1}{1-\lambda}\sqrt{1-\lambda\left(1-\frac{\sigma}{\sigma_0}\right)} - \frac{\lambda}{(1-\lambda)}\frac{V}{W'}. \qquad (21)$$

For the case where $c'_p = c''_p$, formula (21) is simplified as follows

$$\left.\frac{P_R}{P'}\right|_{\sigma=\sigma_0} = \frac{1-\lambda\frac{V}{W'}}{1-\lambda}. \qquad (21a)$$

Figure 7 shows the variation curves P_R/P' depending on λ, according to equation (21a). With small values for the ratio V/W' the improvement in specific thrust and, hence, in efficiency is found to be considerable. Figure 7 also shows the dependence of

the quantity λ on the expansion ratio in the chamber at a rate of regeneration q_R = 0.5 and 1.0. According to the graphs of Fig. 7 for a chamber with an expansion ratio δ = 20 and q_R = 0.5 we have λ = 0.3, which corresponds to P_R/P' = 1.35 at V/W' = 0.1.

Let us compare the rocket parameters with a common and regenerative chamber. For this purpose we first determine the conventional rocket take-off velocity V_{max} in a non-resisting medium.

Equation

$$-Pdt = Wdm - Vdm' \qquad \text{B 134}$$

can be written as follows:

$$-Pdt = \left[W\frac{dm}{dm'} - V\frac{dm'}{dm'}\right]dm'. \qquad \text{C 134}$$

Since

$$\frac{dm}{dm'} = \frac{1}{1-\lambda} \text{ и } \frac{dm'}{dm'} = \frac{\lambda}{1-\lambda}, \qquad \text{D 134}$$

then

$$-Pdt = \frac{W - V\lambda}{1-\lambda}dm'. \qquad \text{E 134}$$

On the other hand, if M is the mass of the rocket, then its thrust P = M(dV)/(dt). Eliminating dt from the expressions obtained, we have

$$MdV = -\frac{W - V\lambda}{1-\lambda}dm'. \qquad \text{F 134}$$

Upon dividing the variables and integrating we find the final

expression for the ratio of rocket take-off velocity to the out-flow rate of the gas from its nozzle:

$$\frac{V_{max}}{W} = \left[1 - \left(\frac{M_к}{M_0}\right)^{\frac{\lambda}{1-\lambda}}\right] \frac{1}{\lambda}, \qquad (22)$$

where M_f and M_0 is the final and initial mass of the rocket.

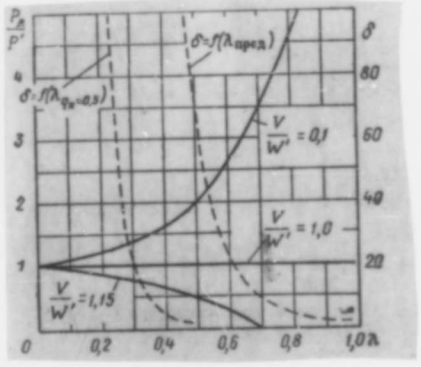

Fig. 7. Variation of specific thrust referred to fuel consumption, depending on the relative quantity of inert substance obtained from outside ($c''_p = c'_p$).

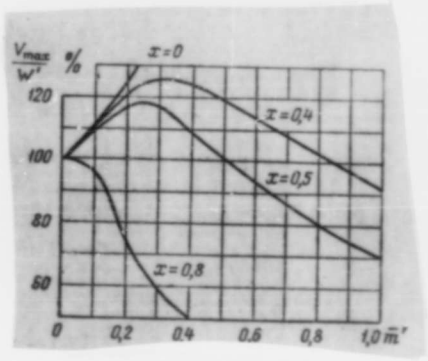

Fig. 8. Variation of the ratio of velocities V_{max}/W' depending on $m' = 1-\lambda$ at varying values for $x = M_f/M_0$ and with $c'_p = c''_p$.

With $\lambda = 0$, formula (22) changes into the Tsiolkovskiy formula.

The gas outflow rate W depends on λ in the following fashion:

$$W = W'\sqrt{\frac{c_p}{c_p^*}} = W'\sqrt{1-\lambda\left(1-\frac{c'_p}{c_p^*}\right)}. \qquad \text{A 135}$$

Substituting this expression in formula (22) we obtain

$$\frac{V_{max}}{W'} = \frac{\sqrt{1-\lambda\left(1-\frac{c'_p}{c_p^*}\right)}}{\lambda}\left[1-\left(\frac{M_к}{M_0}\right)^{\frac{\lambda}{1-\lambda}}\right]. \qquad (23)$$

The change according to forula (23) of the ratio of velocities

V_{max}/W' in the case where $c''_p = c'_{p'}$ with several ratios of final mass to initial mass, is shown by the curves in Fig. 8.

As is seen in Fig. 8, with $\bar{m}' = \frac{m'}{m' + m''} < 0{,}5$ it is possible to obtain a considerable gain in velocity.

As another rocket parameter we can take the distance of its actual flight S_R. Let us assume that the speed of the rocket from the moment of the engagement of the engine and further through the entire time of its operation is constant. The path of the rocket is usually represented as consisting of the active portion where the engine is operating, and the portion where, after the fuel has been spent, the rocket is slowed down and has to overcome the resistance of the medium. As the length of the effective path portion we take the rocket's trajectory from the beginning of its motion to the point where its speed decreases by one half.

Thus, the rocket's trajectory is

$$S' = S'_1 + S'_2 = V't' + S'_2. \qquad \text{A 136}$$

The operating time of the engine is determined from the expression

$$t' = \frac{M_0 - M_к}{m_{сек}}, \qquad \text{B 136}$$

where m_{sec} is the mass consumption per second.

We assume the drag in the active sector of slowed-down rocket motion to be proportional to the square of its speed, i.e.,

$$P' = CV^2 = -M_x \frac{dV}{dt}.$$

C 136

By juxtaposing under these conditions the sectors of the rocket's trajectory S_R and S', we obtain

$$\frac{S_R}{S'} = \frac{\frac{V_R}{V_0}\frac{1-x}{1-\lambda} + x\frac{V_0}{W'}\ln 2}{1-x+x\frac{V_0}{W'}\ln 2}, \tag{24}$$

where $x = V_0/V_R$ for $V_R > V_0$,

V_0 is the rocket's speed at the instant when lagging begins.

Confining ourselves to juxtaposing the length of only the active sectors, we obtain

$$\frac{S_R}{S'} = S_{\text{акт}} = \frac{V_R}{V_0}\frac{1}{1-\lambda} \tag{25}$$

and

$$S_{\text{акт}} = \frac{1}{1-\lambda}\sqrt{\frac{P_R}{P'}} = \sqrt{\frac{1}{1-\lambda}\frac{P_R}{P'}}.$$

D 136

Here, P_R and P' are the specific thrusts referred to a mass unit of fuel. Utilizing formula (21), we obtain

$$S_{\text{акт}} = \frac{1}{1-\lambda}\sqrt{\sqrt{1-\lambda\left(1-\frac{c_p}{c_p'}\right)}-\lambda\frac{V_R}{W'}}. \tag{26}$$

If $c_p' = c_p''$, formula (26) takes the following form:

$$S_{\text{акт}}\Big|_{c_p' = c_p''} = \frac{1}{1-\lambda}\sqrt{1-\lambda\frac{V_R}{W'}}. \tag{26a}$$

The latter expression should be used with small λ, with $x \leqslant 0.4$ and $W_R/W' \leqslant 0.4$. The functions $S_{act} = f(\lambda)$ for two values of V_R/W' according to formula (26a) and $S_R/S' = F(\lambda)$ according to equation (24) for $x = 0.5$ and $V_R / W' = 0.5$ are shown in Fig. 9.

Juxtaposition of rockets by their take-off run and the length of the effective trajectory shows that by utilizing external inert substances the value of regenerative cycles of liquid fuel rocket engines is strongly improved.

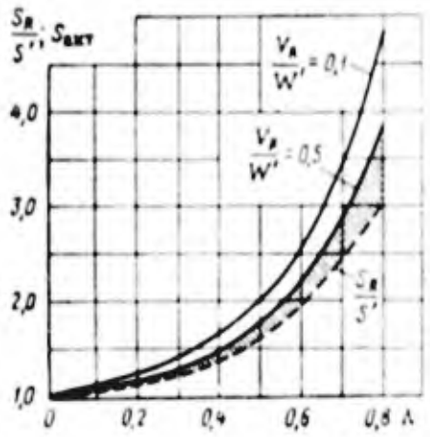

Fig. 9. Variation of the effective rocket trajectory depending on λ ($c_p' = c_p''$, $x = 0.5$).

The following cases may be characteristic for systems with external inert regenerator substances:

- Motion of substance under water;

- Introduction into the regenerator of a working substance for the turbo-pump system;

- Utilization of regenerator heat in composite engines when, for example, heat is transferred to compressed air in ram-jets;

- Obtaining a flow for the air-cooling of models.

The profitableness of regeneration increases as λ increases, i.e., as the consumption of proper mass decreases. The greatest values for λ can be obtained with nuclear engines.

After examining the conditions for regeneration we can draw the following conclusions:

1. Thermodynamic conditions for cycles with external regeneration are considerably more favorable in liquid fuel rocket engines than in pressure cycles.

2. Efficiency of the chamber and, in the case of an increase in its internal temperature, also its specific thrust increase when changing to regenerative cycles, all the more, the smaller the expansion ratio in the cycle and the greater the rate of

regeneration.

3. Utilization in the regenerator of fuel components as cooling agents leads to negligible changes in efficiency and specific thrust (4 to 7%) owing to the low cooling capacity of these components.

4. In the case where the inert substance carried by the fuel ranges within expansion ratios δ = 20 to 80 and relative heat losses q_R = 0.1 to 0.5, specific thrust exceeds adiabatic thrust by (2 to 4) to (15 to 25)%. In this case:

a) Transition to regenerative cycles, while maintaining maximum temperatures in the chamber, does not lead to a decrease in the specific consumption of the working substance.

b) Depending on the type of fuel and the inert substance, utilization of inert heat-transfer agents in the regnerator may lead to some small increase or decrease in specific thrust.

c) Consumption of the calorific part of the fuel per unit thrust and for the acceleration of the rocket up to maximum velocity can be considered reduced by changing to the regenerative cycle.

5. Utilization of external inert substances with δ = 20 to 80, q_R = 0.1 to 0.5 and V_R/W' = 0.1 to 0.5 reduces the thrust as compared to adiabatic thrust by 1 to 15%. Specific thrust referred to

the fuel consumed, ~~in the~~ increases if $V_R/W' \leqslant 1.0$ (see Fig. 7).

6. If an external inert substance is utilized, the acceleration rate of the rocket increases with λ increasing to 0/2 to 0.3 (σ_R 0.3 to 0.5) and with $M_f/M_0 = 0.5$ by 13 to 25%. An increse in M_f/M_0 leads to an increase in the velocity V_{max}.

7. The relative distance of the effective path of a rocket with external inert substance increases as λ or σ_p increase, especially if σ_R 0.9. Within the range of values up to $\lambda = 0.2$ ($\sigma_R \approx 0.5$) the distance of the effective path S_R may increase by 20 to 40%, this increase being promoted by a decrease in the relative rocket velocity V_R/W'.

3. INTERNAL (NOZZLE) HEAT RECOVERY.

Taking into account the conditions for the formation of gas-dynamic losses, it may be safely said that utilization of only external regeneration cannot be considered expedient.

In this case the intake of the regenerator will be placed in the supersonic part of the flow, and wave losses must therefore be considerable.

Moreover, even if wave losses in the regnerator were absent,

friction losses in the supersonic flow with a dufficiently developed friction surface would also be considerable. At the same time, the intensity of the heat flow at the nozzle outlet and, hence, in the regenerator is small. Numerical data show that fuel may be saved with external regeneration, but that this is accompanied by relatively high friction losses.

In order to reduce outlet losses it is necessary to develop a method whereby to reduce losses from shocks or to combine external regeneration with the internal (nozzle) one or, finally, make use only of the latter.

Computation of nozzle regeneration leads to the following expression for the determination of temperature at the end of expansion which takes place in the nozzle regenerator:

$$\left(\frac{T_2}{T_1}\right)^{1+\frac{\bar{q}}{1-\frac{T_2}{T_1}}}=\left(\frac{p_2}{p_1}\right)^{\frac{k-1}{k}}. \qquad (27)$$

where $$\bar{q}=\frac{Q_w+Q_r}{I_1}=\bar{q}_w+\bar{q}_r. \qquad \odot$$

Here Q_r is the heat equivalent to the work of friction forces;

$\bar{q}_w$ is the relative thermal stress of the cooling jackets;

$\bar{q}_r$ is the relative thermal stress of friction forces.

The temperature ratio T_2/T_1 is determined in a simpler way from the following quadratic equation

$$\left(\frac{T_2}{T_2}\right)^2+\left(1-\bar{q}-\frac{T_{2a}}{T_1}\right)\left(\frac{T_2}{T_1}\right)-(1-\bar{q})\frac{T_{2a}}{T_1}=0. \qquad (28)$$

For example, with k = 1.2 and = 20 we obtain T_{ad}/T_1 = = 0.606. If $\bar{q}$ = -1/8, then T_2/T_1 = 0.5 and n = 1.3. Accordingly, with $\bar{q}$ = -4/8, n = 1.86 and T_2/T_1 = 0.25.

The discharge velocity from the regenerative nozzle is determined according to formula

$$\frac{w_2^2}{2g}=\frac{w_{2a}^2}{2g}+\frac{Q_w}{A}+\frac{k}{k-1}RT_{2a}\left[1-\left(\frac{T_2}{T_1}\right)^{\frac{k-1}{k}}\frac{T_2}{T}\right]. \qquad (29)$$

If $\bar{q} \leqslant 0.15$, then we have with sufficiene accuracy

$$\frac{w_2^2}{2g}=\frac{w_{2a}^2}{2g}-L_r+c_pT_1\bar{q}\,\frac{1-\left(\frac{p_2}{p_1}\right)^{\frac{k-1}{k}}}{1+\left(\frac{p_2}{p_1}\right)^{\frac{k-1}{k}}}. \qquad (29a)$$

Figure 10 shows an example xx of the changes in the relative values for q_w and τ along the nozzle xx axis with the neck redius in the regenerator regenerator r_{lim} = 4 mm with an initial dimension without regenerator r_{lim} = 40 mm. Some uncertainties in the computation method and the fact that the effect of structural elements of the regenerator have not been taken into consideration forced us to consider in the given example not the absolute values but their ratios. Maximum thermal load of a wall q_w is obtained

immediately before the critical section, while maximum friction stress $\tau_{w\,max}$ is obtained immediately after the neck. The maximum effect of friction forces, inasmuch as velocity increases along the nozzle axis, falls on a section located further away from the critical section as compared with the spot where $\tau_{w\,max}$. Total heat production q changes in such a way that its peak is located almost in the critical section. The effect of friction forces is so considerable that toward the end of expansion, heat production from negative becomes positive.

Beyond the critical section and after having reached its peak, the effect of friction decreases, although in a considerably slower way than the heat losses from the wall. With q_{cool} = 1.5% in the initial nozzle, in the regenerative nozzle (r_{lim} = 4 mm with 100 nozzles) the calculated consumption amounts to q'_{cool} = 21% in the nozzle ducts and q''_{cool} = 7% in the ducts of the external regenerator. Consequently, regenerative heat exchange amounts to 28% of the value of initial enthalpy. The initial version of these computations is characterized by the following data: T_1 = 3,000° abs; p_k = 22 kg/cm^2; R = 30; k = 1.3; I_{00} = 1,200 cal/kg.

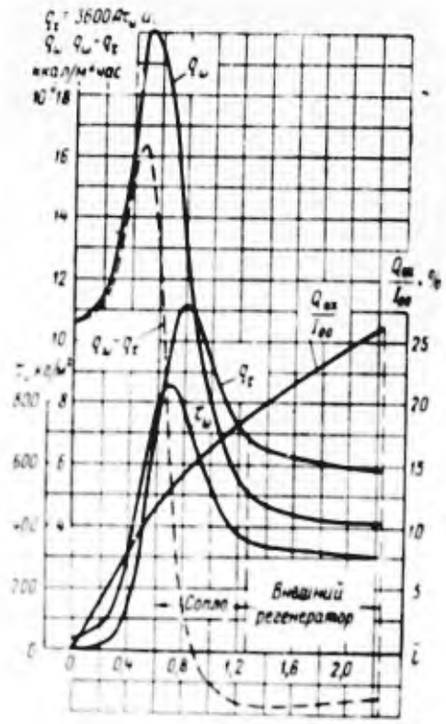

Fig. 10. Thermal characteristic of nozzle with friction and cooling in the presence of external and internal (nozzle) regeneration of heat.

a) kcal/m^2 hour b) nozzle c) external regenerator.

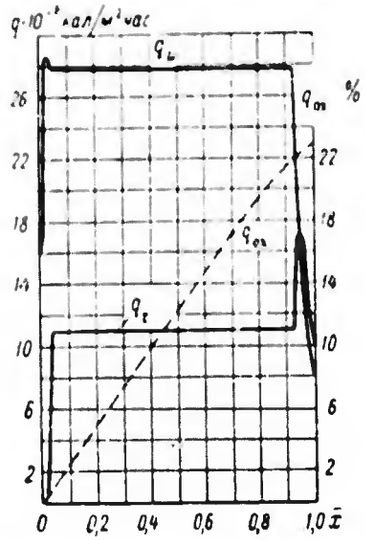

Fig. 11 . Thermal characteristic of nozzle with friction in the presence of internal (nozzle) heat recovery. a) kcal/m^2 hour.

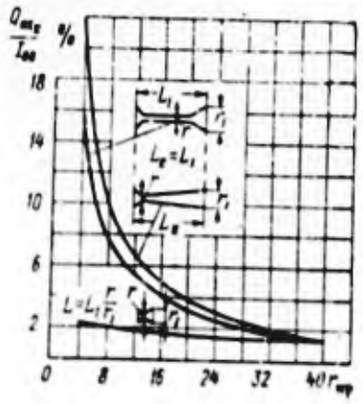

Fig. 12. Variation of regeneration heat depending on the neck radius of nozzle with identical overall consumption for three types of nozzles.

Figure 10 shows clearly that the external regenerator is not sufficiently profitable owing to high friction losses and low thermal stress q_w. By removing the external regenerator it is impossible to increase the quantity of heat transferred to the regenerator by developing the heat exchange surfaces in those places where q_w is high. For example, Fig. 11 shows the thermal characteristic of a regenerator nozzle with a highly developed neck surface. The length of the nozzle regenerator is the same

as that of the outlet nozzle. Nevertheless, on most of the surface of the regenerator nozzle we have high q_w and low q_τ. The problem of cooling the working substances from the external part of the duct is not examined here since we assume that a satisfactory cooling system is possible.

In Fig. 12 we compare the relative heat losses q_{cool} in regenerator nozzles with two profiles: one with a developed neck, and the other with a normal one. In both cases the nozzle lengths are identical and the diameter of the critical section equals 8 mm. Although from a thermodynamic point of view the second nozzle version is more profitible, yet, there is less heat removed in the regenerator while friction losses are greater.

The curve at the bottom of Fig. 12 shows that if instead of one initial nozzle we utilize 100 nozzles geometrically similar to the initial one, heat exchange will not increase considerably while the length of the nozzle unit will be 10 times shorter.

In conclusion we bring Table II which characterizes the effect of regeneration on the specific thrust and thermodynamic efficiency of the chamber. The initial temperature is assumed to be identical for all versions, and water is the inert heat-transfer agent.

TABLE 2

Variation of Specific thrust and Efficiency of Regenerative Chambers

Варианты регенерации	Q_{ox}	Q_r	$P_{уд}$	$\frac{P_{уд}}{P_{уд1}}$	$\frac{C_{уд}}{C_{уд1}}$
Исходный $r_{кр}=40$ мм	0	0	201,2	1,0	1,0
Сопловая регенерация $r_{кр}=4$ мм	—20,5	10,7	229	1,147	0,605
Сопловая и внешняя регенерация $r_{кр}=4$ мм	—28,2	21,5	194,4	0,964	0,56
Сопловая регенерация (сопло с длинной горловиной) $r_{кр}=5$ мм	—23	10,4	218	1,085	0,604

1) Regeneration alternatives 2) Reference r_{lim} = 40 mm 3) nozzle regeneration r_{lim} = 4 mm 4) nozzle and external regeneration r_{lim} = 4mm 5) nozzle regeneration (nozzle with long neck) r_{lim} = 5 mm. 6) Note. In the last two vertical columns, the index "1" denotes the initial version with r_{lim} = 40 mm.

Utilization of regeneration becomes complicated and its advantages diminish owing to the resistances resulting from great velocities of the working substance during expansion. Yet, these resistances are of no decisive importance.

Heat recovery and the presence of resistances in the nozzle

duct result in a considerable improvement of the thermodynamic efficiency of the chamber.

Owing to great friction losses, external regeneration can be successfully utilized in those cases where heat changes into recovery, as, for instance, in composite engines, including liquid fuel rocket engines.

The conditions for the utilization of regeneration improve with increasing adiabatic parameters of the working substance.

COOLING OF SHORT WORKING TURBINE BLADES BY MEANS OF HEAT REMOVAL TO THE COOLED ROOT

By

Engineer A. F. Shtyrlin

One of the main problems at which the gas turbine technology is working at present, consists in producing high-temperature gas turbines. Increased gas temperatures affect, in the first place, the efficiency of the blades on the turbine rotor. For this reason, the principal attention is devoted to increasing the stability of this turbine assembly. The program of investigations directed to solve this problem concentrates on developing materials with greater heat resistance and devising methods for artificial blade cooling.

The possibilities of improving heat resistance of nickel-base alloys has been almost entirely exhausted. New heat-resistant molybdenum- and chromium-base alloys as well as ceramics and metal ceramics are for the time being at the stage of experimentation. For this reason, utilization of turbine blade cooling promises to lead to a faster solution of the problem of producing high-temperature gas turbines. The great advantage of cooled turbines consists in the

possibility of utilizing heat-resistant materials available in great quantities.

1. COOLING METHOD AND POSSIBLE WAYS TO INCREASE ITS EFFICIENCY

One of the simplest methods of cooling working turbine blades consists in removing heat from the blade to the cooled root. This method has been utilized by gas turbine technology for a long time, although basically it was applied for lowering the temperatures of discs and locks (Fig. 1) rather than for the cooling of working blades. Alongside great operating simplicity and reliability, the given system of air cooling is not very efficient. Efforts to improve the rate of cooling lead to an increase in the consumption of air and to an increase in the capacity output for cooling.

The negligible results of such cooling in turbines of ram-jet engines is due mainly to the small values of the coefficient of heat transfer from the disc to the cooling air (α_{air} = 200 to 400 kcal/m^2 degrees x hour) and a relatively high air temperature (t_{air} approximately 200° C).

For this reason, in powerful turbines with long working blades, whose height frequently exceeds 100 mm, the effect of cooling spreads only over 25 to 30% of their height and cannot exert any

substantial effect on the distribution of temperatures in the blade (Fig. 2).

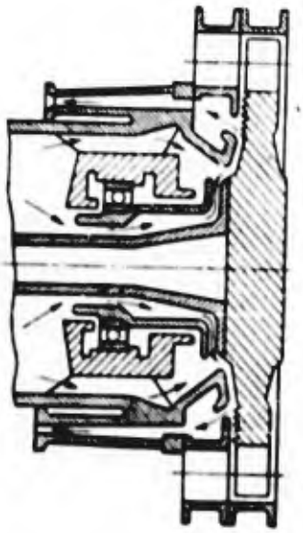

Fig. 1. Design of air cooling system of a turbine disc.

As the power of turbines decreases and, hence, the working blades become shorter, the effect of cooling spreads over a constantly increasing relative height of the blade. As a consequence, the given blade cooling method can be most efficiently utilized only in small-power turbines, i.e., in turbines of turbo-compressors of composite piston engines, turbo-pump units and turbo-starters, gas turbine

engines for motorcars , the first stages of small-power tubro-jet engines and stationary gas turbine plants with high initial gas pressures.

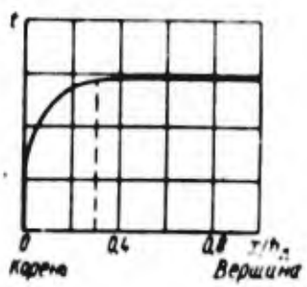

Fig. 2. Temperature distribution along the height of a long blade. a) root b) top.

The efficiency of the given cooling method for short turbine blades can be considerably improved by utilizing a fluid as a cooling working substance. The most commonly used designs of a coolant system

of the roots of working blades are shown in Fig. 3.

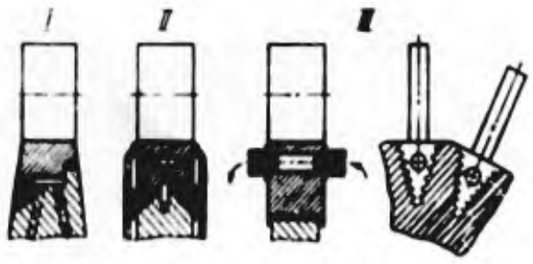

Fig. 3. Diagrams of coolant systems of blade roots. I-blades made in one piece with a top part of the disc, II -blades welded to the disc, III-blades with a "herringbone" lock.

Another possible way for improving the efficiency of the cooling system consists in utilizing various types of covers for the blades, for example, thermal protection of the blades by means of

covers with lower heat conduction, covers made of materials with high heat conduction which improve the transfer of the heat used by the gas to the cooled root, as well as combinations of these covers.

2. DISTRIBUTION OF TEMPERATURES IN THE BLADE AND BLADE COVER

Proceeding from the system of heat flows in Fig. 4, let us make the following possible assumptions:

a) The gas deceleration temperature in the boundary layer t_r^* is considered constant both along the profile and along the height of the blade.

b) The blade temperature t_b is considered constant over the perimeter and transverse section. In long blades, the difference of temperatures at various points of the section, with air cooling of the disc, usually does not exceed 20 to 30°. In the case of short blades and utilization of more efficient cooling of blade roots by means of fluids, this difference of temperatures along the section seems to increase slightly and to attain a maximum near the blade base. Along the transverse section of the blade, maximum temperature will be at the inlet edge, while the minimum temperature will be found in the central part of the blade. Although this

assumption introduces a slight error, it simplifies considerably the problem and makes it possible to solve it for blades not as a three-dimensional problem but as a one-dimensional one.

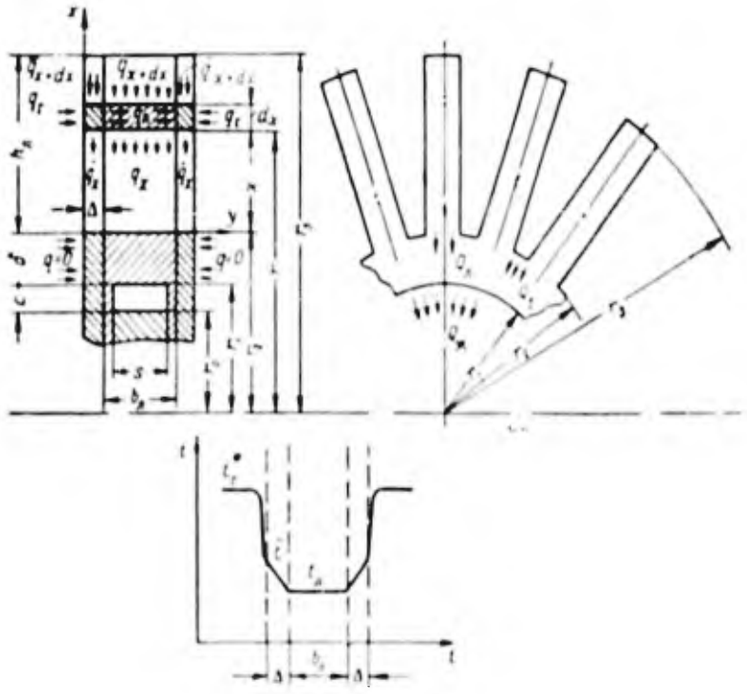

Fig. 4. System of heat flows and temperatures in the blade and blade cover.

c) The heat-transfer coefficient α_2 and the coefficients of heat conduction of the material of the blade λ_b and of the blade

cover λ_{Δ} are considered constant along the height of the blade. Under actual service conditions they vary, but if for the computation we take these coefficients as being average alont the height, the relative error will be small.

In order to solve the problem it is necessary to find:

- The distribution of temperatures along the height of the blade $t_b(x)$;
- The distribution of temperatures in the blade cover $\bar{t}(x,y)$;
- The distribution of temperatures in the disc $t_{\rho}(r)$;
- The quantity of heat Q_r removed from the disc.

Let us write the differential equation of thermal conduction for the blade cover under steady heat conditions

$$\frac{\partial^2 \bar{t}}{\partial x^2} + \frac{\partial^2 \bar{t}}{\partial y^2} = 0 \qquad (1)$$

and let us set up the differential equation of thermal conduction of the blade. For the isolated differential blade element with a thickness dx the heat balance will be written as

$$q_x = q_{x+dx} + q_{\Delta}.$$

A 1/6

where

$$q_x = \lambda_x F_x \left(\frac{\partial t}{\partial x}\right)_x^*; \quad q_{x+dx} = \lambda_x F_x \left(\frac{\partial t}{\partial x}\right)_{x+dx}^*; \quad q_{\Delta} = -\lambda_{\Delta} u_x dx \left(\frac{\partial \bar{t}}{\partial y}\right)_{y=\Delta}.$$

B 1/6

Expanding $(\partial t/\partial x)_{x+dx}$ in a Taylor series and substituting the values q_x, q_{x+dx} and q_b in the equation of heat balance, we obtain the equation of thermal conduction for the blade

$$\frac{d^2\bar{t}}{dx^2} - m^2\left(\frac{\partial \bar{t}}{\partial y}\right)_{y=\Delta} = 0, \qquad (2)$$

where

$$m^2 = \frac{\lambda_\Delta u_\Delta}{\lambda_\Delta F_\Delta}. \qquad \text{C 146}$$

It is necessary to solve differential equations of thermal conduction for the blade and blade cover (1), (2) for a practical case determined by boundary conditions.

Boundary conditions for equation (1) are as follows:

$$\bar{t}(0, y) = t_2; \qquad (3)$$

$$\left(\frac{\partial \bar{t}}{\partial x}\right)_{x=x_1} = 0; \qquad (4)$$

$$-\lambda_\Delta\left(\frac{\partial \bar{t}}{\partial y}\right)_{y=0} = \alpha_1 (t_1' - \bar{t})_{y=0}; \qquad (5)$$

$$\bar{t}(x, \Delta) = t_x; \quad q_\Delta = q_x - q_{x+dx}. \qquad (6)$$

Boundary conditions for equation (2):

$$t_{x=0} = t_2; \qquad (7)$$

(x) The plus sign has been taken for the reason that the direction of the x-axis is opposite to the direction of heat propagation. (this foot footnote refers to formula B 146 - - translator's note).

$$\left(\frac{dt}{dx}\right)_{x=h_3}=0. \tag{8}$$

Keeping in mind condition (6) and equation (2), we have

$$\left(\frac{\partial^2\bar{t}}{\partial x^2}\right)_{y=\Delta}-m^2\left(\frac{\partial\bar{t}}{\partial y}\right)_{y=\Delta}=0. \tag{A 147}$$

Substituting this expression in equation (1) , we can write boundary condition (6) as

$$\left(\frac{\partial^2\bar{t}}{\partial y^2}\right)_{y=\Delta}+m^2\left(\frac{\partial\bar{t}}{\partial y}\right)_{y=\Delta}=0. \tag{9}$$

Thus, the problem amounts to solving the Laplace equation (1) for the blade cover at boundary conditions (3), (4), (5) and (9). To determine the blade temperature it is sufficient to set $y = \Delta$ in the expression $\bar{t}(x,y)$.

Replacing $\bar{t}$ by a new variable $u = \bar{t} - t_2$, let us write differential equation (1) as

$$\frac{\partial^2u}{\partial x^2}+\frac{\partial^2u}{\partial y^2}=0. \tag{10}$$

Boundary conditions (3), (4), (5) and (9) are replaced by the following conditions:

$$u_{x=0}=0; \tag{11}$$

$$\left(\frac{\partial u}{\partial x}\right)_{x=h_3}=0; \tag{12}$$

$$\lambda_3\left(\frac{\partial u}{\partial y}\right)_{y=0}+\varepsilon\alpha_1(t_1^*-t_2-u)_{y=0}=0; \tag{13}$$

$$\left(\frac{\partial^2u}{\partial y^2}\right)_{y=\Delta}+m^2\left(\frac{\partial u}{\partial y}\right)_{y=\Delta}=0. \tag{14}$$

In order to solve equation (10) let us use the classical

Fourier method and let us look for the solution of the equation in the form of a product of two functions:

$$u = X(x)\,Y(y). \tag{15}$$

where X(x) is the function of only x;

Y(y) is the function of only y.

Substituting expression (15) in equation (10) we obtain

$$YX'' + XY'' = 0 \text{ или } \frac{X''}{X} = -\frac{Y''}{Y} = -\gamma^2, \qquad \text{A 148}$$

where γ is a constant quantity.

The solutions of equations

$$X'' + \gamma^2 X = 0 \tag{16}$$

and

$$Y'' - \gamma^2 Y = 0 \tag{17}$$

for the
have the form

$$X = C_1 \sin \gamma x + C_2 \cos \gamma x, \tag{18}$$

$$Y = A \operatorname{sh} \gamma y + B \operatorname{ch} \gamma y. \tag{19}$$

Consequently, the expression of function u(x,y) will be

$$u = (C_1 \sin \gamma x + C_2 \cos \gamma x)(A \operatorname{sh} \gamma y + B \operatorname{ch} \gamma y). \tag{20}$$

We find the integration constants from boundary conditions:

$$u_{x=0} = 0, \text{ т. е. } C_2 = 0, \qquad \text{при } x = 0; \qquad \text{B 148}$$

$$\left(\frac{\partial u}{\partial x}\right)_{x=h_2}=0, \text{ т. е. } -C_1\gamma\cos\gamma h_2=0, \quad \text{при } x=h_2.$$

C 148

Constant C_1 cannot be equal to zero since in this case the entire solution will become zero. Function $\cos \gamma h_2$ will equal zero only if $\gamma h_2=(2n+1)\frac{\pi}{2}$, where n = 0, 1, 2, 3 .....

Hence

$$\gamma=\gamma_n=\frac{(2n+1)\pi}{2h_2}. \tag{21}$$

Substituting (21) in equation (20) we obtain a countless number of particular solutions. The general solution consists of the sum of particular solutions, i.e.,

$$u=\sum_{n=0}^{\infty}(A_n\operatorname{sh}\gamma_n y+B_n\operatorname{ch}\gamma_n y)C_n\sin\gamma_n x. \tag{22}$$

Introducing functions u(x,y) and its derivatives in boundary conditions (13) and (14) we obtain

$$\alpha_1(t_1'-t_2)=\sum_{n=0}^{\infty}(\alpha_1 B_n-\lambda_2\gamma_n A_n)C_n\sin\gamma_n x \tag{23}$$

and

$$\sum_{n=0}^{\infty}\{A_n[\gamma_n^2\operatorname{sh}\gamma_n\Delta+m^2\gamma_n\operatorname{ch}\gamma_n\Delta]+B_n[\gamma_n^2\operatorname{ch}\gamma_n\Delta+\gamma_n m^2\operatorname{sh}\gamma_n\Delta]\}\sin\gamma_n x=0. \tag{24}$$

The latter equality will be true only if

$$\left.\begin{aligned}A_n&=-[\gamma_n\operatorname{ch}\gamma_n\Delta+m^2\operatorname{sh}\gamma_n\Delta],\\ B_n&=[\gamma_n\operatorname{sh}\gamma_n\Delta+m^2\operatorname{ch}\gamma_n\Delta].\end{aligned}\right\} \tag{25}$$

Substituting the values found for the coefficients A_n and B_n in equation (23) we obtain

$$\varepsilon\alpha_r (t_r^* - t_2) = \sum_{n=0}^{\infty} C_n \beta_n \sin \frac{(2n+1)\pi x}{2h_1}, \tag{26}$$

where

$$\beta_n = \varepsilon\alpha_r [\gamma_n \operatorname{sh} \gamma_n \Delta + m^2 \operatorname{ch} \gamma_n \Delta] + \gamma_n \lambda_n [\gamma_n \operatorname{ch} \gamma_n \Delta + m^2 \operatorname{sh} \gamma_n \Delta]. \tag{27}$$

Thus, function $\varepsilon\vartheta_r (t_r^* - t_2)$ in expression (26) is expanded in a Fourier series

$$f(x) = \sum_{n=0}^{\infty} b_n \sin \frac{(2n+1)\pi x}{2h_1}. \tag{A 149}$$

The coefficients of the Fourrier series can be found with the aid of the well-known expression (1):

$$b_n = \frac{2}{h_1} \int_0^{h_1} f(x) \sin \left[\frac{(2n+1)\pi x}{2h_1} \right] dx \tag{B 149}$$

or

$$b_n = C_n \beta_n = \frac{2}{h_1} \int_0^{h_1} \varepsilon\alpha_r (t_r^* - t_2) \sin \left[\frac{(2n+1)\pi x}{2h_1} \right] dx = \frac{4\varepsilon\alpha_r (t_r^* - t_2)}{\pi (2n+1)}. \tag{C 149}$$

whence

$$C_n = \frac{4\varepsilon\alpha_r (t_r^* - t_2)}{\pi} \frac{1}{(2n+1)\beta_n}. \tag{28}$$

Keeping in mind that $t = t_2 + u$, and introducing in function (22) the quantities A_n, B_n and β_n, we obtain finally the reference dependence for the determination of temperatures at any point of the blade cover

$$\bar{t} = t_2 + \frac{4\varepsilon\alpha_r (t_r^* - t_2)}{\pi} \times$$

$$\times \sum_{n=0}^{\infty} \frac{\gamma_n \operatorname{sh} \gamma_n (\Delta - y) + m^2 \operatorname{ch} \gamma_n (\Delta - y)}{\gamma_n (\varepsilon\alpha_1 + \lambda_\Delta m^2) \operatorname{sh} \gamma_n \Delta + (\varepsilon\alpha_r m^2 + \gamma_n^2 \lambda_\Delta) \operatorname{ch} \gamma_n \Delta} \frac{\sin \gamma_n x}{2n+1} \quad (29)$$

where

$$\gamma_n = \frac{(2n+1)\pi}{2h_\Delta}; \quad m^2 = \frac{\alpha_\Delta u_\Delta}{\lambda_\Delta F_\Delta}; \quad n = 0, 1, 2, 3, 4 \ldots$$

A149 (29)

The temperature of the blade is equal to the temperature of its cover with y = Δ (see boundary condition (6)), hence

$$t_\Delta = t_2 + \frac{4\varepsilon\alpha_r (t_1^* - t_2) m^2}{\pi} \times$$

$$\times \sum_{n=0}^{\infty} \frac{1}{\gamma_n (\varepsilon\alpha_1 + \lambda_\Delta m^2) \operatorname{sh} \gamma_n \Delta + (\varepsilon\alpha_1 m^2 + \gamma^2 \lambda_\Delta) \operatorname{ch} \gamma_n \Delta} \frac{\sin \gamma_n x}{2n+1}. \quad (30)$$

Dependences (29) and (30) make it possible to determine the temperature at any point of the blade cover and the blade itself if the temperature of its base is known.

Let us examine the heat flows in the turbine disc and determine the temperature of the turbine base. The portion of the turbine disc from the inner cooled surface to the blade base can be regarded as the ring wall. Taking into account that in a turbine with such a blade cooling system no additional air cooling of the disc surface is effected, the heat flows across the edge surfaces of this ring may be regarded as equally zero. The design diagram can be represented in the following way: heat is conveyed from the cicular turbine blade grid to the outer ring surface, while from the inner surface, heat is

removed by the coolant (see Fig. 4), i.e.,

$$Q_{реш} = Q_ж \text{ или } Q_л + Q_т = Q_ж. \tag{31}$$

The quantity of heat transferred to the disc through the transverse sections of all the blades of the turbine rotor can be written as

$$Q_л = z_л \lambda_л F_л \left(\frac{\partial t}{\partial x}\right)_{x=0} = z_л \lambda_л F_л \frac{2\varepsilon\alpha_т (t_1^* - t_2)}{\pi} \times$$

$$\times \sum_{n=0}^{\infty} \frac{\gamma_n}{(2n+1)[\gamma_n(\varepsilon\alpha_т + \lambda_л m^2)\operatorname{sh}\gamma_n\Delta + (\varepsilon\alpha_т m^2 + \gamma_n^2\lambda_л)\operatorname{ch}\gamma_n\Delta]} \tag{32}$$

The heat flow from the gas to the disc surface in the inter blade ducts equals

$$Q_т = \alpha_т (2\pi r_2 b_л - z_л F_л)(t_1^* - t_2). \tag{33}$$

Hence, the heat flow from the grid to the outer ring surface equals

$$Q_{реш} = Q_л + Q_т = (t_1^* - t_2) C, \tag{34}$$

where

$$C = \frac{2z_л \lambda_л F_л \varepsilon\alpha_т m^2}{\pi} \times$$

$$\times \sum_{n=0}^{\infty} \frac{\gamma_n}{(2n+1)[\gamma_n(\varepsilon\alpha_т + \lambda_л m^2)\operatorname{sh}\gamma_n\Delta + (\varepsilon\alpha_т m^2 + \gamma_n^2\lambda_л)\operatorname{ch}\gamma_n\Delta]} + \alpha_т (2\pi r_2 b_л - z_л F_л) \tag{35}$$

If the edges are thermally insulated, the heat flow through the ring is determined by expression [2]

$$Q_б = 2\pi b_л \frac{\lambda_б}{\ln \frac{r_2}{r_1}} (t_2 - t_1). \tag{36}$$

while the temperature of the ring wall is

$$t_6 = \frac{t_2 \ln \frac{r}{r_1} + t_1 \ln \frac{r_2}{r}}{\ln \frac{r_2}{r_1}}. \qquad (37)$$

The heat transferred from the inner disc surface to the coolant equals

$$Q_ж = \alpha_ж 2\pi r_1 (t_1 - t_ж) b_д. \qquad (38)$$

Keeping in mind that $Q_{grid} = Q_r$, and solving simultaneously equations (34), (36) and (38) we obtain the temperature of the blade socket

$$t_2 = \frac{t_ж + t_г^* \frac{CR}{\pi b_д}}{1 + \frac{CR}{\pi b_д}}, \qquad (39)$$

where

$$R = \frac{1}{2\lambda_д} \ln \frac{d_2}{d_1} + \frac{1}{\alpha_ж d_1}, \qquad (40)$$

and the temperature of the disc wall washed by the coolant

$$t_1 = t_ж + \frac{(t_г^* - t_2) C}{\alpha_ж \pi d_1 b_д}. \qquad (41)$$

3. PARTICULAR CASES

The calculated dependences ~~for~~ obtained for the general case make it possible to find the distribution of temperatures in the blade and disc at any possible value for thermal conduction of the material of blade covers. Computation of the dependences, however, becomes fairly complex and laborious. For particular cases, the

solution of the problem can be considerably simplified on account of a slight deterioration in accuracy. Let us examine these cases.

One-layer blade covers with $\lambda_\Delta \ll \lambda_l$.

As is known, blade covers with low thermal conduction increase thermal resistance and, hence, reduce the heat-transfer coefficient on the blade surfaces. The high-temperature gradient which arises in the blade cover, increases considerably the surface temperature and reduces heat flow from the gas to the blade. In blade covers with $\lambda_\Delta \ll \lambda_l$ the temperature gradient in the direction of the x-axis will be considerably less than along the y-axis. For this reason, we may disregard the heat flowing over the blade cover along the blade, i.e., assume

$$\bar{q}_x \approx 0$$

(A 152)

and assume that heat propogates only in the blade cover only in the direction of the y-axis.

The differential equation of thermal conduction for the blade cover takes the form

$$\frac{\partial^2 \bar{t}}{\partial y^2} = 0. \qquad (A2)$$

The equation of thermal conduction for the blade remains the same,

The solution of the system of two differential equations (2) and (12) together with boundary conditions (5), (6), (7) and (8) yield the following calculating formulas:

Temperature of blade cover

$$t(x, y) = t_r^* - (t_r^* - t_2)\frac{y + \frac{\lambda_\delta}{\varepsilon\alpha_r}}{\Delta + \frac{\lambda_\delta}{\varepsilon\alpha_r}}\frac{\operatorname{ch} k(h_\lambda - x)}{\operatorname{ch} kh_\lambda}, \tag{13}$$

where

$$k = \sqrt{\frac{\varepsilon\alpha_r u_\lambda}{\lambda_\lambda F_\lambda}\left(\frac{1}{1 + \frac{\varepsilon\alpha_r\Delta}{\lambda_\lambda}}\right)}; \tag{B 152}$$

(1)

Temperature of the blade

$$t_\lambda = t_r^* - (t_r^* - t_2)\frac{\operatorname{ch} k(h_\lambda - x)}{\operatorname{ch} kh_\lambda}; \tag{14}$$

Temperature of blade socket

$$t_2 = \frac{t_\infty + t_r^*\frac{C_1 R_1}{\pi b_\lambda}}{1 + \frac{C_1 R_1}{\pi b_\lambda}}, \tag{15}$$

where

$$C_1 = z_\lambda F_\lambda \lambda_\lambda k \operatorname{th} kh_\lambda + \alpha_1(\pi d_2 b_\lambda - z_\lambda F_\lambda),$$
$$R_1 = \frac{1}{2\lambda_k}\ln\frac{d_2}{d_1} + \frac{1}{\alpha_\infty d_1}; \tag{C 152}$$

temperature of the inner disc wall cooled by a fluid

$$t_1 = t_\infty + \frac{t_r^* C_1}{\alpha_\infty \pi d_1 b_\lambda}; \tag{16}$$

(1) This formula has the same form as that for the blade without a cover [2]; the difference consists only in the parameter k.

temperature of the ~~xis~~ disc

$$t_0 = \frac{t_2 \ln \frac{r}{r_1} + t_1 \ln \frac{r_2}{r}}{\ln \frac{r_2}{r_1}}; \qquad (47)$$

quantity of heat removed by the coolant

$$Q_{\text{реш}} = (t_r^* - t_2) C_1;$$
$$Q_\lambda = \frac{\lambda_\lambda 2\pi b_\lambda}{\ln \frac{r_2}{r_1}} (t_2 - t_1);$$
$$Q_\alpha = \alpha_\alpha (t_1 - t_\alpha) \pi d_1 b, \qquad (48)$$

One-layer blade cover with $\lambda_\Delta \gg \lambda_\lambda$.

If thermal conduction of the blade cover is considerably greater than thermal conduction of the blade material, the temperature gradient in the blade cover in the direction of the y-axis will be small and we can assume that

$$\frac{\partial t}{\partial y} = 0. \qquad (53)$$

Blade covers of this type, while increasing the heat-transfer coefficient, improve the transfer of heat from the blade to the fluid and even out the temperature both along the height and the perimeter of the blade. The solution of the given problem yields the same dependences as in the preceding case (43) and (44), but with a new parameter

$$k = \sqrt{\frac{\varepsilon \alpha_r u_\alpha}{\lambda_\lambda F_\lambda + \lambda_\Delta u_\Delta \Delta}}. \qquad (49)$$

Two-layer Blade Covers with $\lambda_{\Delta 1} \gg \lambda_b \gg \lambda_{\Delta 2}$

If the working blades are made of conventional heat-resistant, poorly heat-conducting alloys of the type YalT, EI437, etc., two-layer blade covers may turn out to be more efficient than one-layer ones. The following combination seems to offer the best alternative:

The first (cover placed) on the blade consists of material with good thermal conduction $\lambda_{\Delta 1} \gg \lambda_b$;

The second cover has a poor thermal conduction $\lambda_{\Delta 2} \ll \lambda_b$.

When solving this problem let us assume

$$\left(\frac{\partial \bar{t}}{\partial \nu}\right)_{s_1} = 0 \text{ и } (\bar{q}_1)_{s_1} = 0$$

B 153

The calculated dependences are the same as the preceding ones [(43) and (44)], but once again with a new parameter

$$k = \sqrt{\frac{\varepsilon_2 a_2}{\lambda_{\Delta 1} a_{\Delta 1} \delta_1 + \lambda_2 F_2}\left(\frac{1}{1 + \frac{\varepsilon_2 \delta_2}{\lambda_{\Delta 2}}}\right)}.$$

A 154

4. RESULTS OF TESTS AND THEORETICAL COMPUTATIONS

The calculated dependences obtained from the solution of the theoretical problem make it possible to single out the field of application, the qualitative and quantitative picture of effectiveness of cooling turbine blades with and without covers.

All of the tests data set forth in the present paper were obtained under statistical conditions on a grid of five blades with an active profile with the following geometric data: h_b = 25 mm; b_b = 20 mm; u_b = 60.4 mm, F_b = 108 mm^2. As a coolant we used kerosene.

The theoretical computations, the results of which are shown in Figs. 9, 10, 12, 13, 14, 15 and 16, were carried out for the rotor: d_{mean} = 0.15 m; h_b = 21 mm; b_b = 15 mm; F_b = 52 mm^2; u_b = 46 mm; δ = 20 mm; z_b = 45; α_1 = 4,000 kcal/m^2 degrees x hour; α_2 = 15,000 kcal/m^2 degree x hour; λ = 20 kcal/m x degree x hour.

Blades without cover

The experimental check of the theoretical solution, carried out with a blade without cover operating under statistical conditions (Fig. 5), showed that the scattering of experimental points does not exceed 20 to 30°, while the maximum relative error resulting from inaccuracies in computation and the assumptions admitted, amounts to 4 to 5%. The effectiveness of blade cooling (see formula (44)) depends on the temperature of its base t_2, its height h_b and the parameter k.

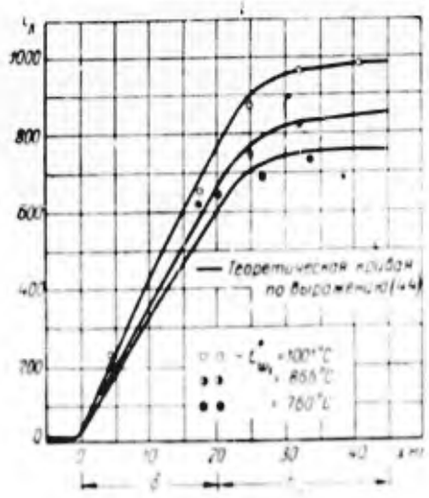

Fig. 5. Juxtaposition of the theoretical and experimental distribution of temperatures in a blade without cover. $\delta_{r.mean} = 9.2$; $\alpha_{r.mean} =$ 2,000 kcal/m^2 degrees x hour; $\alpha_r = 13{,}000$ to 15,000. 1) theoretical curve for expression (44).

The temperature of the blade's socket t$_2$ at great values for α_r is basically determined by the distance δ (Fig. 6). For this reason, when designing working blades with this cooling system, the distance from the cooling duct to the blade's socket must be minimal.

Owing to great thermal resistance of the blade towards the cooling duct, sizeable cooling can be obtained only with short blades

the height of which does not exceed 30 to 40 mm, and with small values for parameter k. This is achieved in the following cases:

1) With small heat flows across the turbine rotor blades determined by the quantity $\Sigma\alpha_1$;

2) With a satsifactory thermal conduction of the turbine blade material;

3) If utilizing blades with a small outer heating surface and a large transverse section, i.e., with a smaller quantity u_b/F_b.

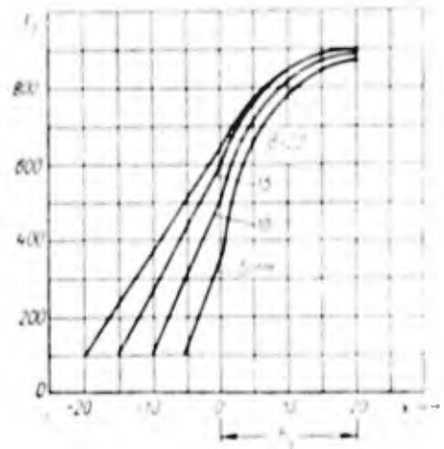

Fig. 6. Effect of distance δ on the temperature of the blade socket. t^*_r = 1,000° C; $\Sigma\alpha_1$ = 450 kcal/m^2 degrees x hour.

Computations carried out for an operating turbine and variable degree of partiality (Fig. 7) show that the blade actually begins to cool only with $\varepsilon\alpha_r < 15{,}000$ kcal/m^2 degrees hour (with $\varepsilon < 0.5$). The tests have confirmed these computations. Figure 8 gives the results of temperature measurements in the blade with varying effectiveness of heat transfer with the gas. With $\alpha_r > 1{,}600$ kcal/m^2 degrees x hour ($\delta_r > 7.3$) the effectiveness of blade cooling does not exceed $t^*_r - t_{b\,mean} = 50$ to 70°, while with $\alpha_r < 1{,}600$ kcal/m^2 degrees x hour it sharply increases.

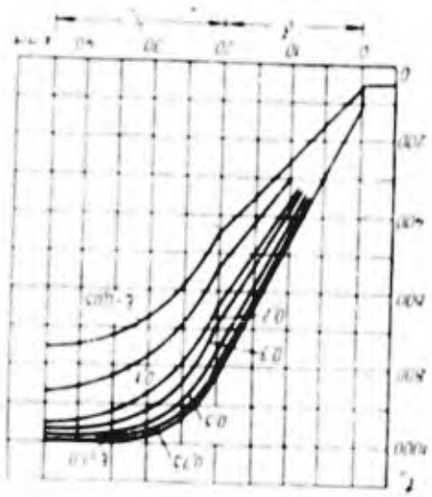

Fig. 7. Effect of degree of partiality of turbine on the effectiveness of blade cooling: a) kcal/m^2 degrees x hour.

Thermal conduction of the blade material has a decisive bearing on this type of cooling. The heat-resistant, nickel- base alloys of the type YalT, EI69, EI437 etc., utilized at the present time have a fairly low coefficient of thermal conduction ranging from 10 to 30 kcal/m degrees x hour. Such low thermal conduction makes it impossible to achieve an effective cooling of the blade, hence it is desirable to use heat-resistant alloys with a higher thermal conduction.

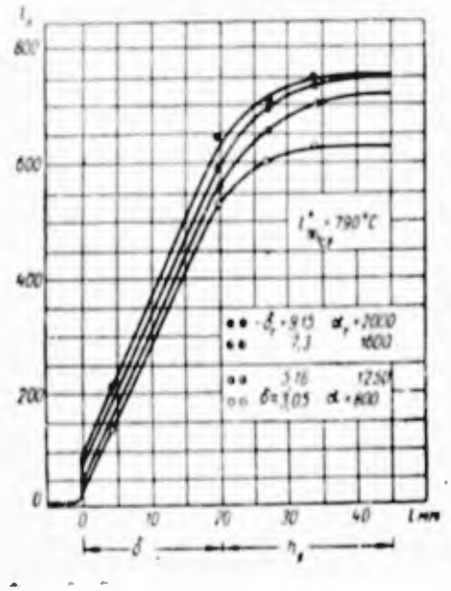

Fig. 8. Experimental distribution of temperature in blades depending on the intensity of heat flow.

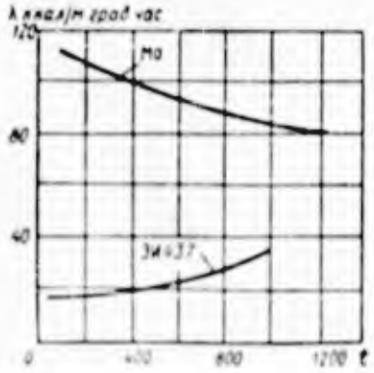

Fig. 9. Thermal conduction of a nickel alloy EI437 and sintered molybdenum.

Heat-resistant materials with the greatest future, whose utilization is expected to begin in the nearest future, are molybdenum-base alloys. These alloys have a high heat resistance and an excellent thermal conduction. Figure 9 shows a comparison between the coefficient of thermal conduction of a nickel alloy EI437 and sintered molybdenum. High thermal conduction of these alloys improves the transfer of heat to the cooled root and makes it possible to lower

considerably the blade temperature (Fig. 10) . With increasing blade dimensions, and especially of its chord b_b , the transverse section F_b increases somewhat more rapidly than the perimeter u_b , which also leads to a certain decrease in the blade temperature.

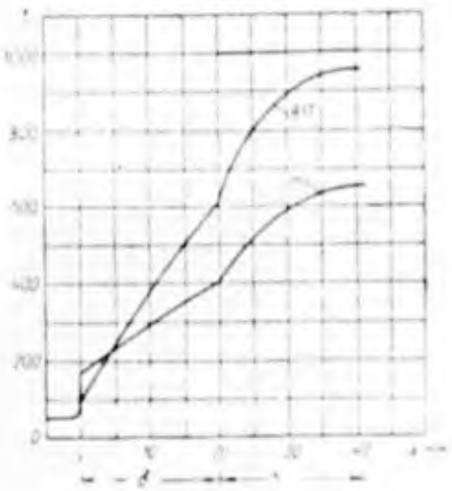

*$t_r = 100°C$; $\alpha_r = 400$.

Fig. 10: Effect of thermal conduction of material on the distribution of temperatures in the blade. a) kcal/m^2 degrees x hour; b) kcal/m degrees x hour c) YalT.

With the given cooling method, the inlet and outlet edges of the top part of the blade are least subject to cooling, hence failure and pitting begin from these spots of the blade. Figure 11 shows a plane grid of aluminum blades which has been subjected to tests at temperatures of advancing gas $t^{*}_{g1} \approx 550$ to 600°C. The temperature of the blade's socket was 350° C while that of the top part was approximately 500°C. Failure of the edges occurred because of overheat of blade spots difficultly accessible to cooling.

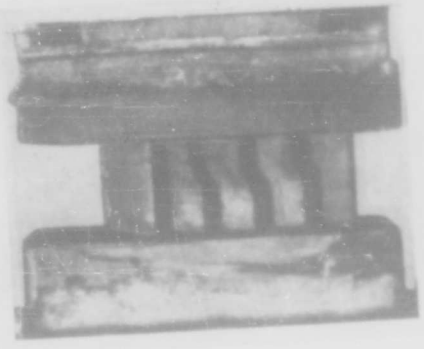

Fig. 11. Experimental grid with failed edges in the top part of the blade.

Blades with Covers

Comparison of the distribution of temperatures in the blade computed according to accurate dependences (29) and (30), and approximate dependences (43) and (44), showed a fairly satisfactory agreement of the results obtained (Fig. 12). For this reason all the subsequent theoretic analyses were carried out according to simpler approximate dependences.

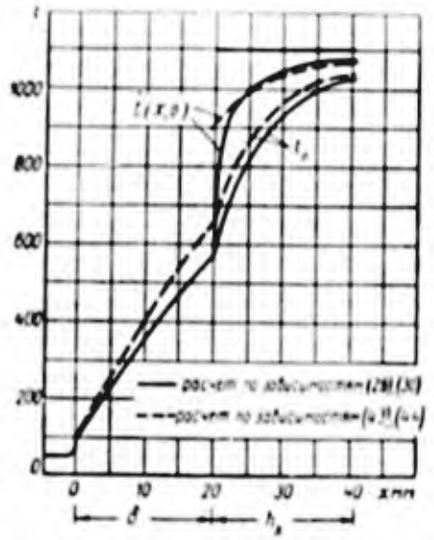

Фиг. 12 Сравнение температур лопатки с покрытием, рассчитанное по точным и приближенным зависимостям

$t_г^*$=1100° C; $\alpha_г$=800 ккал/м² град час; λ=0,5 м; $\lambda_з$=0,3 ккал/м град час.

Fig.12. Comparison of temperatures of blades with covers computed according to accurate and approximate dependences. a) computation according to dependences (29),(30) b) computation according to dependeces (43),(44) c) kcal/m^2 degrees x hour d)kcal/m degrees x hours.

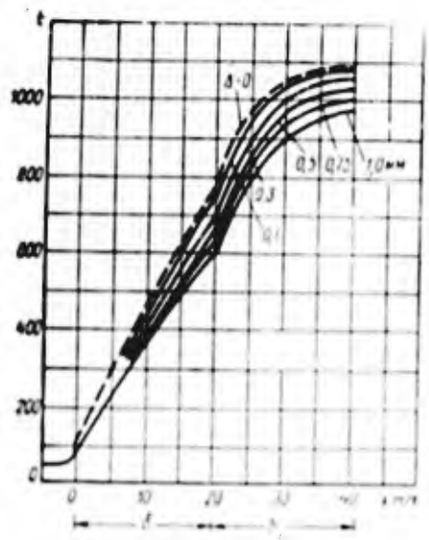

Fig. 13. Effect of the thickness of blade covers with low thermal conduction on blade temperature. a) kcal/m degrees x hours; b) kcal/m degrees x hours.

The effectiveness of decreasing blade temperatures depends on the thickness and thermal conduction of the covering material. The thicker the cover and the lower its thermal conduction, the lower the blade temperature. With a cover thickenss Δ = 0.5 mm and λ_Δ = 0.3 kcal/m x degrees x hours the blade temperature, as compared with blades with no covers, decreases by 50 to 100° (Fig. 13). As

the cooling duct approaches the root up to 7 mm under identical conditions, the blade temperature decreases already by 90 to 130°. Thermal conduction of the blade cover material has a considerable bearing on the temperature of the blade. For more probable cover thicknesses up to Δ = 0.5 mm, covers with λ_Δ > 1 kcal/m x degrees x hours are nearly ineffective (Fig. 14). For this reason, covers of operating turbine blades should be made of materials with the least possible thermal conduction. High temperature gradients arise in these covers. For example, in a section x = 5 mm with λ_Δ = 0.3 kcal/m x degrees x hours we have Δt = 130°, while for λ_Δ = 1 kcal/m x degrees x hours we have Δt = 50° (see Fig. 14).

Covers with good thermal conduction improve the transfer of heat from the blade to the cooling duct, lower considerably the temperature of the upper blade portion and somewhat increase the temperature of the blade's socket (Fig. 15).

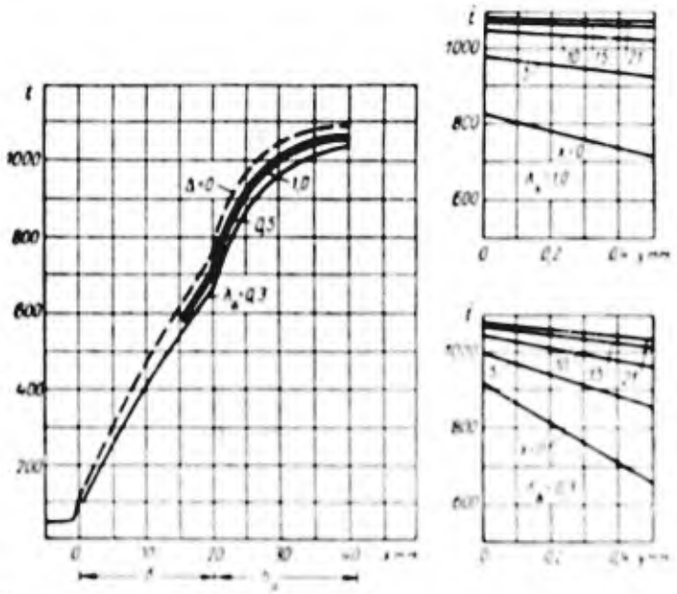

Fig. 14. Effect of thermal conduction of blade covers on blade temperature. a) kcal/m² degrees hours.

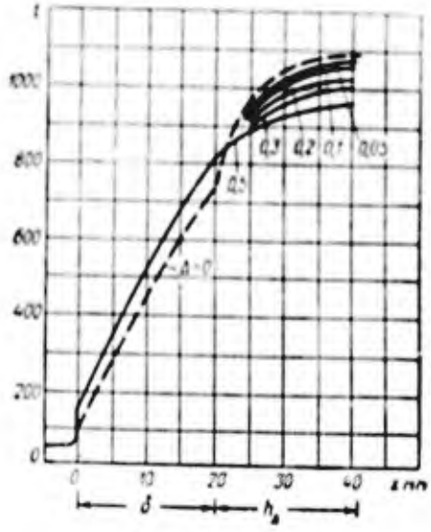

Fig. 15. Effect of cover thickness with high thermal conduction on temperature distribution in blade. a) kcal/m degrees hours ; b) kcal/m degrees hours .

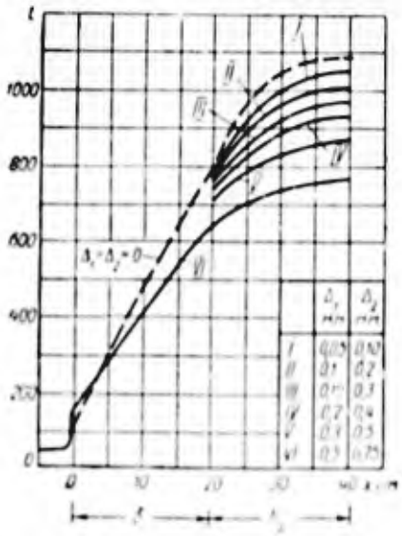

Fig. 16. Effect of two-layer covers on blade temperature.

a) Kcal/m^2 degrees hours b) Kcal/m degrees hours.

More effective in this respect are two-layer covers (Fig. 16). Even with a small overall thickness of the cover $\Delta_1 + \Delta_2 = 0.3$ to .6 mm the temperature of the blade, and especially of its upper part, drops considerably.

CONCLUSIONS

1. The approximate dependences (43) and (44) obtained by us can be used only for preliminary computations. More precise computa-

tions should be undertaken with the more accurate formulas (29) and (30).

2. An efficient utilization of the given cooling method is possible only in the case of short operating blades with heights not exceeding in 30 to 40 mm.

3. It is necessary that the distance between the cooling duct and the blade root be [redacted] as small as possible.

4. An effective cooling of short blades made of heat-resistant, nickel ~~nickel~~-base alloys can only be obtained if $\varepsilon\alpha_\lambda < 1{,}500$ kcal/m^2 degrees x hours.

5. If heat-resistant materials with higher thermal conduction are utilized, effectiveness of blade cooling can be improved.

6. As a thermal insulation of blades, covers with the lowest possible coefficient of thermal conduction should be used. Covers with $\eta_\delta > 1$ kcal/m x degrees x hours are ineffective.

7. For blades made of conventional heat-resistant materials, two-layer covers attain the highest degree of effectiveness.

REFERENCES

1. Romanovskiy P. I., Ryady Fur'ye. Teoriya Polya. Analiticheskiye i Spetsial'nyye Funktsii. Preobrazovaniye Laplasa (Fourier series.

Field theory. Analytical and special functions. Laplace Transformation), Gostekhizdat (State Technical Press), 1957.

2. Mikheyev M. A., Osnovy Teploperedachi (Fundamentals of Heat Transfer) Gosenergoizdat (State Press for Power Engineering), 1956.

3. Zhiritskiy G. S. , Aviatsionnyye Gazovyye Turbiny (Aeronautical Gas Turbines), Oborongiz, 1950.

ON THE POSSIBILITY OF UTILIZING BINARY COMPOUNDS FOR MODEL STUDY OF TURBINES

By

Candidzate of Technical Sciences V. M. Tyugin

An analysis of the possibility of utilizing turbines in various fields of technology requires knowledge of turbine characteristics in the wide range of changes occurring to the parameters of its operation. Devising reliable methods for the computation of turbine characteristics represents a difficult task. More accurate turbine characteristics are obtained from tests carried out on stands. Tests where the parameters of turbine operation are identical with the corresponding parameters under actual service conditions yield the most accurate results, yet, they present considerable difficulties from a technical point of view. For this reason, the most widespread type of turbine tests (and turbo-engines in general) are model studies of geometrically similar specimens. It is known, that in the case of such tests the eqaulity of the basic similarity criterions must be maintained. For steady-state operations, without considering heat transfer, these criteria are

as follows:

1. The number $M = c/a^*$, accounting for compressibility (c being the rate of flux, and a^* the velocity of sound in the same section).

2. The number $Re = c\varrho l/\eta$, accounting for the effect of viscosity forces (ϱ , η and l which are, respectively, density, dynamic viscosity and the characteristic geometric dimension).

3. The index of the adiabatic curve $k = c_p/c_v$ which characterizes the thermodynamic properties of the working substance (c_p and c_v being specific heat).

4. The ratio u/c which determines the proportionality of the velocity triangle (u being the peripheral turbine velocity).

Instead of the ratio u/c we use the criteria M_u or λ (the M_u and λ numbers for peripheral velocity u).

We were unable to maintain in practice the exact equality among all the criteria mentioned above. In fact, when utilizing as a model working substance slightly heated air (combustion products), owing to a great difference in temperatures the index of the adiabatic curve k_{mod} was found to be different from k_{nat}. An increase in temperature, as well as the trend to keep $Re_{mod} = Re_{nat}$,

increases the power of the turbine during tests. This renders more complex the test ewuipment utilized. In order to avoid the difficulties, we resorted to dimensional modeling, (testing reduced models) and to tests with reduced numbers Re_{mod} Re_{nat}, thus reducing the accuracy of tests. A basically new method of model studies of turbines was proposed by Prof. A. V. Kvasnikov in MAI in 1949. This method consists in utilizing as working substances high-molecular gases and vapors with small specific gas constants R, which makes it possible to reduce considerably the turbine shaft horsepower during tests. This eliminates the necessity in reduced-scale modeling. A basic difficulty arising with this experimental method consists in that the index of the adiabatic curve of high-molecular gases and vapors differs considerably in magnitude from the index of the adiabatic curve of combustion products: k_{mod} k_{nat}.

Thus, the problem of model studies of high-molecular working substances is basically the problem of model tests under conditions of inequality of one of the above basic similarity criteria, viz., the index of the adiabatic curve k. This is indeed a complex problem which requires special attention. In a paper (5) of recent publica-

tion it is shown that even in such relatively simple turbo-engines as single-staged axial turbines and centrifugal compressors, special testing methods based on the conservation of approximate similarity of operating conditions of turbo-engines are required if as working substances we use such substances which have different indices of the adiabatic curve ($k_{mod} \neq k_{nat}$).

Such a method for testing single-staged action turbines is proposed by V. A. Tselikov (6). The fact that experimental data from tests carried out with air (k = 1.39 to 1.4) and carbon tetrachloride CCl_4 (k = 1.1) support this method shows that in the given case it is possible to obtain a satisfactory simulation of turbine operations under test conditions.

Yet, for multi stage axial compressors and turbines, the method of model tests with single-component heavy substances with adiabatic indices different from the adiabatic index of the natural working substance is bound to run into serious difficulties. For some types of turbo-engines, it may even turn out to be completely inapplicable. The difficulties connected with the difference of k_{mod} from k_{nat} can be avoided if as a working substance for turbine

model tests we use a mixture of two gases where $k_{mod} = k_{nat}$. This mixture will henceforth be called binary mixture. It is obtainable by mixing high-molecular gas where $k_{mod} < k_{nat}$, with one of the rare gases (He, Ar, Kr and Xe). As is known, they have $k_{mod} = 1.66 > k_{nat}$. In addition to difficulties of purely practical order, the possibility of utilizing such mixtures for turbine model tests depends on the solution of at least two basic problems:

1. Determining the demixing degree of these compounds on working turbine blades;

2. Determining the thermodynamic equilibrium of expansion processes of such mixtures.

The present paper is devoted to the study of these problems.

1. STRATIFICATION OF BINARY MIXTURE

Stratification of a binary mixture consists in the effect of centrifugation by centrifugal forces of the mixture component which is heavier by molecular weight. The effect of centrifugal forces on the gas between the blades of a working turbine wheel reveals itself in two perpendicular planes, viz., along the radius and in the direction of the normal to the blade (Fig. 1). The evaluation of the degree

of possibile stratification in various directions made for the parameters of model tests corresponding to the parameters of the natural operation of one of the aviation type high-pressure turbines, assuming an infinitely long time of permanence of one of the prospective binary mixtures (mixture of 54% Ar and 46% CCl_4) on the working blades of a standard jet turbine, shows that the most dangerous direction for the stratification of the mixture is the direction of the normal to the blade and that the characteristics of physical properties of the mixture in the section near the top and the root of the blade differ rather substantially. In particular,

$\bar{R}_{cap} = R_{top} / R_{root} = 200\%$ and $\bar{k}_{cap} = k_{top} / k_{root} = 125\%$.

The latter result requires that the mixture stratification process be investigated with regard to time. From a physical point of view the stratification system of a binary mixture consisting of various molecules represents a molecular process of gas diffusion complicated by the fact that, in addition to diffusion of high-molecular gas under the action of centrifugal forces, there will take place a natural diffusion of the same gas owing to varying concentration. After a certain period of time these processes must find

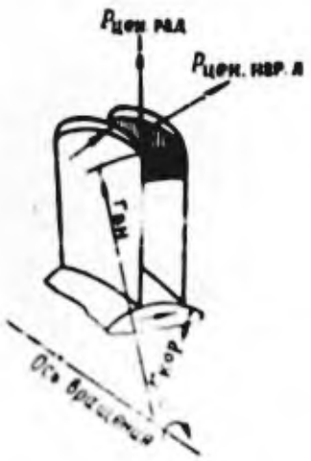

Fig. 1. Forces acting on the gas between turbine blades.

a) P cen.rad b) P cen.nor.b c) r ext d) r cor e) rotation axis.

an equilibrium, the condition of continuity of action being maintained. † An accurate solution of this problem as applied to the flow of gas in the ducts of a working turbine wheel runs into considerable difficulties. For this reason, as a model of the phenomenon under investigation, let us study the problem of the variation in time of the concentration of one of the mixture components placed in a long cylinder with a base and with an assigned initial distribution of the concentrations along the cylinder length and an assigned character of acting external forces (Fig. 2).

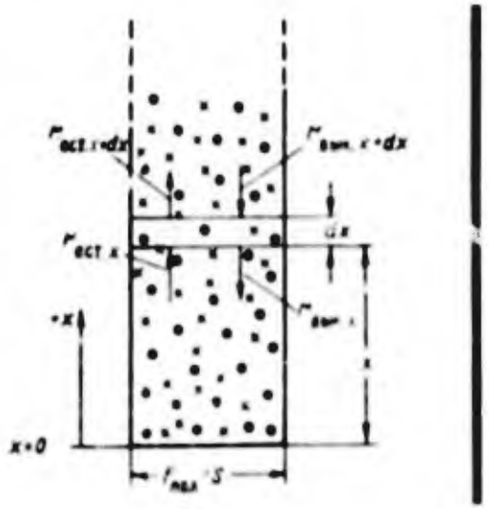

Fig. 2. Diagram of the phenomenon under investigation.

The mixture is represented schematically by different symbols. Let us determine the volume of the mixture enclosed in the cylinder with base S and height dx and let us examine the variation in the quantity of one of the components in this volume. For the process of natural diffusion in gases the following equation is true:

$$dM = -D\left(\frac{\partial \rho}{\partial x}\right) S\, d\tau, \qquad (1)$$

where dM is the mass of the gas which has flowed through the section under investigation;

$\delta\rho/\delta x$ is the density gradient in the direction of diffusion;

S is the section;

τ is the time;

D is a constant which depends on the nature of the gas and diffusion conditions.

Using expression (1) for one of the mixture components, we find the variation of the component mass in the [redacted] volume as a result of natural diffusion (the effect of the side walls is disregarded)

$$dM_{ест} = D\frac{\partial^2\rho}{\partial x^2} S\,dx\,d\tau \qquad (2)$$

For the diffusion of gas under the action of external forces (forced diffusion) we may write the following expression:

$$dM_{выт} = (V_ф)_x S\,d\tau. \qquad (3)$$

where V is the rate of forced diffusion.

Hence we find the variation of the component mass as a result of forced diffusion in the singled-out volume

$$dM_{выт} = -\frac{\partial(V_ф)_x}{\partial x} S\,dx\,d\tau \qquad (4)$$

The minus sign denotes that the directions of forced and natural diffusion are opposed.

The change of gas mass in the singled-out volume in time is

$$dM = \frac{\partial \rho}{\partial \tau} S dx d\tau. \tag{5}$$

Since this variation of mass occurs as a result of diffusion, we obtain from expressions (2), (4) and (5)

$$\frac{\partial \rho}{\partial \tau} = D \frac{\partial^2 \rho}{\partial x^2} - \frac{\partial}{\partial x} (V \rho), \tag{6}$$

The density of the substance is proportional to its concentration C, hence the differential equation obtained can be rewritten as

$$\frac{\partial C}{\partial \tau} = D \frac{\partial^2 C}{\partial x^2} - \frac{\partial}{\partial x} (VC) \tag{7}$$

In order to solve this equation it is necessary to assign initial and boundary conditions. As a boundary condition we use that of the equality of gas molecule flows on the basis of the cylinder

$$\left(D \frac{\partial C}{\partial x}\right)_{x=0} = VC \tag{8}$$

Before assigning the initial condition let us find the rate of forced diffusion V. The amount of the component transferred under the action of external forces in analogy with (1) can be written as

$$dM_{forc} = D \left(\frac{\partial \rho}{\partial x}\right)_x S d\tau. \tag{9}$$

Substituting dM_{forc} by expression (3) we obtain

$$V_x = \frac{D \left(\frac{\partial \rho}{\partial x}\right)_x}{\rho_x}. \tag{10}$$

In the case under investigation the variation of density along

the radius must be due to the effect of forces imitating centrifugal forces which develop on the turbine blades. Since the latter are variable in accordance with the height of the blade, the forces replacing them must be variable according to the height of the cylinder. Yet, in this case, equation (8) is not integrated by (1). Moreover, the model of the phenomenon would be physically unreal. It is simpler to assume these forces to be constants determined, for example, by the heavy "weight" of molecules. The required degree of "weighting" can be found in the following way. The change in density of the gas along the turbine blade radius is expressed in the general case by the differential equation

$$\frac{\partial \rho}{\partial r} = \frac{\rho}{RT_g} r\omega^2 \qquad (11)$$

By averaging according to the mean geometric blade radius r, we obtain

$$\left(\frac{\partial \rho}{\partial r}\right)_{cp} = \frac{\rho_{cp}}{R_i T_g} r_{cp}\omega^2 \qquad (12)$$

Here R_i is the constant of the gas component whose concentration is of interest to us;

T is the gas temperature;

ω is the angular velocity.

In computing (12) we may assume $\delta q/\delta r = dq/dr$, where dq/dr is determined from equation (11).

In order to conserve $\left(\frac{dp}{dx}\right)_{cp} = \left(\frac{dp}{dr}\right)_{cp}$ in the constructed model, we have to take $r_{cp}\omega^2 = x_{cp}\omega^2$. Knowing the relationships between r, x and ω, this can be done easily. Then for $V_{x\,mean}$ we obtain

$$V_{x\,cp} = \frac{D}{R_i T_g} x_{cp}\omega_i^2 = \text{const} \qquad (13)$$

Velocity $V_{x\,mean}$ is directed towards the cylinder base.

The initial condition has to be assigned in the following fashion. In the turbine, the forced molecule motion under the effect of centrifugal forces will be directed towards the blade top. For this reason, in the constructed system of phenomena the cylinder base has to play the part of the wall of the turbine body. It can readily be shown that once the gas hits the working turbine blades, it is compressed by centrifugal forces in such a way that the distribution of the concentration along the blade radius can be expressed by the dependence

$$C_r = C_0 e^{\beta_r}, \qquad (14)$$

where

$$\beta_r = \frac{U_0^2}{2gR_{cm}T}\left[\left(\frac{r}{r_0}\right)^2 - 1\right].$$

Here $T = T_r = \text{const}$;

R_{mix} is the constant of the gas mixture which has not yet been subjected to stratification;

U_o is the surrounding velocity on the inner radius.

With a limited height of the working blade, pressure and, hence, concentration at its top will be specific ($C_{ext} = 1$). In accordance with what was stated about V_{mean} let us assume for the model $C_{r,\tau} = 1$, and the initial distribution of the concentration of the component along the cylinder height as being governed by the law

$$C_{r,\tau=0} = Ae^{-az}, \qquad (15)$$

where $a = \frac{\omega^2 r_0}{RT}$.

Such an initial distribution can be obtained with an abrupt shift of the cylinder from its horizontal position into a vertical one.

Thus, for the solution of the problem we have the equation of the process (7) boundary conditions (8) and initial conditions (15). When designing the model nothing was said about the second mixture component. Let us assume that it is weightless, whence we are justified in regarding the results of the computation as excessive.

First of all, by substituting

$$C = C^* e^{\frac{Vx}{2D} - \frac{V^2 t}{4D}} \tag{16}$$

we transform equation (7) into the following one:

$$\frac{\partial C^*}{\partial t} = D \frac{\partial^2 C^*}{\partial x^2} \tag{17}$$

This equation does not contain terms depending on forced gas diffusion. Hence it is an equation of free gas diffusion, which in its external form recalls the basic equation of heat conduction for one-dimensional problems. The boundary and initial conditions can be written in the form

$$\left(\frac{\partial C^*}{\partial x}\right)_{x=0} = \frac{V}{2D} C^*_{x=0} \tag{18}$$

$$C^*_{t=0} = Ae^{-x\left(x + \frac{V}{2D}\right)} \tag{19}$$

The analogy of differential equation (18) and boundary condition (19) with the relationships for one of the problems of heat conduction, set forth in (2), makes it possible to write immediately the general solution in the form of

$$C^* = \frac{1}{2\sqrt{\pi D t}} \int_0^\infty \left[\Phi(z) e^{-\frac{(x-z)^2}{4Dt}} + \Phi(-z) e^{-\frac{(x+z)^2}{4Dt}}\right] dz, \tag{20}$$

where

$$\Phi(-z) = \Phi(z) - \frac{V}{D} e^{\frac{Vz}{2D}} \int_0^z \Phi(\xi) e^{\frac{V}{2D}\xi} d\xi. \tag{21}$$

Consequently, the problem consists in that on the basis of the

initial condition in the form of (19) we find from (21) the function $\Phi(-\alpha)$ and, substituting it in the general solution (20), carry out integration. Assuming $\Phi_1(\alpha) = \Phi(\alpha) = Ae^{-\alpha\left(\alpha+\frac{V}{2D}\right)}$ and performing integration, we obtain

$$\Phi(-\alpha) = A\left\{e^{-\alpha\left(\alpha+\frac{V}{2D}\right)} + \frac{V}{D\alpha}e^{-\alpha\left(\alpha+\frac{V}{2D}\right)} - \frac{V}{D\alpha}e^{-\alpha\frac{V}{2D}}\right\}. \qquad (22)$$

Substituting this expression in the general solution (20) we have

$$C^* = \frac{A}{2\sqrt{\pi D x}}\left\{\int_0^\infty e^{-\frac{(\alpha-x)^2}{4Dx}-\alpha\left(\alpha+\frac{V}{2D}\right)}d\alpha + \int_0^\infty e^{-\frac{(\alpha+x)^2}{4Dx}-\alpha\left(\alpha+\frac{V}{2D}\right)}d\alpha + \right.$$
$$\left. + \int_0^\infty \frac{V}{D\alpha}e^{-\alpha\left(\alpha+\frac{V}{2D}\right)-\frac{(\alpha+x)^2}{4Dx}}d\alpha - \int_0^\infty \frac{V}{D\alpha}e^{-\frac{V}{2D}\alpha-\frac{(\alpha+x)^2}{4Dx}}d\alpha\right\}. \qquad (23)$$

We shall take integrals in sequence.

By complementing the exponent of the subintegral expression of the first integral up to a complete square and utilizing substitution of $z = \frac{\alpha-(x-2aDx-Vx)}{2\sqrt{Dx}}$, we can reduce the integral to the following form:

$$I_1 = 2\sqrt{Dx}\int_{z_0}^{\infty} e^{-z^2}dz = 2\sqrt{Dx}\left[\int_0^{\infty} e^{-z^2}dz + \int_{z_0}^{0} e^{-z^2}dz\right],$$

where $z_0 = -\frac{x-2aDx-Vx}{2\sqrt{Dx}}$.

The first of the integrals obtained is a Gauss integral which, as is known, equals $\sqrt{\pi}/2$.

Let us write the second integral as

$$\int_{z_0}^{0} e^{-z^2}dz = \int_0^{-z_0} e^{-z^2}dz.$$

This integral is a part of Gauss' error function

$$\operatorname{erf}(z)=\frac{2}{\sqrt{\pi}}\int_0^z e^{-z^2}dz, \qquad \text{B 169}$$

whose numerical values are tabulated in (3). Thus, in the general solution, the first integral was found to equal

$$I_1=2\sqrt{D\tau}\left|\frac{\sqrt{\pi}}{2}+\frac{\sqrt{\pi}}{2}\operatorname{erf}\left(\frac{x-2aD\tau-V\tau}{2\sqrt{D\tau}}\right)\right|e^{\frac{(x-2aD\tau-V\tau)^2-x^2}{4D\tau}}. \qquad \text{C 169}$$

Omitting for shortness the computation of the remaining integrals in the general solution (23) we write their expressions in their final forms:

$$I_2=\int_0^{\tau} e^{-\frac{(\alpha+x)^2}{4D\tau}-\alpha\left(\alpha+\frac{V}{2D}\right)}d\alpha=B_2 2\sqrt{D\tau}\left|\frac{\sqrt{\pi}}{2}-\right.$$

$$\left.-\frac{\sqrt{\pi}}{2}\operatorname{erf}\left(\frac{x-2aD\tau-V\tau}{2\sqrt{D\tau}}\right)\right|;$$

$$I_3=\int_0^{\tau}\frac{V}{Da}e^{-\frac{(\alpha+x)^2}{4D\tau}-\alpha\left(\alpha+\frac{V}{2D}\right)}d\alpha=B_3\frac{V}{Da}2\sqrt{Da}\left|\frac{\sqrt{\pi}}{2}-\right. \qquad \text{D 169}$$

$$\left.-\frac{\sqrt{\pi}}{2}\operatorname{erf}\left(\frac{x-2aD\tau-V\tau}{2\sqrt{D\tau}}\right)\right|;$$

$$I_4=\int_0^{\tau}\frac{V}{Da}e^{-\frac{(\alpha+x)^2}{4D\tau}-\frac{V}{2D}\alpha}d\alpha=B_4\cdot 2\sqrt{D\tau}\left|\frac{\sqrt{\pi}}{2}-\right.$$

$$\left.-\frac{\sqrt{\pi}}{2}\operatorname{erf}\left(\frac{x+V\tau}{2\sqrt{D\tau}}\right)\right|,$$

where

$$B_2=B_3=e^{\frac{(x-2aD\tau-V\tau)^2-x^2}{4D\tau}}\ ;\quad B_4=\frac{V}{2Da}e^{\frac{(x+V\tau)^2-x^2}{4D\tau}}. \qquad \text{E 169}$$

Thus, we obtain the intermediate solution C*. Substituting the expression of individual integrals I_1, I_2, I_3 and I_4, and taking into account (14), we obtain after transformation

$$C=\frac{A}{2}e^{\frac{V}{2D}x-\frac{V^2\tau}{4D}}\left\{2e^{\frac{(x-2aD\tau-V\tau)^2-x^2}{4D\tau}}+\frac{V}{aD}e^{\frac{(x-2aD\tau-V\tau)^2-x^2}{4D\tau}}\left|1-\right.\right.$$

$$\left.\left.-\operatorname{erf}\left(\frac{x-2aD\tau-V\tau}{2\sqrt{D\tau}}\right)\right]-\frac{V}{aD}e^{\frac{(x+V\tau)^2-x^2}{4D\tau}}\left[1-\operatorname{erf}\left(\frac{x+V\tau}{2\sqrt{D\tau}}\right)\right]\right\}. \qquad (24)$$

It can readily be seen that the solution obtained satisfies the initial condition with $\tau = 0$.

Let us investigate what happens with $\tau = \infty$. In this case, on account of the general factor $e^{\frac{V_1}{2D} - \frac{V_1}{4D}}$, all of the terms of the solution excepting the last one turn to zero and the solution is obtained in the form

$$C_{\tau=\infty} = -\frac{A}{2}\frac{V}{D_M} e^{\frac{V}{D}x} \times \left[1 - \operatorname{erf}\left(\frac{x + V_1}{2\sqrt{D\tau}}\right)\right]. \quad \text{A 170}$$

Taking into account the sign of V, the last term of eqn is

$$\operatorname{erf}\left(\frac{x + V_1}{2\sqrt{D\tau}}\right) - \quad \text{B 170}$$

and, hence, we finally obtain

$$-\frac{2}{\sqrt{\pi}}\int_0^{-\infty} e^{-x^2} dx = -1$$

$$C_{\tau=\infty} = -\frac{AV}{D_M} e^{\frac{V}{D}x}. \quad (25)$$

Since velocity $V < 0$, the expression obtained yields $C_{\tau=\infty} > 0$.

Let us return to the solution of equation (24) and let us use it for the mixture Ar+CCl$_4$. Figure 2 shows the concentrations of the vapors of the heavy component of the CCl$_4$ mixture along the height of the cylinder with $\tau = 0$ and $\tau = \infty$, computed with the aid of expressions (19) and (25) and the aid of equality (12), where $R = R_{CCl_4} \approx 5.5$.

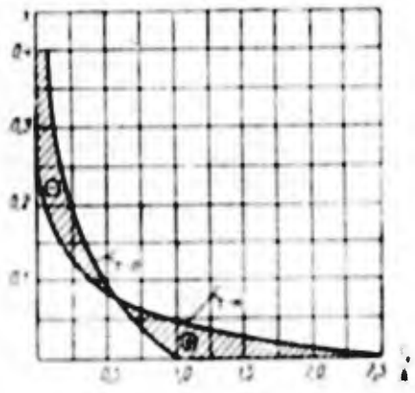

Fig. 3. Distributions of concentrations along the height of cylinder. 1 -concentration of CCl_4 with $\tau = 0$, $x = 0$.

The computations were effected for a turbine with $r_0 = 240$ mm, $r_{ext} = 345$ mm, $U = 250$ m/sec. The temperature of model tests was set equal to $T = 320°$ abs. As is seen from the results, the descrepancies between $C_{x, \tau = 0}$ and $C_{x, \tau = \infty}$ are considerable and for the tip of the blade ($x = 0$) amount to 255%. For the evaluation of the possible degree of stratification of the binary mixture in the turbine, however, it is interesting to note the change in the concentration for the final time interval. We assume

it equalling 5 sec (which exceeds by several thousands of times the time the binary mixture stays on the working turbine blades during model tests) and compute $C_{x = 0, \tau = 5}$ for CCl_4. To do this it is necessary to determine beforehand the diffusion coefficient D and the diffusion velocity V under the action of "conditional" forces of gravity. To determine the diffusion coefficient D let us use the dependents $D = 1/3\ \bar{V}L$ (4), where L is the mean length of the free path of molecules; $\bar{V}$ is the mean quadratic velocity of molecule motion.

According to dependence (4) found experimentally, the values for L and $\bar{V}$ are found to be linked with the values for viscosity η and density ρ of xx the gas:

$$\eta = 0.499\rho\bar{V}L. \qquad (171)$$

The value for viscosity of the mixture can be determined according to the viscosity of the components and the composition of the mixture. In particular, for the mixture Kr + CCl_4 with T = 290° abs viscosity of the mixture was found to equal η = $= 1.54 \times 10^{-6}$ kg x sec/m^2. Density of the mixture at the working blade roots with model test parameters corresponding to ground operation conditions of the turbine, was found to equal [redacted]

$g = 0.0569$ kg x sec^2/m^4. Computations according to the above dependences and utilization of expression (13) yielded the following results:

$$D = 1{,}315 \cdot 10^6 \ м^2/сек;$$
$$V_{ср} = 3{,}48 \cdot 10^{-4} \ м/сек; \qquad \text{В 171}$$
$$V_{ср}/D = 19{,}2 \ м^{-1}.$$

Let us go back to solution (7А) and compute the change in concentration on the bottom of the cylinder ($x = 0$). Without bringing all of the computations in their entirety, we write the final expression for $C_{x=0,\tau=\tau}$ in the form of (7А)

$$C_{x=0,\tau=\tau} = \frac{A}{2} e^{-0{,}32 \cdot 10^{-3}} \left[2e^{0{,}32 \cdot 10^{-3}} - \frac{19{,}2}{7{,}51} e^{0{,}32 \cdot 10^{-3}} \times \right.$$
$$\left. \times [1 - \operatorname{erf}(1{,}95 \cdot 10^{-3})] + \frac{19{,}2}{7{,}51} e^{0{,}32 \cdot 10^{-3}} [1 - \operatorname{erf}(0{,}9 \cdot 10^{-3})] \right] \approx 1{,}02A. \qquad \text{С 171}$$

Consequently, after 5 sec have elapsed, the concentration on the bottom of the cylinder will change approximately by 2%. Actually, the change in the mixture parameters will be even smaller, since when solving the differential equation and the definition of the numerical values for the effective "forces of gravity" the second component of the mixture (Ar) was considered weightless. Moreover, when the mixture flows through the flow area of the turbine, it mixes intensively in passing from one stage to another.

Thus, the results of the investigation undertaken by us lead us to conclude that stratification of binary mixtures on working turbine blades with model test parameters is impossible. This allows us to give a positive answer to the question of applicability of these mixtures from the point of view of their stratification.

2. THERMODYNAMIC EQUILIBRIUM OF THE DISCHARGE PROCESS OF BINARY MIXTURES

The necessity of evaluting the thermodynamic equilibrium of the discharge process of binary mixtures is due to the fact that binary mixture components are gases sharply differing among one another in their physical properties, and, in particular, having sharply differing adiabatic parameters. Thus, for example, for the components of the Ar + CCl_4 mixture mentioned earlier the adiabatic parameters with T = 50 to 150°C are equal to 1.66 and 1.1, respectively.

As is known, temperature variation during adiabatic gas expansion depends greatly on the magnitude of the index of the adiabatic curve. As a consequence thereof one may fear that during rapid processes (discharge from turbine nozzles) the temperatures

of binary mixture components will not be balanced, and that this may be the cause for the thermodynamic nonequilibrium of the process. The balancing of temperatures of mixture components during discharge is rendered difficult by the fact that the parameters of model tests (in particular, pressure and temperature) are considerably below the natural ones. As a consequence, the number of molecule collisions decreases, i.e., the processes of energy exchange between molecules are inhibited. Unfortunately, the extent of this paper does not make it possible to undertake a thorough analysis of this problem, hence we shall confine ourselves to bringing only the final conclusions.

According to the general physical premises the equilibrium of the process, characterized by the equality of temperatures of mixture components during discharge, is not impaired if the duration of the process is no less than the time interval between two molecule collisions. We carried out an investigation with the nozzle of a turbine of a liquid fuel rocket engine. As is known, turbines of this class operate with great expansion rates. This leads to high gas discharge velocities from turbine nozzles ($V \gg 2.5$). The purpose of the investigation consisted in juxtaposing the number of

actual and required molecule collisions of the components of the binary mixture Ar + CCl_4 necessary for balancing the temperatures of mixture components in the discharge area of a shortened turbine nozzle of a liquid fuel rocket engine (δ = 25, nozzle length 50 mm, initial discharge temperature T = 300°C, initial pressure $p_{0\ mod}$ = 11.1 absolute atmospheres). The investigation consisted in computing the number of collisions approaching the central ones and determining the quantity of energy transferred by heavy "hot" CCl_4 molecules to Ar molecules. To do this, all energy forms of CCl_4 molecules were reduced to the energy of progressive motion (due to the corresponding increase in mass efficiency), while molecule collision was regarded as the collision of elastic spheres.

The results of the juxtaposition turned out to be as follows: if for the balancing of the energies of CCl_4 and Ar molecules at the end of expansion on the 3-mm long nozzle area about two central impacts are required, then the number of impacts available, which can be regarded as central, equals about 1%. Thus, if we take into account that unused besides the 10/head-on impacts there will be a huge number of oblique impacts between CCl_4 and Ar molecules during discharge, it becomes obvious that the temperature of mixture

components will be balanced instantly, and, hence, thermodynamic steadiness of the process is fully ensured. In the case of slower processes in conventional turbines, this statement is evenmore justified.

On the basis of the above results we can draw the conclusion that the applicability of binary compounds as model turbine tests is fully ensured both from the point of view of stratification of mixtures and from that of thermodynamic equilibrium of the gas expansion process in the turbine.

REFERENCES

1. Kamke E., Spravochnik po Obyknovennym Differentsial'nym Uravneniyam (Handbook for Normal Differential Equations), IL, 1951.

2. Frank F. and Mizes R., Differentsial'nyye i Integral'nyye Uravneniya Matematicheskoy Fiziki (Differential and Integral Equations of Mathematical Physics), ONTI, 1937.

3. Segal V. I. and Semendyayev K. A., Pyatiznachnyye Matematicheskiye Tablitsy (Five-Unit Mathematical Tables), Akademiya Nauk SSSR (Academy of Sciences of the USSR), 1950.

4. Key and Lebi, Spravochnik Fizika-Eksperimentatora (Handbook of Experimental Physics, translated from the English, edited by

Frank-Kamenetskiy), IL, 1949.

5. Gaygerov V. I., Vliyaniye Svoystv Rabochego Tela na [illegible] Tsentrobezhnogo Kompressora i Gazovoy Turbiny, Trudy [illegible] iesledovatel'skoy Laboratorii Dvigateley (Effect of the [illegible] of the Working Substances on the [illegible] Compressors and Gas Turbines, Proceedings of [illegible] Laboratory of Engines), No. 4, [illegible].

6. Tselekov V. A., Modelirovaniye [illegible] Gazom (Simulation of Turbine Operation with [illegible] Academy of Sciences of the USSR, [illegible].

UNCLASSIFIED